Dynamics of hot electrons in ultra-thin metallic films and small structures

Dissertation

Ron Porath

Vom Fachbereich Physik der Universität Kaiserslautern zur Verleihung des akademischen Grades „Doktor der Naturwissenschaften“ genehmigte Dissertation

Betreuer: Prof. Dr. Martin Aeschlimann

Zweitgutachterin: Prof. Dr. Ch. Ziegler

Datum der wissenschaftlichen Aussprache:
06.12.2002

D 386

Introduction

Thin-film knowledge and nanometer-structure technology play a crucial role in the high-tech industries. Whilst the major exploitation of thin films has been in microelectronics, there are numerous applications in communications, optical electronics, coatings of all kind, and in energy generation and conservation strategies. The "roadmap" of the semiconductor industry brings about the strongest need to the production and understanding of thin-films, small structures and semiconductor-metal junctions. In order to fabricate tiny electric circuits, with diameters of about 90nm (possible since 2002) or even smaller ones, it is essential to intensify the research on this topic. Not only the formation and generating of nanometer structures are known to be quite intricated, but also the electron behaviour in such solids with limited extensions.

The dynamics of electrons in a solid crystal has been of enormous interest since the beginning of the 20th century. A short time after the discovery of the electron, Drude developed his theory on the electric conductivity in metals[1]. Already in his visionary work in the year 1900, the term *relaxation time* of the electrons, that is of huge importance to this thesis, played an essential role. He described the relaxation time of excited electrons as the mean time between two scattering processes, which lead the electrons to return to the equilibrium after a disturbance (e.g. by scattering on phonons or defects).

For *thermally* excited electrons as well as for electrical resistivity, the scattering at phonons and defects play a decisive role. On the other hand, at *optical* excitation, electrons are produced with some eV above Fermi energy, and primarily relax via inelastic electron-electron interaction. A simple theoretical description of the relaxation time (or *lifetime*) of those so-called *hot electrons* was given by Landau in his theory of Fermi-liquids[2]. According to this theory, an excited electron scatters with a cold electron, which is located below the Fermi energy. Because of Pauli's exclusion principle, both electrons have to occupy free states above the Fermi energy after the interaction. Thus, the scattering probability and therefore the relaxation time depend critically on the accessible phase space, i.e. the amount of possible scattering partners and final states.

During the 20th century's sixties to eighties, many theoretical research works were made concerning the energy dissipation of electrons in smaller dimensions, in advance of the experimental methods. Landau's

[1] [Dru00]
[2] [Lan57]

theory of the Fermi-liquid was thereby extended in many aspects. The extension that is important to this present thesis is related to the scattering and relaxation behaviour of hot electrons in a two-dimensional electron gas. For such a 2d gas, Giuliani and Quinn[3] described an electron-electron interaction, which adds to the known energy dependent relaxation time a factor that is logarithmically dependent of the energy. This additional factor is a consequence of the electron confinement in a 2d crystal.

Since the development of ultra-short, tuneable laser systems in recent years, mainly based on Ti:sapphire crystal medias, a large variety of modern (experimental) research fields have expanded the knowledge of the dynamics of photoexcited hot electrons in solid states of different dimensions. Examples for the used methods are fs-photochemistry[4], (magneto) electronics[5], second harmonic generation[6], as well as the time (and spin) resolved two-photon photoemission technique (TR-2PPE)[7], transmission observations[8], and others. By these means, the dynamics of optically excited electrons has been investigated intensively in metals, semiconductors and adsorbates.

These observations have shown that electron dynamics depends not only on the phase space, but also on the excitation energy, the electron density of states, i.e. the band structure, dimensionality and morphology, as well as on screening of the excited electrons and of their spins[9].

The time-resolved two-photon photoemission, which is used in this thesis, is known to be adequate for the analysis of electronic states and the dissipation of their momenta and energies in solids. It is of enormous importance for the theoretical, the experimental and the industrial research, to achieve clarity on the dissipation of energy and momentum of electrons in small structures, after optical excitation. Only with a clear understanding of this dynamics, controlling and realizing new developments in the field of nano technology will be possible.

This thesis is organized as follows: the first chapter deals with the theoretical description of electrons in a bulk and at surfaces of metals and semiconductors, the interaction of light with a medium and the classical dispersion theory. This will lead directly to the concept of plasmons that became more and more important at analyses of photoexcitation experiments. The 3d-Fermi-liquid theory will be briefly sketched and applied to electron-electron interaction in 2d and smaller structures.

---

[3] [GQ82]
[4] [Zew98]
[5] [Wol01]
[6] [Lam99]
[7] [Hai95], [SAE+94], [HKWE96], [ABP+97], [PO97]
[8] [LRWM01]
[9] [BA02]

The theory of photoemission (PE), two-photon photoemission (2PPE) and time-resolved two-photon photoemission (TR-2PPE) in chapter two will explain the background of the measurements. Its experimental requirements will then be described in chapter three.

Chapter four, which discusses new results, will begin with an introduction about known facts of electron dynamics in thin films. Subsequently the results of different observed systems will be explained in details. Starting with ultra-thin layers of silver on HOPG, new effects in silver films on GaAs and finally in deposited silver layers on MgO will be shown.

An outlook, the drawn conclusions and the appendix will complete this thesis.

I. Electrons in the bulk, at the surface, and in small particles

This chapter introduces the reader into fundamental facts in the context of the electronic behaviour in solids of different dimensions. For explanation concerning the crystal structure of those solids and of recent developments in producing different structures, see appendix 1.

a. Electronic wave functions in the bulk and at the surface

The knowledge of the electronic structure of solids is based on Bloch's theorem: As soon as atoms are brought together, the outer-shell electrons participate to form the chemical bond. The N-particle Schrödinger equation for the outer-shell electrons is of course too difficult to manage. It is replaced by a one-particle equation for an electron moving in an effective crystal potential. This effective potential contains the Coulomb attraction by the nuclei, the Coulomb repulsion by the core electrons (which are not participating in the chemical bonding), and the Coulomb repulsion between the outer shell electrons. Within this so-called single-electron approximation, each electron of mass m arising from the outer-shell is treated as independent particle. Associated with it is an Hamiltonian of the simple form:

$$\mathrm{H} = -\frac{\hbar^2}{2\mathrm{m}} \cdot \Delta + \mathrm{V}(\vec{\mathrm{r}}) \qquad \textbf{(I.1.1)}$$

which is involved in the time-independent Schrödinger equation

$$\mathrm{H}\psi = \mathrm{E}\psi \qquad \textbf{(I.1.2)}$$

where the potential energy term $V(\vec{r})$ can be calculated in principle using e.g. the Hartree-Fock approximation.

This single-electron approximation is a dramatic simplification of the manybody problem of an electronic system in a solid, but has produced

some useful results. The key element of the success of this approximation is that the effective potential carries the main symmetry of the problem, namely the translation symmetry:

$$\vec{\mathrm{T}} = \mathrm{n}_1 \cdot \vec{\mathrm{a}}_1 + \mathrm{n}_2 \cdot \vec{\mathrm{a}}_2 + \mathrm{n}_3 \cdot \vec{\mathrm{a}}_3 \qquad \textbf{(I.1.3)}$$

$$\mathrm{V}(\vec{\mathrm{r}} + \vec{\mathrm{T}}) = \mathrm{V}(\vec{\mathrm{r}}) \qquad \textbf{(I.1.4)}$$

With $\vec{\mathrm{a}}_{1,2,3}$ being the vectors of the primitive cell, and $\mathrm{n}_{1,2,3}$ are integers. This fact allows drawing very important conclusions without knowing the precise form of $V(\vec{r})$. Consequently, the Schrödinger equation, which describes the motion of the electron in this effective potential, is invariant with respect to any operation $\vec{\mathrm{T}}$. This puts some constraints on the eigenfunctions of the system. In fact, let now $\psi(\vec{r})$ be the wave function of an electron in an eigenstate. Then $\psi(\vec{r}+\vec{T})$ is also a solution belonging to the same eigenstate.

$$\psi(\vec{\mathrm{r}} + \vec{\mathrm{T}}) = \mathrm{const} \cdot \psi(\vec{\mathrm{r}}) \qquad \textbf{(I.1.5)}$$

Thus, up to a constant, the two wave functions $\psi(\vec{r})$ and $\psi(\vec{r}+\vec{T})$ are the same. The constant must be of absolute value 1. Otherwise, repeating the translation $\vec{T}$ would modify the electron density. The most general wave function, which fulfils the equation, $\psi(\vec{r}+\vec{T}) = const \cdot \psi(\vec{r})$ is (Bloch's theorem):

$$\begin{aligned} &\psi(\vec{\mathrm{r}}) = \mathrm{e}^{\mathrm{i}\vec{\mathrm{k}}\vec{\mathrm{r}}} \cdot \mathrm{u}_{\vec{\mathrm{k}}}(\vec{\mathrm{r}}) \\ &\mathrm{u}_{\vec{\mathrm{k}}}(\vec{\mathrm{r}} + \vec{\mathrm{T}}) = \mathrm{u}_{\vec{\mathrm{k}}}(\vec{\mathrm{r}}) \\ &\vec{\mathrm{k}} \in 1.\ \mathrm{Brillouin\ \ zone} \end{aligned} \qquad \textbf{(I.1.6)}$$

$\vec{k}$ is a label for the various eigenstates. A very important property of $\vec{k}$ is that, in order for the constant to be of absolute value 1, $\vec{k}$ must be a vector with real components. It is possible to show that $\vec{k}$ can be reduced into the first Brillouin zone. In general, to each value $\vec{k}$ there is an infinite number of different discrete eigenvalues $E(\vec{k})$. Such eigenvalues belong to the same $\vec{k}$-vector but to different bands. Additionally, simple calculations[10] lead to the result that a potential with translation symmetry produces a series of bands separated by gaps situated at the edge of the

[10] Consider a chain of atoms, which is a 1d-solid with lattice constants a and reciprocal lattice vectors $\mathrm{g}_\mathrm{n} = \mathrm{n} \cdot 2\pi/\mathrm{a},\ \mathrm{n} = 0, \pm 1, \pm 2, \ldots$

Then the solution of the Schrödinger equation may be determined by using the (Fourier-) ansatz: $\psi_k(x) = e^{ikx} \cdot \sum_{g_n} c_{g_n} e^{-ig_n x}$ and $V(x) = \sum_{g_n \neq 0} v_{g_n} e^{-ig_n x}$

Brillouin zone. The wave functions at band edges are standing waves. Within the gap, there are no possible eigenstates with real[11] $\vec{k}$.

By breaking the translation symmetry, as it is the situation for a semi-infinite solid (surface), it is possible to calculate that there are indeed possible eigenstates in the gap, so-called "surface states". Those appear due to the fact that here $\vec{k}$ can be taken as a complex vector to satisfy the Schrödinger equation in the gap[12]. The eigenfunctions interpolate between the two standing waves below and above the gap. The most important feature of the electron wave functions therein is that their amplitudes are exponentially vanishing toward the bulk. This means, the probability of the electrons being at or near the surface is almost 1. Concluding, the broken translation symmetry at the surface changes the electronic behaviour and there arise newly possible electronic eigenstates.

For 3d semi-infinite solids, the situation is geometrically more complicated, although many of the simple results obtained for the 1d chain can be generalised. There are a lot of bands and different types of surface states, which are either occupied or not, and thus incorporate the electronic system. A typical example is the complex band structure of copper, shown partially in Fig. 1.

One of the clearest and simplest derivations for the existence of surface states and so-called image states (localised in front of a surface) has been summarised in appendix 2.

[11] For $\vec{k} \in \mathbb{C}$ the solution of the Schrödinger equation would become exponentially large for $\vec{k} \to \infty$, and could not satisfy the translations symmetry

[12] The resulting band structure is called *the complex band structure*.

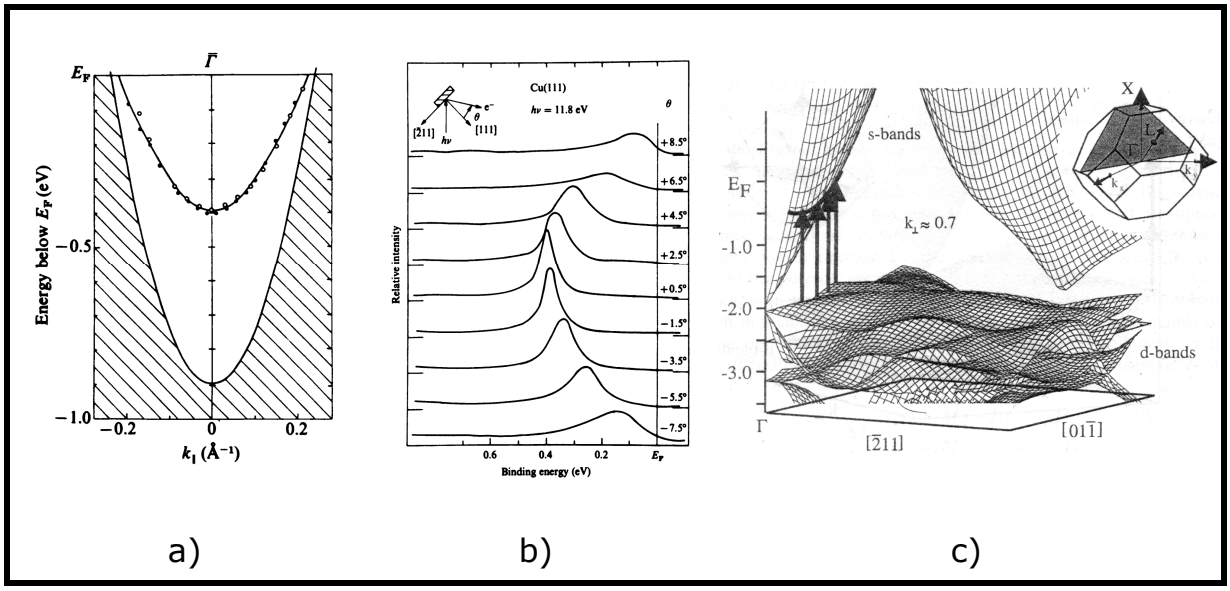

Fig. 1: Band structure and spectra of Cu(111). Data from [Kev83], pictures from [Zan88] (a, b) and [Ben98] (c)

a) Dispersion of the Cu(111) surface state with projection of the bulk bands.

b) Photoemission energy distribution curves from the surface state of Cu(111) at different angles.

c) A part of the bulk band structure of Cu(111) with possible excitation paths from d-bands into the s-bands.

b. The electronic system at a *clean* surface

Looking at the electronic system from a more macroscopic point of view, it is known, that because of Heisenberg's uncertainty principle, the density of the electrons may not drop to zero immediately at the surface. There is an exponentially vanishing probability to observe the bulk electrons in the vacuum. That phenomenon, called "spilling out" of the electron density, is the origin of the necessity to impose an additional work to bring an electron to a macroscopic distance from the solid. This energy is typically a few eV and is called *work function* ϕ.

For the further description, examine Fig. 2. Considering metals, a dipole layer may formally describe a surface electron density, with a positive charge[13] in the bulk in front of a negative surface charge[14] (Jellium model). That dipole layer is therefore build up, because the negative electron clouds neutralize the positive ions for a test charge in the vacuum.

[13] Build up by the positive atomic residue
[14] The negative electrons

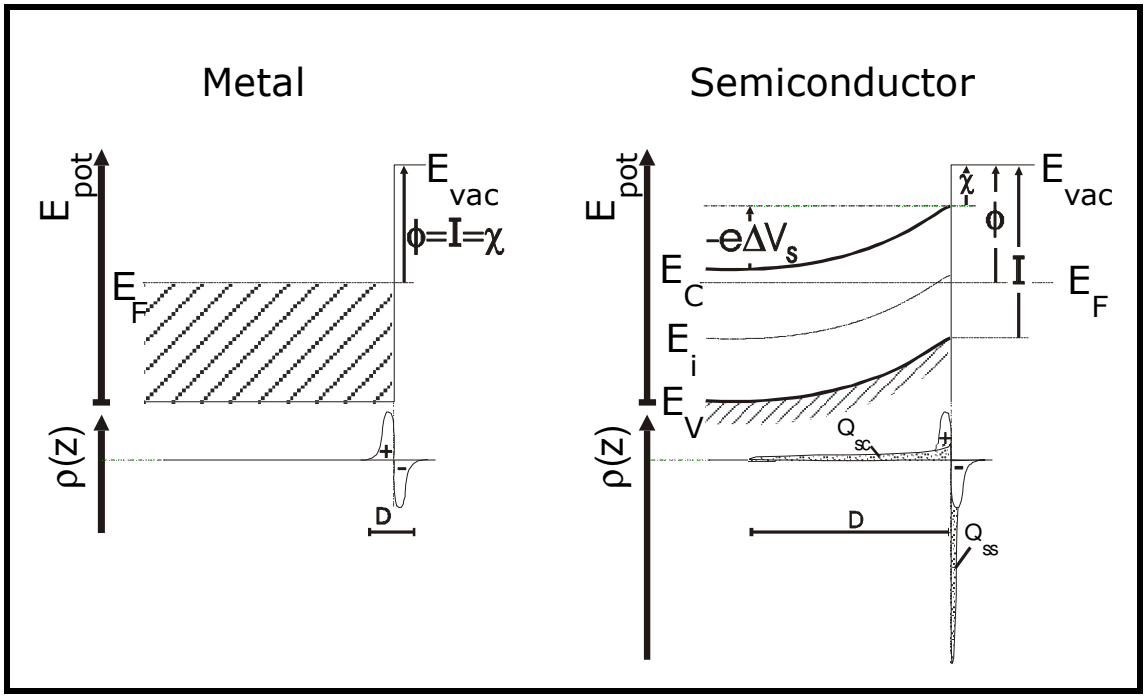

Fig. 2: Schematical comparison of surfaces at a metal and at a semiconductor. The Debye-length D could extend at semiconductors up to 1000nm (after [GZ94]). The variables are:

E_F: Fermi level	**E_{vac}: Vacuum level**	**$-e\Delta V_s$: Band bending**
E_C: Conduction band edge	**ϕ: Work function**	**Q_{SC}: Space charge**
E_V: Valence band edge	**I: Ionisation energy**	**Q_{SS}: Surface charge**
E_i: Intrinsic conduction level	**χ: Electron affinity**	**$\rho(z)$: Charge density**

There is also such a dipole layer at semiconductors. Even at clean semiconductor surfaces, an additional surface charge may raise caused by the localised charge in surface states (coming from e.g. defect states or from dangling bonds[15]). This is the normal case. Because of the extended radius of action of the raised electronic fields, caused by the lower amount of compensating, movable charge carriers, there arises at semiconductors a so-called band bending, with range D (=Debye-length). This is easy to understand by assuming, without loss of generality, the surface charge to be negative. Then there is a positive space charge in the bulk, which prevents the electrons to vanish from the solid. The bulk electrons "feel" therefore an increased barrier that has to be surmounted to transverse through the surface into the vacuum. This is equal to a band bending to higher energies. Accordingly, a positive surface charge produces a band bending to lower energies, because the electron emission is eased.

[15] Dangling bonds arises at surfaces of semiconductors (C, Si, Ge), where the overlap of their sp^3-hybridorbitals is not as strong as in the bulk, because of the different shapes of the orbitals at the surface.

In an electronic band structure, there are some specific energy levels, which are essential to describe many experiments, like e.g. photoemission[16]. Three of them are the following variables: *vacuum level* (E_{vac}), *Fermi level* (E_F) and *work function* (ϕ). E_F is the energy difference between the energy of all electrons and the energy of all electrons except one. The *vacuum level* describes the minimum energy that an electron must have, to take it out of the solid. These three variables are related one to the other by[17]:

$$\phi = E_{vac} - (E_N - E_{N-1}) = E_{vac} - E_F \qquad \textbf{(I.1.7)}$$

For a semiconductor more vocabulary is needed, because of the absence of continuous electronic state bands in the region of the Fermi level. In addition to the terms of the metal case, one uses the *band gap energy* (E_g), the *electron affinity* (χ) as the distance between conduction band and vacuum level, the *ionisation energy* (I) as the distance between valence band and vacuum level, the *band bending* ($e\Delta V_s$), the *valence band edge* (E_V) and the *conduction band edge* (E_C). So, the *work function* at semiconductors is defined as:

$$\begin{aligned} \phi &= E_{vac} - E_F \\ &= \chi + (E_C - E_F) - e\Delta V_s \\ &= I - (E_F - E_V) - e\Delta V_s \end{aligned} \qquad \textbf{(I.1.8)}$$

An interesting property of clean semiconductors, with unfilled electronic states at the surface caused by dangling bonds (or from any other effects), is the phenomenon of *Fermi level pinning*, i.e. the independence of the sample work function to bulk doping. The Fermi level is pinned because the density of surface states is much larger than the density of bulk donor/acceptor states. The Fermi level at the surface needs not to change very much to accommodate any charge flow needed to equilibrate the surface to the bulk. This happens e.g. at Si (silicon) and at GaAs.

The details explained for a semiconductor, remain the same also for an insulator. There may also for example occur a band bending, and there could also arise any surface state in the vicinity of the Fermi level, mainly when the surface undergoes a reconstruction. However, in the gap of an insulator there are not only states at the Fermi level. It is a known fact, that an insulator normally shows a few more states in the gap, coming from so-called F-centres. They arise because of vacancies of negative ions in the bulk or at the surface, or because of point defects[18]. Those F-centres concentrate bound electrons or holes and produce therefore

[16] See also the legend to Fig. 2

[17] E_N is the whole energy, accumulated by all N electrons

[18] A point defect is e.g. a substitution of an atom by another element. Other examples are explained on the pages 129ff

localised states in the gap. And of course those states may be excited by electromagnetic waves. That is the reason for their name "F-centres" from the German word *Farbe* (English: colour); the insulators show a specific colour, after being optically excited. One finds different F-centres for different insulators. They build energy bands of up to about 1eV size, and they may lie anywhere in the gap. Some examples will illustrate that: F-centres have been found at the MgO-surface at 2.3eV above valence band[19], at 1eV above valence band and at the Fermi level[20]. In Appendix 5 both, the absorption and the emission of radiation containing F-centres are depicted.

The F-centres arise at the doping process. One of the most important application of F-centres are laser-media, like Ti:sapphire. Many radiative transitions in F-centre crystals have already been used for laser emission in the red and infrared region (from 620nm till 3000nm). The generation of picosecond pulses by F-centre lasers has also been reported[21], and the femtosecond pulses are known to exist.

c. Adsorbates[22] on the surface

What happens to the surface electronic system if any adatoms are deposited on it?

It is quite clear, that an adlayer, which fills (i.e. hybridises) the dangling bonds of a cut solid, will change the electronic compound on the surface. But also "neutral" atoms on a "neutral" surface do change it, because of moving charge centres. The reason for a change is of course to strive for lowering the total energy.

In surface physics, one compares the *binding energies* E_b of the adatoms on the surface, and distinguishes between the *physisorption* class ($E_b < 0.5$eV/atom = 50kJ/mol), and the *chemisorption* ($E_b > 0.5$eV/atom) one.

At *physisorption*, the geometric and electronic structure of the adatoms and of the surface stay mainly unchanged. The physical reasons for physisorption are interactions, between adsorbed particles and substrate atoms, like those between molecules in the gas phase. There, attractive and repulsive forces are known, which result in the Lennard-Jones-Potential. The attractive forces come from van-der-Waals interactions, whereas the repulsive force is a consequence of the Pauli principle. At surfaces, there are interactions of adatoms with many underlying atoms,

[19] [HDZ80]
[20] [SSC00]
[21] [BFG90]
[22] The term "adsorbate" does not state here for unintended "dirt", like contamination in bad vacuums, but mainly for the controlled deposited coverage.

which result in a sum of all those potentials. On metals, the interaction with the Fermi sea leads to additional attractive force. All those forces often cause a relaxation of the substrate surface, which obviously brings a change in the charge structure.

In contrast to the physisorption, the *chemisorption* of particles at the substrate surface leads to dramatical changes in the electronic structure of both the adatoms and the surface. The adsorbed atoms become bound via chemical bonding to the atoms of the surface. This strong attraction leads in some cases to the enhanced dissociation of fractions of deposited molecule compounds.

An adsorbate lying on a substrate implies, among others, the following two important consequences:

1) Change of the substrate's work function

The induced adsorbate dipole[23] changes the substrate's work function by affecting the electron affinity: $\Delta\phi=\Delta\chi$. This change is directly correlated to the amount of adatoms covered. So, it leads to the often-used method, to lower the work function by controlled deposition of alkali atoms (mostly Cs or Na), see Fig. 3. In photoelectron spectroscopy this feature is a standard way to get access to energetically lower lying electrons, without altering the surface heavily.

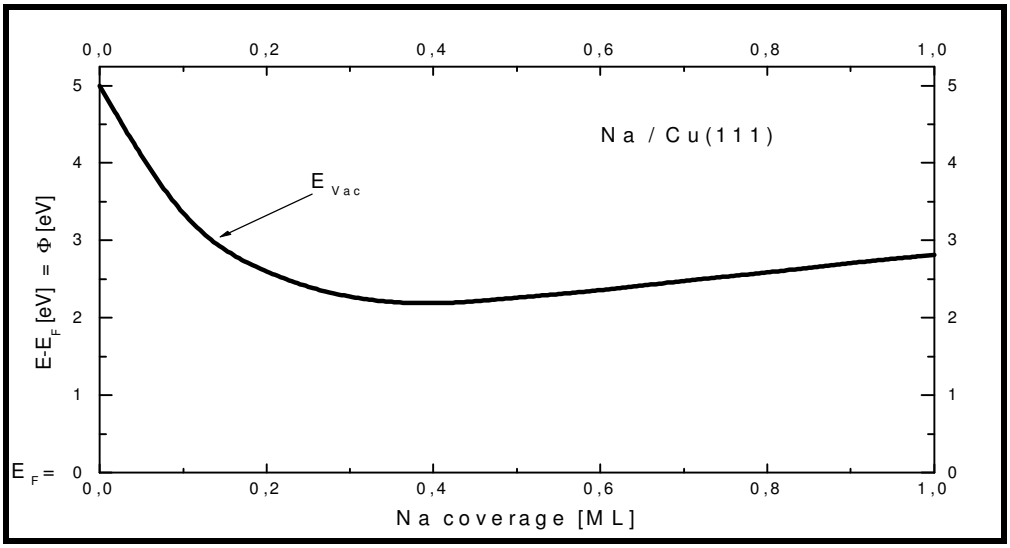

Fig. 3: Change of the work function of Cu(111) by deposition of Na. It is possible to lower the work function by about 3eV using only a coverage of 0.3ML Na. From [FSFS94]

[23] Exactly spoken, its component perpendicular to the surface

2) Induced Schottky barrier

On a semiconductor, which is covered with small amount of adatoms, there is - beside the self-induced band bending of a clean surface (explained above) - an additional band bending $e\Delta V_s$ to higher (lower) energies, because of the charge transfer to (from) the acceptor (donor) adsorbate from (to) the surface, which produces a space charge on the interface, and hinders (simplifies) the electron emission. The density of states needed to form such a junction can be small, on the order of $10^{11}cm^{-2}$. Additionally, a negligible effect, influencing the work function through the diffusion of doping atoms from adsorbate into the bulk and therefore a change of $\Delta(E_F-E_V)$ should also be mentioned here. For a complete sketch of the influence to a photoemission spectrum, see Fig. 17 Seite 48.

Because of the high importance of the mentioned *junction*, not only to those experiments described in this work, but also to the physics of MOSFETs (Metal-Oxide-Semiconductor-Field-Effect-Transistor), it is necessary to take a more precise view on it. Without loss of generality, the following will concern about the applied case: metal on p-type semiconductor. Other systems with n-type and/or different work functions behave correspondingly.

The following explanation relates to Fig. 4. Right after deposition of adatoms, and before thermodynamical equilibrium the system looks like the situation in Fig. 4a). There are a (measurable) metal work function ϕ_M, and a (measurable) electron affinity χ of the semiconductor.

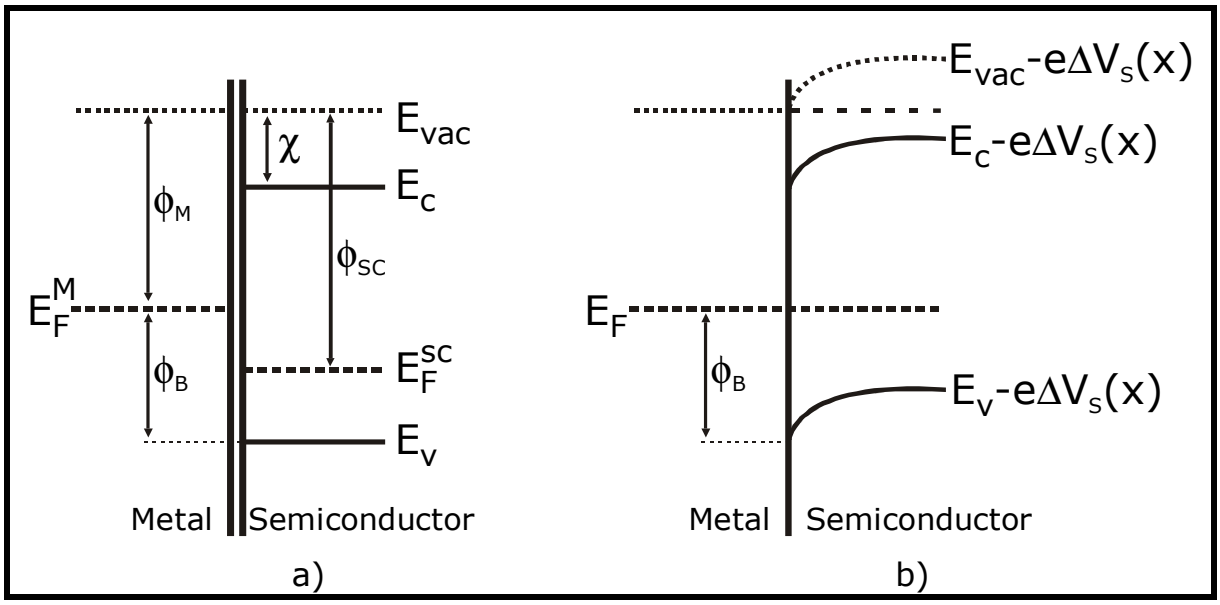

Fig. 4: The spatial behaviour of the metal-semiconductor Schottky-junction
a) Before thermodynamical equilibrium
b) After: the Schottky contact. All Energies are related to the vacuum level.

Usually, a new energy ϕ_B of the semiconductor holes, which move into the metal, is defined here. It is called *Schottky-barrier* (typically some tenth of eV). By moving electrons from the metal to the semiconductor, one finally gets the thermodynamical equilibrium, seen in Fig. 4b). Thereby, a space charge on the interface is being build, which is connected to a spatial changing electrostatic potential $\Delta V_S(x)$. The energy levels of the semiconductor get a shift of $-e\Delta V_S(x)$, the *band bending*. This leads to a contact potential (defined the same way as with two metals):

$$U_K = [\Delta V_S(\infty)-\Delta V_S(0)] = \frac{1}{e}\left[E_F^{SC} - E_F^M\right]. \qquad \textbf{(I.1.9)}$$

For p-type semiconductors:

if $E_F^{SC} > E_F^M$ (i.e. $\phi_{SC} < \phi_M$) it is called *ohmic contact* $\Rightarrow$ upwards band bending
if $E_F^{SC} < E_F^M$: it is called *Schottky contact* $\Rightarrow$ downwards band bending

It is vice versa for n-type semiconductors, where ϕ_B is taken as ϕ-χ.

With means of the Poisson equation one gets the spatial width of the barrier (= depth of the band bending = Debye-length):

$$x_B = \sqrt{\frac{2\varepsilon\varepsilon_0}{eN_D}\left|\Delta V_s(0)\right|} \qquad \textbf{(I.1.10)}$$

Taking the values of the used p-type GaAs:

- dielectric function $\varepsilon = 10.9$
- electrical field constant $\varepsilon_0 = 10^7/4\pi c^2$
- number of doping atoms $N_D = 10^{19}cm^{-3}$
- band bending $e\Delta V_S(0) = 0.1 - 0.5eV$

Finally the *Debye-length* becomes: $x_B = 5\text{-}10nm$.

The contact of an *insulator* to a *semiconductor* leads to bended bands both at the semiconductor and at the insulator side. The strength is higher at the semiconductor, but the Debye-length is longer at the insulator part. It is even possible to consider the vacuum as an insulator, which produces the same band bending at the semiconductor as if the vacuum were an insulator.

d. Dielectric properties of electrons in solids

In this section, a brief discussion will show the interaction of light with a medium and will be followed by the classical dispersion theory, which leads to the *Lorentz model* and to the *Drude model*. It delivers the basics for the ensuing plasmon theory.

1) The interaction of light with a medium

In order to study the interaction of light with a medium, the medium is taken as isotropic, so that there is no spatial variation in the dielectric function ε.

Starting with the well-known Maxwell equations inclusive the material equations ($\vec{D} = \varepsilon\vec{E}$ and $\vec{B} = \mu\vec{H}$) for the dielectric displacement D and the magnetic field strength H. ε is the dielectric function, μ is the magnetic permeability. With those equations and the conductivity σ coming from Ohm's law ($\vec{J} = \sigma\vec{E}$) for free electrons, the *wave equation* for the plane wave of the impinging electro-magnetic (e. m.) field propagating in an energy-absorbing medium can be written down:

$$\nabla^2 \vec{E} = \frac{\varepsilon\mu}{c^2}\frac{\partial^2 \vec{E}}{\partial t^2} + \frac{4\pi\sigma\mu}{c^2}\frac{\partial \vec{E}}{\partial t} \qquad \textbf{(I.1.11)}$$

The conductivity σ should be called the optical conductivity, because the energy absorption is arising from transitions accompanying photon absorption. For sufficiently long wavelengths (far infrared), the transverse optical conductivity approaches the ordinary dc electric conductivity (for isotropic materials).

Now, one considers the *propagation of a single e. m. plane wave* within an isotropic medium. Thus the electric field is:

$$\vec{E} = \vec{E}_0 \cdot e^{i\hat{q}r - i\omega t} \qquad \textbf{(I.1.12)}$$

where the direction E_0 of the electric field is perpendicular to the wave vector $\hat{q}$. In order to describe energy dissipation of the wave, $\hat{q}$ should be taken as a complex number. The combination of both equations above ((I.1.11) and (I.1.12)) leads to the relation:

$$\hat{q}^2 = \mu \frac{\omega^2}{c^2}\left(\varepsilon + i\frac{4\pi\sigma}{\omega}\right) \qquad \textbf{(I.1.13)}$$

A complex refractive index $\hat{n}$ is to be defined such that

$$\begin{aligned} \hat{q} &= \frac{\omega}{c}\hat{n} \\ &= \frac{\omega}{c}(n + ik) \end{aligned} \qquad \textbf{(I.1.14)}$$

where n is the (ordinary) refractive index and k is the extinction coefficient. It follows that (I.1.12) can be written as

$$\vec{E} = \vec{E}_0 \cdot e^{-\frac{\omega k}{c}\frac{\hat{q}\vec{r}}{|\hat{q}|}} \cdot e^{i\frac{\omega n}{c}\frac{\hat{q}\vec{r}}{|\hat{q}|} - \omega t} \qquad \textbf{(I.1.15)}$$

The first exponential factor in (I.1.15) describes the attenuation of the wave amplitude with distance. An absorption coefficient thereby, which describes the fractional decrease in intensity I with distance, is defined as

$$\alpha = -\frac{1}{I}\frac{\partial I}{\partial r} \qquad \textbf{(I.1.16)}$$

with I the intensity of the e. m. wave. Since the intensity is proportional to the square of the wave amplitude E_0, one finds with (I.1.15) $\alpha = 2\omega k/c = 4\pi k/\lambda$, where λ is the wavelength of the light in vacuum[24].

The second exponential factor in (I.1.15) describes a wave travelling with phase velocity c/n, hence the earlier identification of n as the refractive index.

One defines a complex dielectric function $\hat{\varepsilon} = \varepsilon_1 + i\varepsilon_2$, where ε_1 is the old (ordinary) dielectric function ε that appears in the usual versions of the Maxwell equations when the properties of the medium are included. Then equations (I.1.13) and (I.1.14) can be used to obtain expressions for ε_1

[24] Using the absorption coefficient α, it is easy to calculate the penetration depth d (= extinction length) of light in a material. One assumes an exponential attenuation of the light intensity with the distance x.

$$I(x) = I_0 \cdot e^{-\alpha \cdot x}$$

From the condition, that the penetration depth d should decrease to $I(d)=1/e \cdot I_o$ the result is straightforward (note: k is the absorption coefficient of the complex refractive index)

$$\boxed{d \approx 0.08 \cdot \lambda/k}$$

with d and λ both in [nm].

and ε_2 in terms of n, k and σ

$$\begin{aligned} \varepsilon_1 &= (n^2 - k^2)/\mu \\ \varepsilon_2 &= 2nk/\mu = 4\pi\sigma/\omega \end{aligned} \qquad \textbf{(I.1.17)}$$

Those equations show that ε_1 and ε_2 are not independent quantities. They are (as well as n and k) related in a quite fundamental way by means of the Kramers-Kronig dispersion relations.

2) The classical dispersion theory

In this section, a simple but helpful phenomenological approach will be developed, in order to reach an understanding of the optical properties of solids. The classical dispersion theory explained by *Lorentz* and *Drude* will be described. This approach is largely 'ad hoc', but still a useful starting point for developing a feeling on electrodynamic response of metals and insulators.

The *Lorentz model* considers the situation of electrons bound to the nucleus of the atom (like a small mass bound to a large mass by a spring, see Fig. 5). The following description assumes therefore an *insulator* with electrons bound to their nucleus. The situation of a *metal* is analysed later.

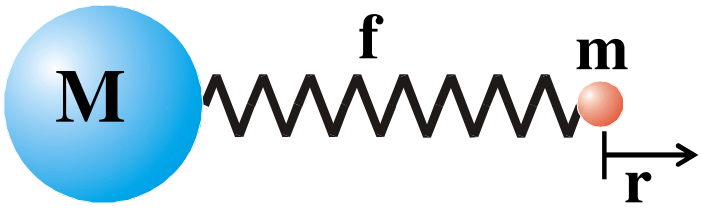

Fig. 5: A simple model for an electron (mass m), bound to a nucleus (mass M >> m). Within the Lorentz model, the electrons are taken as bound to the nucleus of the atom via an attractive force f (first-order approximation).

The motion of such a bound electron is then described by

$$m\ddot{\mathbf{r}} + m\Gamma\dot{\mathbf{r}} + m\omega_0^2\mathbf{r} = -e\mathbf{E}_{loc} \qquad \textbf{(I.1.18)}$$

where m is the electronic mass, e is the magnitude of electronic charge. The field E_{loc} is the local field acting on the electron as a driving force, and can be taken to vary in time as exp(-iωt). The second term represents viscous damping and provides for an energy loss mechanism. The third term ($m\omega_0^2 r$) is a Hooke's law restoring force, where $\omega_0^2 := f/m$.

Note: this Lorentz model does only consider electrons in insulators, but not in metals, because, there is not such a strong attractive force at metals.

Taking the ansatz $\mathbf{r}(t) = \mathbf{A}\cdot\exp(-i\omega t)$, then the (complex) solution to equation (I.1.18) is

$$\mathbf{r} = \frac{-e\mathbf{E}_{loc}}{m}\frac{1}{(\omega_0^2-\omega^2)-i\Gamma\omega} \qquad \textbf{(I.1.19)}$$

One meaning of (the real part of) this result is the following: The only time-dependence appears in the term of $\mathbf{E}_{loc}$, i.e. the electron oscillates around the nucleus with the frequency ω of the impinging e. m. wave. The amplitude of this oscillation is small, because of the large denominator, i.e. the electron is localised (bound). The stronger the force f is, or the larger the frequency ω of the e. m. wave is, the smaller is the amplitude of the oscillation.

The induced dipole moment ($\mathbf{p} = -e\cdot\mathbf{r}$) is:

$$\mathbf{p} = -e\cdot\mathbf{r} = \frac{e^2\mathbf{E}_{loc}}{m}\frac{1}{(\omega_0^2-\omega^2)-i\Gamma\omega} \qquad \textbf{(I.1.20)}$$

One now assumes that the displacement $|\mathbf{r}|$ is sufficiently small that a linear relationship exists between $\mathbf{p}$ and $\mathbf{E}_{loc}$, namely $\mathbf{p} = \alpha(\omega)\cdot\mathbf{E}_{loc}$, where $\alpha(\omega)$ is the frequency-dependent atomic polarizability.

If there are N atoms per unit volume, the macroscopic polarisation is:

$$\mathbf{P} = N < \mathbf{p} > = N\hat{\alpha}\left\langle \mathbf{E}_{loc} \right\rangle = \chi_e \mathbf{E} \qquad \textbf{(I.1.21)}$$

In eq. (I.1.21) the allowed[25] assumption $<\mathbf{E}_{loc}> = \mathbf{E}$ between the microscopic and the macroscopic field was made.

With $\mathbf{P}=\chi\mathbf{E}$, $\mathbf{D}=\mathbf{E}+4\pi\mathbf{P}$ and $\mathbf{D}=\varepsilon\mathbf{E}$, one gets the complex notation $\hat{\varepsilon} = 1 + 4\pi N\hat{\alpha}$ and therefore the *complex dielectric function* in the *Lorentz model*:

$$\hat{\varepsilon} \;=\; \varepsilon_1 + i\cdot\varepsilon_2 \;=\; 1 + \frac{4\pi N e^2}{m}\frac{1}{(\omega_0^2 - \omega^2) - i\Gamma\omega} \qquad \textbf{(I.1.22)}$$

If N_j is the density of electrons bound with resonance frequency ω_j, then eq. (I.1.22) can be generalised in the following way:

$$\hat{\varepsilon} \;=\; 1 + \frac{4\pi e^2}{m}\sum_j \frac{N_j}{(\omega_j^2 - \omega^2) - i\Gamma_j\omega} \qquad \textbf{(I.1.23)}$$

This eq. (I.1.23) has the same form[26] as the quantum mechanical formula for the dielectric function, built by optical electron transitions between two atomic states, which are separated by $\Delta E_j = \hbar\omega_j$. But the meanings of some corresponding terms are quite different. For example, in eq. (I.1.23) ω_j is the resonance frequency of a bound electron, and not a transition between two atomic states. Nevertheless, it is surprising that two different models of two different systems correspond so well.

The deduced dielectric function expresses the behaviour of the optical excitation of electrons in an insulator. It is worthwhile to write down the two components of the dielectric function in eq. (I.1.22) separately:

$$\begin{aligned} \varepsilon_1 &= 1 + \frac{4\pi N e^2}{m}\frac{(\omega_0^2 - \omega^2)}{(\omega_0^2 - \omega^2)^2 + \Gamma^2\omega^2} \\ \varepsilon_2 &= \frac{4\pi N e^2}{m}\frac{\Gamma\omega}{(\omega_0^2 - \omega^2)^2 + \Gamma^2\omega^2} \end{aligned} \qquad \textbf{(I.1.24)}$$

By means of those ε_1 and ε_2, it is possible to determine easily the *complex refractive index* $\hat{n}$, via $\varepsilon_1 = n^2 - k^2$ and $\varepsilon_2 = 2nk$:

---

[25] It has been shown in [Deg96] that this assumption preserves the essential features of the description of the optical properties.

[26] [Jac83]

$$\begin{aligned} n &= \sqrt{\frac{1}{2}\left[\sqrt{\varepsilon_1^2+\varepsilon_2^2}+\varepsilon_1\right]} \\ k &= \sqrt{\frac{1}{2}\left[\sqrt{\varepsilon_1^2+\varepsilon_2^2}-\varepsilon_1\right]} \end{aligned} \qquad \textbf{(I.1.25)}$$

And finally, one also gets the frequency dependence of the *reflectivity* $R(\omega)$, by using the Fresnel equations for the reflectivity in normal incidence[27]:

$$R = \frac{(1-n)^2+k^2}{(1+n)^2+k^2} \qquad \textbf{(I.1.26)}$$

A model calculation for ε_1, ε_2, n, k and R is depicted in the *left parts* of Fig. 6 - Fig. 8, pages 23ff. Thereby, the resonance frequency ω_0 has been set arbitrarily to $\hbar\omega_0$=4eV. This value could be considered as a band gap energy of the illustrated insulator, because there, both frequencies ω_0 and ω match together, and the energy transfer is optimal.

Four principal regions may be recognised easily in those figures (from small value of $\hbar\omega$ to higher frequencies):

Region I: $\omega << \omega_0$, $\varepsilon_2 = 2nk \approx 0$, and $\varepsilon_1 = n^2-k^2 > 1$.
One may conclude, that $k\approx 0$, $n>1$ and $\varepsilon_1=n^2$.
Thus, region I is characterised by nearly no absorption ($k\approx 0$), a small reflectivity ($R\approx 0$) and *high transparency* (1-R),

Region II: $\omega \approx \omega_0$, $\varepsilon_2 \approx$ max., $\varepsilon_1^2+\varepsilon_2^2 >> 0$, therefore $k >> 0$.
It is characterised by *strong absorption*.

Region III: $\omega >> \omega_0$, $\varepsilon_1 < 0$, $\varepsilon_2 \approx 0$, therefore $n \approx 0$, $k \approx \sqrt{\varepsilon_1}$, $R \approx 1$.
The electrons of the insulator respond as if they were free electrons. This is because the photon energy is much larger than the binding energy of the electrons. The insulator thus has a metallic *reflectance*. Then, for $\Gamma \to 0$ it follows $R(\omega)\to 100\%$ (total reflection region)

Region IV: ε_1 small and > 0
The system is again transparent

[27] See e.g. [Deg96]

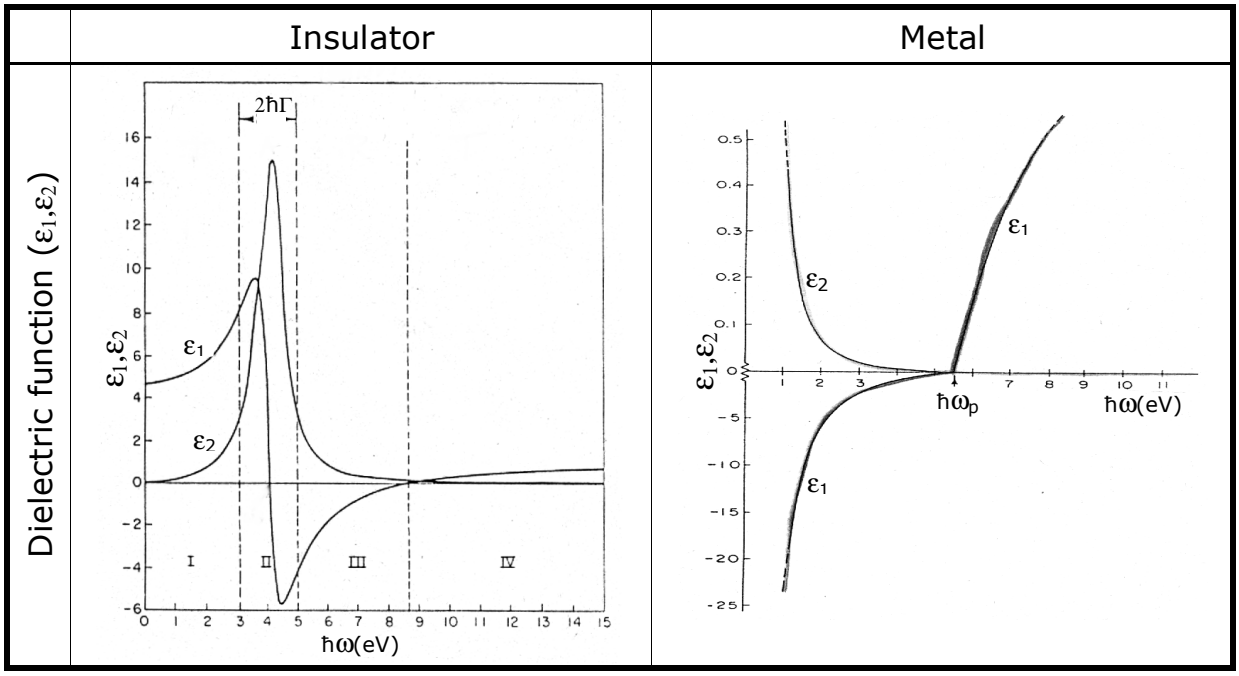

Fig. 6: Schematic curves for the *dielectric function*. Drawings from [Deg96].

Left: for an insulator, calculated with means of the Lorentz model using $\hbar\omega_0$=4eV, $\hbar\Gamma$=1eV and $4\pi Ne^2/m$=60.

Right: for a metal with means of the Drude model, using $\hbar\omega_p$=5.5eV and $\hbar\Gamma$=0.02.

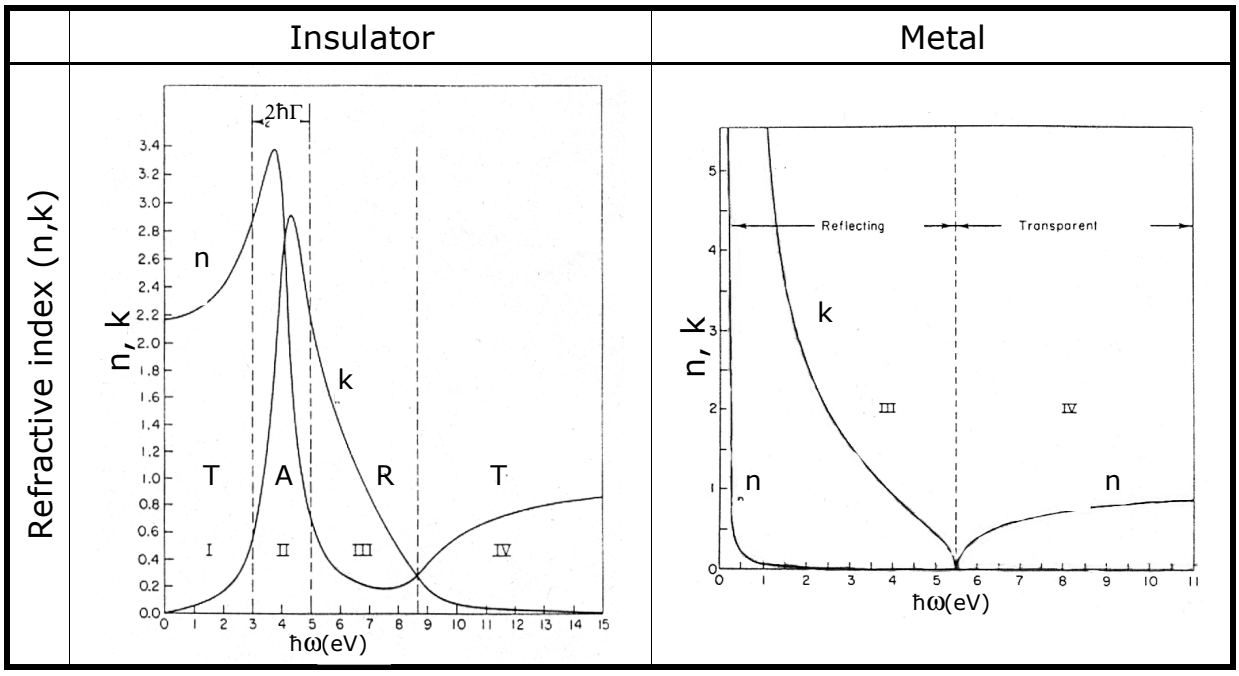

Fig. 7: Schematic curves for the *refractive index*. Drawings from [Deg96].

Left: for an insulator, calculated with means of the Lorentz model using $\hbar\omega_0$=4eV, $\hbar\Gamma$=1eV and $4\pi Ne^2/m$=60.

Right: for a metal with means of the Drude model, using $\hbar\omega_p$=5.5eV and $\hbar\Gamma$=0.02.

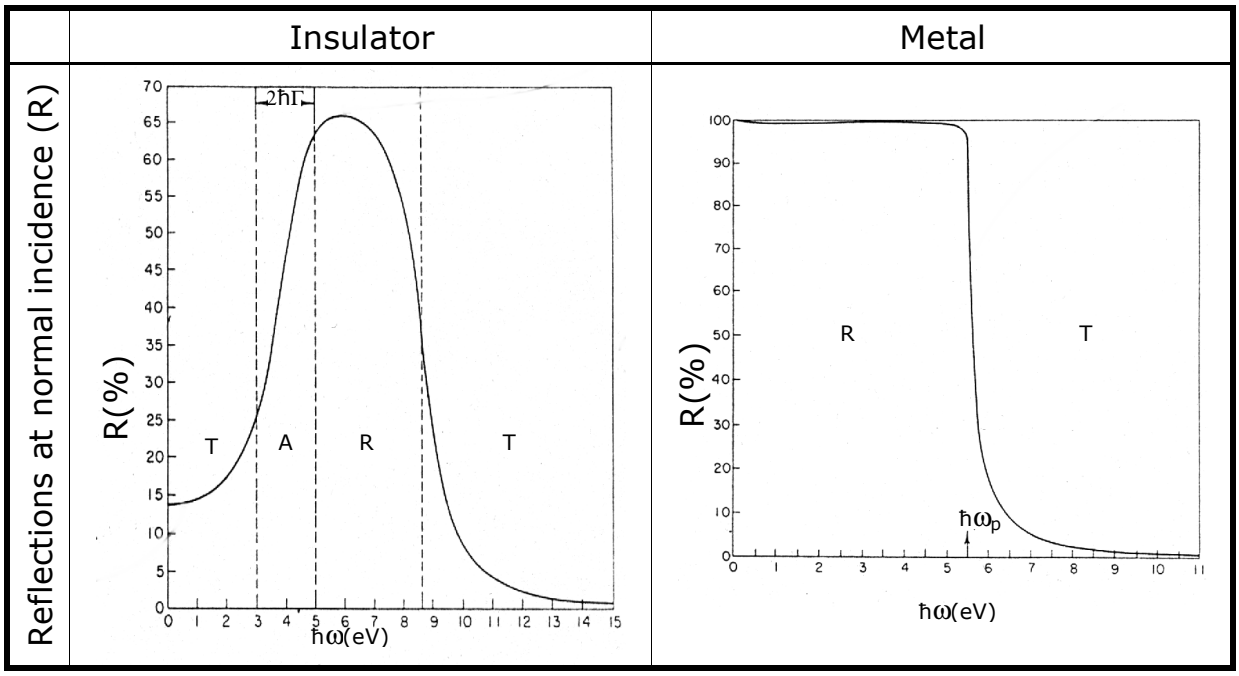

Fig. 8: Schematic curves for the *reflectivity at normal incidence*. Drawings from [Deg96].

Left: for an insulator, calculated with means of the Lorentz model using ħω0=4eV, ħΓ=1eV and $4\pi Ne^2/m=60$.

Right: for a metal with means of the Drude model, using ħωp=5.5eV and ħΓ=0.02.

Now the *case of a metal* is considered (*right parts* of Fig. 6 - Fig. 8). The conduction electrons of a metal are not bound (f = 0 in Fig. 5). Furthermore, because the wave function for a free electron is distributed fairly uniformly throughout the metal, the field acting on the electrons is just the average field. Thus, there is no need to invoke corrections for the local field. Taking then $\omega_0 = 0$ in the *Lorentz model* (eq. (I.1.18)ff), one obtains the solution to eq. (I.1.18) as:

$$\mathbf{r} = -\frac{-e\mathbf{E}_{loc}}{m}\frac{1}{\omega^2 + i\Gamma\omega} \qquad \textbf{(I.1.27)}$$

In accordance to the analysis above, and considering the real part of this solution. Again, the only time-dependent factor is $\mathbf{E}_{loc}$. There is no "binding force", and therefore the electrons in a metal act (in this simple model) as free mass, following exactly the oscillating e. m. wave, with frequency ω. The amplitude of the electron's oscillation diverges for small ω, and vanishes for large frequencies.

The *dielectric function* for a *metal* in the *Drude model* becomes:

$$\varepsilon_1 = 1 - \frac{4\pi Ne^2}{m}\frac{1}{(\omega^2+\Gamma^2)}$$
$$\varepsilon_2 = \frac{4\pi Ne^2}{m}\frac{\Gamma}{\omega(\omega^2+\Gamma^2)} \qquad \textbf{(I.1.28)}$$

The origin of the viscous damping term for a free-electron metal is the scattering of electrons associated with electrical resistivity or with electron-electron collisions (Drude damping).

As the *Drude model* is obtained directly from the *Lorentz model* simply by setting $\omega_0 = 0$, the optical properties of a free-electron metal should resemble those for an insulator at frequencies higher than ω_0. The *right parts* of Fig. 6 - Fig. 8 display the *dielectric function* ($\hat{\varepsilon}$), the *optical constants* (n, k), and the *reflectivity* (R) for a Drude model metal. For such an ideal free electron metal two regimes may be defined[28], one at frequencies[29] $\omega<\omega_p$ (i.e. below the plasma frequency for which $\varepsilon_1(\omega_p)=0$, see next section), where $R(\omega)$ approaches unity, and one at $\omega>\omega_p$, where $R(\omega)$ decreases with increasing frequency and the metal is transparent.

In this simple model, the microscopic explanation for the reflectivity of a metal is the following: for frequencies up to a sharp limit (ω_p), the electrons may follow the impinging e. m. wave; they become excited, and oscillate with the same frequency. The excited electrons emit photons of the same energy. The accumulation of all photons builds the reflected beam. For higher frequencies the electrons may not follow, may therefore not be excited, and thus the metal becomes transparent for this e. m. wave.

But, what happens exactly at ω_p?

To answer this question one can think of a kind of resonance, describing the ability of the electrons to become oscillated with the impinging e.m. wave. At low frequencies $\omega<\omega_p$ the electrons can follow the oscillation of the e.m. wave, and the oscillation radius become increasingly stronger the closer ω and ω_p are. For $\omega>\omega_p$ the oscillation is too fast, the electrons can not follow, and the crystal becomes transparent. At $\omega=\omega_p$ the amplitude **r** would diverge. However, it is evident that in a crystal with infinity dimensions, an electron oscillation of infinity extension[30] will collapse the system in any way. And this could be seen at $\omega=\omega_p$: $\varepsilon_1=0$, k=0, n=0,

---

[28] Up to now, this definition is quite arbitrary. The meaning of this choice will become clear later.

[29] $\omega_p^2 := \frac{4\pi Ne^2}{m}$ (see later)

[30] This means: divergence

R drops fast. Of course the physical reason for such a cut-off frequency is coming from the given formulae $\mathbf{D}=\mathbf{E}+4\pi\mathbf{P}$ and $\mathbf{P}=\chi\mathbf{E}$, which set up (in accordance to the insulator case) a macroscopic polarisation of the electronic system. This macroscopic polarisation can not be hold at a diverging electron moving, and collapse therefore at $\omega=\omega_p$.

It is quite impressive how accurate the Drude model is. Such a simple deviation leads to results comparable to real metals, as shown in Fig. 9a) for silver.

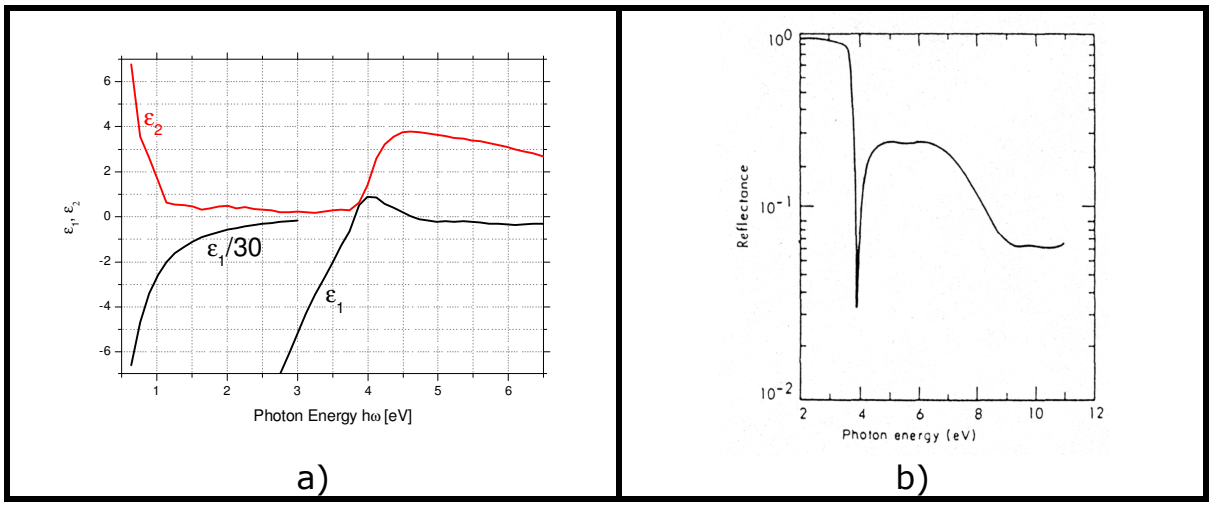

Fig. 9: a) The dielectric function of silver. Adopted from [JC72]
b) The reflectance of silver. From [Deg96]

Fig. 9b) shows the real reflectance of silver. At 3.9eV, the reflectance drops sharply, then rises almost immediately. The reflectance well into the vacuum-ultraviolet region is characteristic for interband transitions spread over a wide spectral region. The sharp decrease in reflectance at 3.9eV identifies (seemingly) the plasma frequency[31], which corresponds to the zero crossing of $\varepsilon_1(\omega)$ (with $d\varepsilon_1/d\omega>0$). However, the reason $\varepsilon_1(\omega)$ passes through zero at $\hbar\omega=3.9$eV, and not at $\hbar\omega=9.2$eV (i.e. the *true or unscreened plasma frequency*) as calculated for silver using a free-electron model, is because of the influence of the d states which lie 4eV below the Fermi energy in silver. The effect of the d states is to make a positive contribution[32] to $\varepsilon_1(\omega)$ and so shift to lower energies the point at which $\varepsilon_1(\omega)$ passes through zero. Almost immediately, there is a rise in $\varepsilon_2(\omega)$ because of real transitions from d states.

[31] The considered deduction (Drude model) of the plasma frequency is too simple. In real metals, bulk-plasmons may not be excited by divergenceless transverse e. m. waves. This means: the plasma frequency, where the reflectance drops, seems to be calculated by the equation in the footnote 29, but instead, in real metals the drop in reflectance at a specific frequency is generated by interband transitions. Because of the fact, that a plasma oscillation would give the same drop in reflectance, the cut-off frequency is often called plasma frequency.

[32] Via interband transitions

The *screened plasma frequency* can be thought of as a collective oscillation of the conductive electrons (s electrons) screened by the bound d electrons. Thus, there are then contributions like in an insulator (interband transitions), and contributions like in a metal (intraband transitions).

e. The concept of plasmons

The meaning of plasmons has already been used a few times in the last section. Now, the concept of plasmons will be described in more details.

A plasma is a medium with the same density of positive and negative charges. From a phenomenological point of view, one can look at the conduction electrons as a negative collection in front of the positive ions. The net charge is zero, because of a uniform background density of positive ions. Now, imagine that a region of electron charge has been uniformly translated by a distance δx without disturbing the remainder of the system (i.e. the ions). This leaves a region of thickness δx having a net positive charge density and creates another region of net negative charge density. Because of the force between the two regions of unbalanced charge, they will be attracted towards each other. In the absence of a damping mechanism, there will be an overshoot leading to the preview situation, but with the charges reversed. The system will continue to oscillate in this manner at a characteristic frequency known as the *plasma frequency*. The oscillations are called the (longitudinal) plasma oscillations, and their energy quanta are called *plasmons*. For example, a collective behaviour of the free-electron gas may be taken as a plasmon. Typical values for metals (bulk) lie in between 3eV and 20eV; this shows, that plasmons cannot be excited by thermal excitation.

In addition to the section above, the plasma frequency may be defined as the frequency at which[33] $\varepsilon_1(\omega)=0$. Then - in the case of free electrons only, and assuming $\omega \gg \Gamma$ – one obtains from (I.1.28):

$$\begin{aligned} 0 &= \varepsilon_1(\omega_p) \\ &= 1-\frac{4\pi Ne^2}{m}\frac{1}{\omega^2} \\ &= 1-\frac{\omega_p^2}{\omega^2} \end{aligned} \qquad \textbf{(I.1.29)}$$

with the plasma frequency

$$\omega_p^2 = \frac{4\pi Ne^2}{m} \qquad \textbf{(I.1.30)}$$

On first sight, it is astonishing, that there is a relation between the optical parameter ε_1 and the plasma frequency ω_p, although a plasma may not be excited in bulk material by (transversal) e. m. waves. As mentioned

[33] This definition has its origin in the fact, that with $D=\varepsilon_0\hat{\varepsilon}E$ and $\varepsilon_1=0$ there is no moveable dielectric medium. However, there may still be a phase shift between e. m. wave oscillation and plasma oscillation, caused by $\varepsilon_2\neq 0$.

before, this derivation of a plasma frequency is deduced without any limitation to the e. m. wave. Although it does not fit to the situation in a bulk, it helps to build models for other oscillating systems, where transversal e. m. waves may excite plasmons, as it will be seen later.

For the following chapters, one should distinguish between three types of different plasmons:

1. Bulk plasmons in a 3d solid
2. Surface plasmon in the surface layer or in interfaces
3. Mie plasmons in structures of small dimensions, like nanoparticles

1) Bulk plasmons

The so-called bulk plasmons are collective oscillations of the conduction electrons in a 3d solid. Those oscillations are longitudinal density fluctuations. As bulk plasmons are longitudinally polarised, they do not couple directly to transverse electromagnetic waves. Spectroscopy of those plasmons requires the interaction with electromagnetic fields of charged particles like fast electrons. An ideal tool to excite bulk-plasmons, are fast (but nonrelativistic) electrons, which interact quasistatically via their Coulomb-field "flying" with them: EELS (Electron-Energy-Loss-Spectroscopy).

The excitation of those bulk plasmons cannot take place in the current case of interaction with red and blue light.

Additional note: According to [Rae80] there exists a possibility to excite bulk plasmons with light via the surface of the crystal. The electric field falling on the boundary of a solid under an angle α against the normal has a component E_z normal to the surface (z-direction), which is discontinuous due to a surface charge layer. Due to this changed distribution a finite gradient of the electron density (n) may be produced by E_z of the light and leads to an additional force (~dn/dz), which pushes the metal electrons along the z-direction according to the frequency of the light and thus produces longitudinal density oscillations of the electrons or bulk plasmons.

2) Surface plasmons

The concept of surface-plasmons was introduced shortly after the discovery of bulk plasmons in metals. In recent years surface-plasmons have been observed in a wide range of materials using both electron and photon spectroscopy. In addition, significant progress has been made towards a systematic use of surface-plasmons as a diagnostic tool to investigate the surface charge profile of metals.

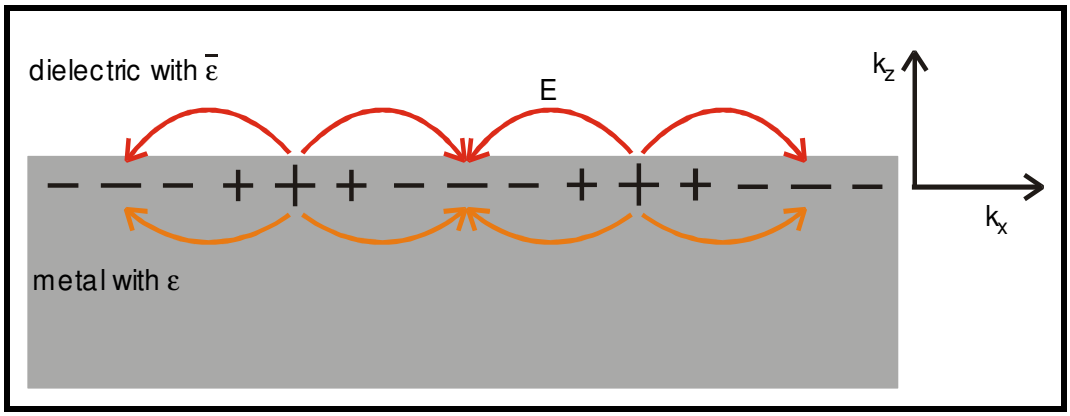

Fig. 10: The charges and the electric field lines of surface-plasmons propagating in a surface along the x-direction. Note: the electromagnetic field is a p-polarised wave (i.e. does not have only k_x and k_y components), because of the non-vanishing component of its electric field in the z-direction[34].

These charge fluctuations[35] are accompanied by a mixed transversal and longitudinal electromagnetic field (see Fig. 10), which disappears at $|z|\to\infty$, and has its maximum in the surface (z=0); this is typical for surface waves. This localisation explains the sensitivity of surface plasmons to surface properties.

The field of a surface plasmon is described by

$$E = E_0^{\pm} \exp[+i(k_x x \pm k_z z - \omega t)] \qquad \textbf{(I.1.31)}$$

with "+" for $z \geq 0$, "-" for $z \leq 0$, and with imaginary wave vector component k_z, which causes the exponential decay of the field E_z. The wave vector is defined by $k_x=2\pi/\lambda_p$, where λ_p is the wavelength of the plasma oscillation. With means of the Maxwell equations, it becomes clear that the wave vector k_x is continuous through the interface (see Fig. 10), and the dispersion relation can be written as

$$k_x = \frac{\omega}{c}\sqrt{\frac{\varepsilon \cdot \bar{\varepsilon}}{\varepsilon + \bar{\varepsilon}}} \qquad \textbf{(I.1.32)}$$

where ε is the complex dielectric function in the surface and $\bar{\varepsilon}$ in the dielectric outside (e.g. vacuum). This means, the frequency ω of these longitudinal charge oscillations is connected with the wave vector k_x by an

[34] S-polarised surface oscillations (i.e. only k_x and k_y components) do not exist, since E_y is continuous in the surface, the surrounding is isotropic and thus no inhomogeneous surface charge may be produced. To break the symmetry and thus create a local density change, it needs the discontinuous of the electric field perpendicular to the surface.

[35] Which can be localised in the z-direction within the Thomas-Fermi screening length of about 1Å

implicit dispersion relation $\omega(k_x)$, which can be determined by starting from Maxwell's equations.

The value of the surface-plasmon frequency for a free electron gas approaches[36]:

$$\omega_{sp} = \frac{\omega_p}{\sqrt{1+\bar{\varepsilon}}} \xrightarrow{\bar{\varepsilon}=1 \text{ in vacuum}} \omega_{sp} = \frac{\omega_p}{\sqrt{2}} \qquad \textbf{(I.1.33)}$$

The surface-plasmon frequency is therefore smaller than the plasma frequency in bulk.

The phase velocity of the surface-plasmon is always smaller than the speed of light in the adjacent dielectric medium. Thus, without participation of another system, which may take off momentum the surface-plasmon cannot decay or become excited radiatively[37]. Even the decay into other surface-plasmons of smaller energy is not possible. Any structural feature, which breaks the symmetry of the plane surface, however, may give rise to coupling: surface roughness, phonons, etc. Another way to excite surface-plasmons is the use of an evanescent wave; see more details in [Rae88]. To emphasize: Surface-plasmons may be excited by light (p-polarised), by means of special configurations, where the momentum may be altered.

The frequency of a surface-plasmon is not a constant value, but depends on its surrounding. Any adsorbate on the surface, for example, lowers the surface-plasmon frequency, because of the effect of depolarisation. The coverage of oxide on aluminum changes, e.g., the frequency from 10eV to 7eV.

At the junction of two metal layers (or metal/semiconductor with many charge carriers), there appear three surface-plasma frequencies:

1. interface plasmon at $metal_1$/dielectric junction $\rightarrow \omega_1$
2. interface plasmon at $metal_2$/dielectric junction $\rightarrow \omega_2$
3. interface plasmon at $metal_1$/$metal_2$ junction $\rightarrow \omega_3$

The frequencies relate as $(\omega_3)^2 = (\omega_1)^2 + (\omega_2)^2$, for thick layers, where $k_x d >> 1$. For thin layers, the frequencies depend strongly on the thickness.

---

[36] The discontinuous of $E_z(z=0^{\pm}) \sim \pm k_z$ and the condition $\varepsilon(\omega)\cdot E_z(0^-) = \bar{\varepsilon}\cdot E_z(0^+)$ imply $\varepsilon(\omega) = -\bar{\varepsilon}$ and finally with the Drude model $\varepsilon(\omega) = 1-\omega_p^2/\omega^2 = -\bar{\varepsilon}$ one gets the result above.

[37] In this chapter only the normal case of *non-radiative* plasmon are considered, which has an imaginary k_z wave vector component. The unusual case of *radiative* plasmons shows real k_z, and therefore a standing wave in the z-direction. They can decay into photons, as well as been created by photons.

3) Mie-plasmons

The collective electron oscillations in small metal particles (nanoparticles) are confined in all three directions. They are called particle plasmons or Mie-plasmons. The sizes of those particles lie in between 10nm-200nm.

Incident light excites electrons in the whole particle, which leads to a charge dipole[38] over the full diameter (Fig. 11), and of course, one cannot define a wave vector k for the Mie-plasmon. It does not need any additional means to excite those Mie-plasmons with light, because of the possibility of the particle surface to fit every momentum and energy, desired.

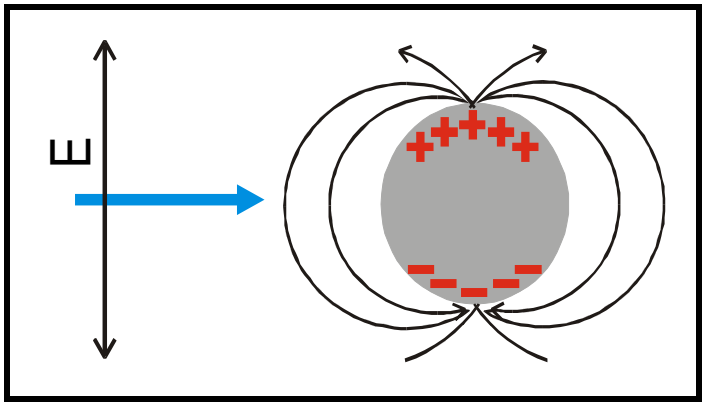

Fig. 11: The excitation of a Mie-plasmon in a nanoparticle is possible with light

It is now quite impressive to apply the same classical dispersion theory, used for insulators and metals, to the system of Mie-plasmons:

The charge dipole acts as an attractive force, the same way as seen in the Lorentz model for insulators. The mass μ is the sum of all electron masses, and the force F takes effect for each electron, due to all ions. Therefore $\omega_0^2 = F/\mu$ is in the same order of magnitude, as ω_0^2 in the Lorentz model for one electron.

There are also damping mechanisms as radiation damping, surface scattering, electron-electron scattering, …[39], which lead to a damping constant Γ.

Although the Mie-plasmons are metals, there is a resonance frequency $\omega_0 \neq 0$, but its origin is not the same as for insulators.

The resulting equation of motion, adopted from eq. (I.1.18) page 20 is

$$\mu\ddot{\mathbf{r}} + \mu\Gamma\dot{\mathbf{r}} + \mu\omega_0^2\mathbf{r} = -Q\mathbf{E}_{loc} \qquad \textbf{(I.1.34)}$$

[38] Electrons with all-over charge Q in front of the positive ions (~Jellium model)
[39] see e.g. in [Sch02]

Its solution with the ansatz $r(t)=Ae^{-i\omega t}$ is

$$\mathbf{r} = \frac{-Q\mathbf{E}_{loc}}{\mu}\frac{1}{(\omega_0^2-\omega^2)-i\Gamma\omega} \qquad \textbf{(I.1.35)}$$

An important difference to systems considered before is the fact that the amplitude of the system's oscillation is restricted to the half of the diameter d of the particle. Therefore $0 \le |r| \le d/2$, and thus:

$$\left|\frac{\mathbf{d}}{2}\right| \geq \left|\frac{-Q\mathbf{E}_{loc}}{\mu}\frac{1}{(\omega_0^2-\omega^2)-i\Gamma\omega}\right| \qquad \textbf{(I.1.36)}$$

This limitation implies the important fact that the Mie-plasmon *may not* be excited at its own resonance frequency ω_0, but only apart from it at a frequency $\omega \notin]\omega_0 - x/2, \omega_0 + x/2[$ (see Fig. 12). This means also that the Mie-plasmon does not oscillate at its intrinsic resonance frequency, but at a redshifted or blueshifted frequency. Surprisingly, this region x is – in this simple model - almost not dependent of the particle's diameter d, nor the resonant frequency ω_0, nor the amplitude of the electric field E_0. It is only (weakly) dependent of the damping Γ. The interval x is about[40] 14meV for a realistic calculation[41]. A consequence of this forbidden frequency band is, that there is no absorption or reflection of the incident light.

[40] To calculate a realistic systems, values from [Sch02] has been taken: d~50nm, ω_0~3eV, E_0~1000V/m, Γ~0.4eV

[41] With the values of footnote 40 and Γ~0.0eV: x~10meV.
With Γ~1.0eV: x~80meV

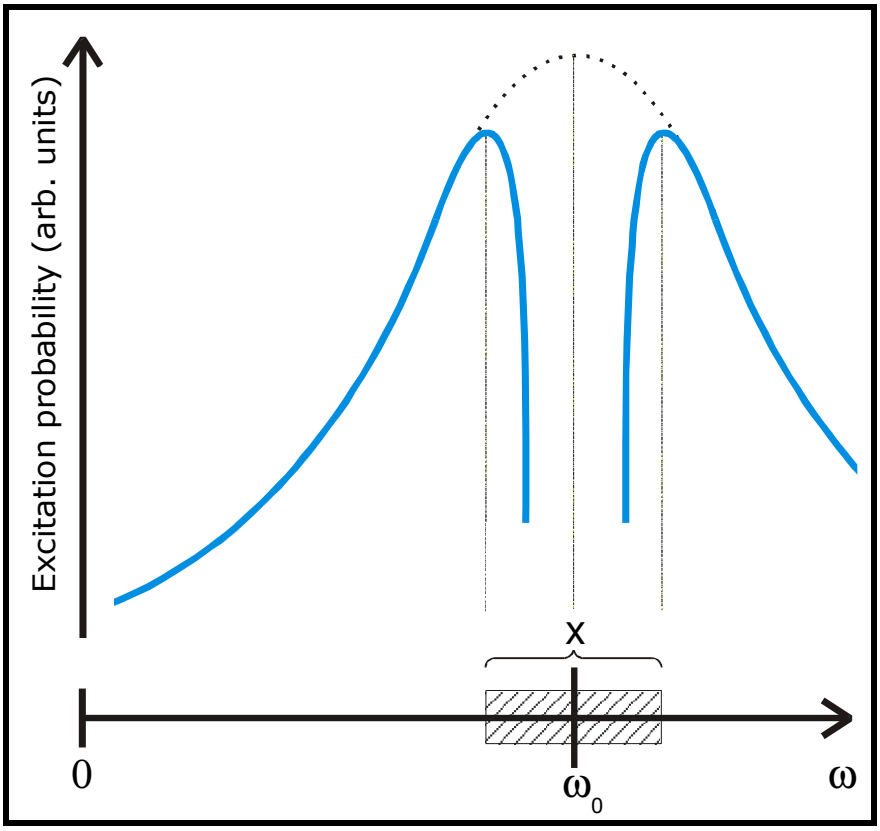

Fig. 12: The Mie-plasmon may not be excited at its intrinsic resonance frequency, but only apart from $\omega_0 \pm x/2$.

Apart from this model, in reality it is obvious that the surroundings[42] around the particle does strongly influence the Mie-plasmon frequency. In fact the Mie-plasmon frequencies of those small silver particles show an *blueshift* with *decreasing radius* as a consequence of the reduced s-d interaction in the region, where 5s electrons spill out into the vacuum. Since part of the density fluctuations associated with the Mie-resonance oscillate with the unscreened plasma frequency, this mechanism leads to an increase of the resonance frequency.

A comparison of the three different plasmons (bulk, surface, Mie) shall give an overview of principal plasmon frequencies. All values were theoretically calculated for silver[43]:

[42] Given by the dielectric function $\bar{\varepsilon}$
[43] [Lie93]

- **Bulk-plasmon**
  ω_p=9.2eV (unscreened[44])
  $\omega_p^* \approx \omega_p / \sqrt{\mathrm{Re}\,\varepsilon_d}$ ≈3.9eV (screened)

- **Surface-plasmon**
  $\omega_s = \omega_p / \sqrt{2}$ =6.5eV (unscreened)
  $\omega_s^* \approx \omega_p / \sqrt{1+\mathrm{Re}\,\varepsilon_d}$ ≈3.6eV (screened)

- **Mie-plasmon** in the large particle limit (~100Å)
  $\omega_M = \omega_p / \sqrt{3}$ =5.3eV (unscreened)
  $\omega_M^* \approx \omega_p / \sqrt{2+\mathrm{Re}\,\varepsilon_d}$ ≈3.5eV (screened)

Of course, those values may shift by many reasons, like size, shape, surrounding media, etc. This has been nicely shown by F.R. Aussenegg et al.[45], which are able to produce nanoparticles of different sizes and shapes, lying in an array. They can tune the resonance frequency of the Mie-plasmons in a wide range of the visible light. It is, for example, possible to produce elliptical nanoparticles (Fig. 13), which show two different resonances.

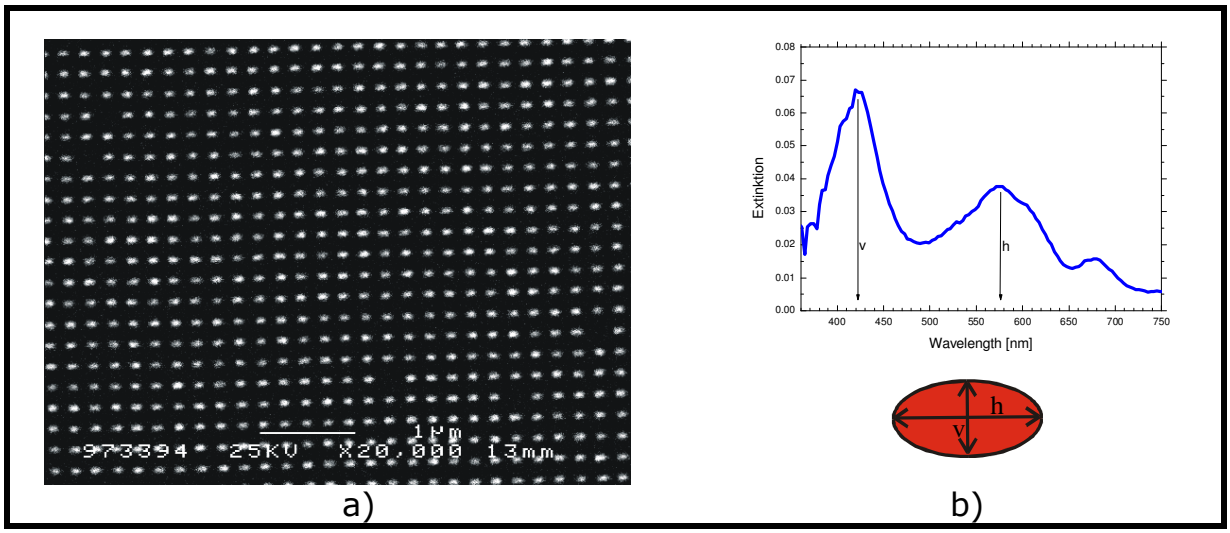

Fig. 13: a) SEM picture of lithographically fabricated nanoparticles on ITO
b) Extinction spectrum and orientation of the nanoparticle array

[44] Unscreened plasma frequency: The calculation uses simple models without taking any additional influences into account
Screened plasma frequency: Possible compensating effects, like screening of the electrons by the bound d-electrons, are considered.

[45] For example in [LLA99]

Previous optical experiments[46] showed that the frequency of the surface plasmon of a thin Ag film increases linearly with the inverse of the layer thickness, while for nanosized clusters the Mie-resonance frequency increases with the inverse of the cluster radius[47]. Both dependences are determined by the same physical effect, i.e., the reduction of the surface to volume ratio[48].

F. Moresco et al.[49] investigated the plasmon confinement in ultra-thin continuous Ag films, and found that for continuous thin films, the plasmon frequency[50] at a vanishing wave vector (as in light) scales with the surface-to-volume ratio of the grains, i.e. with the Mie-resonance of separated clusters, instead of with inverse thickness. This indicates a confinement of the plasmons into single domains, in spite of metallic conductivity.

The importance of Mie-plasmons to this work comes from the fact that Mie-plasmons (and also surface plasmons) may decay into single particle excitations (= electron-hole-pair = eh-pair). In addition, it is known, that Mie-plasmons produce a field enhancement[51], because of the internal polarisation. This field enhancement increases the amount of photoelectrons, which has lately been seen in a PEEM-experiment of Ag/GaAs[52]. H.-G. Rubahn[53] indicates the following connection: "It is expected that for ultra-thin films (below 16nm for Au) the exact value of the relaxation time constant depends on the surface morphology, i.e., the shapes and sizes of the discontinuous distribution of islands. One then enters the regime of 'supported metal clusters' (…)"

For more details, especially the damping mechanisms of Mie-plasmons have a look at M. Scharte's work [Sch02].

[46] [BRA95]
[47] [TKML93]
[48] [Lie97]
[49] [MRHH99]
[50] Which he did not specify further, i.e. he did not distinguish between surface- and Mie-plasmons
[51] [Sch02]
[52] [BA02]
[53] [Rub99]

f. The lifetime of excited electrons

In this chapter, a single electron is considered, which shall have an energy some eV above the Fermi level. It does not interest here, why or how this electron gained this higher energy. Because of possible lower lying empty final states, the system tries of course to lower its total energy, and therefore this electron suffers different relaxation processes. The time before being relaxed is called the *lifetime* of this electron.

As principal relaxation processes, the following two can be distinguished:

1. *Inelastic relaxation* (inelastic lifetime): It is intuitively clear that an electron, after having gained some energy, will dissipate its excitation energy, simply by trying to reach the thermalisation state. The first process is the relaxation of the electron from the higher energy level to a lower one. The most important[54] process thereby is the electron-electron scattering, between an electron above E_F and one below E_F. Other possibility to lose energy is by emitting a photon or by exciting a plasmon. At highly doped semiconductors the scattering of electrons with holes is another dominant event.

2. *Elastic relaxation* (elastic lifetime): A not yet thermalised electron may also take part on processes, which only change its wave function's phase. Included are here processes like electron-phonon interaction and the scattering of electrons with defects and impurities.

The electron-electron interaction, which is the most dominant relaxation process[55] in a metal, shall be analysed here in more details:

1) Fermi-liquid theory (FLT)

The inelastic electron-electron scattering, which usually takes place after optical excitation of electrons in a metal, is well described by Landau's Fermi-liquid theory. It is based on the concept of quasi-particles. Landau's FLT is a general theory for degenerated[56] Fermi systems. Examples for this are the electron system in solids and ^{3}He-atoms. The electron system is a rather unusual case in FLT, compared to the uncharged ^{3}He Fermi system: The electron-electron interaction is long-range and therefore there appear some specific features.

The basic idea for the transition from a Fermi *gas* (non-interacting Fermions) to a Fermi *liquid* (interacting Fermions) is, that the main part of

[54] Mainly for metals
[55] Usually, it is taken (in a 1st-order approximation) as the only process that happens in metals
[56] Several quantum states may have the same energy

the interaction may be redefined, in order to have weakly interacting quasi-particles instead of strong (=fully) interacting particles (Fig. 14).

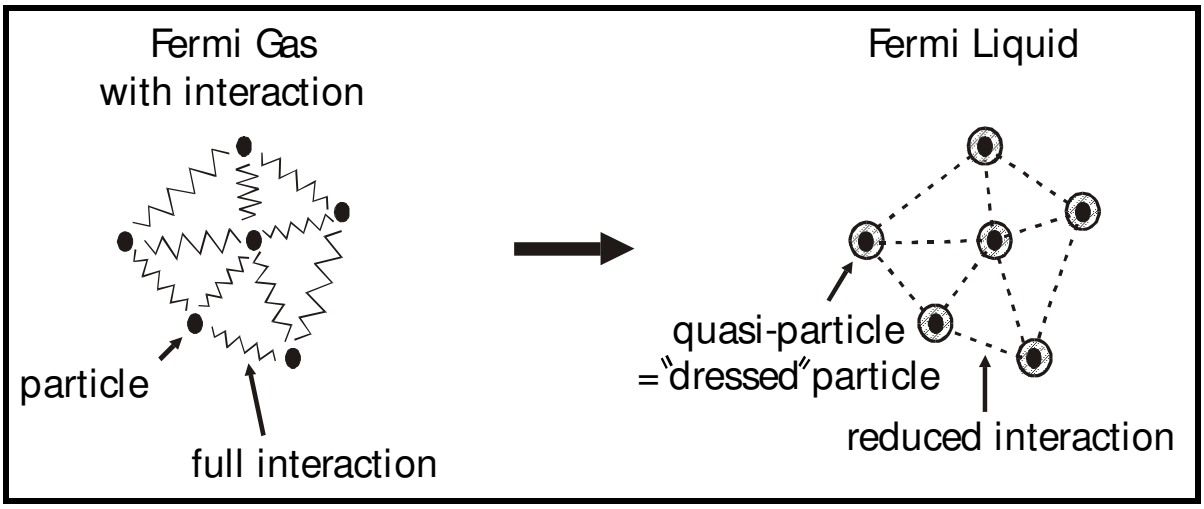

Fig. 14: The transition from a Fermi gas to a Fermi liquid

One of the most important results of the FLT is the description of the electron-electron scattering (exactly: scattering of quasi-particles). Roughly spoken, it shows that an excited electron (with energy > E_F) scatters with another electron lying below the Fermi level. Both have to take unoccupied states above the Fermi level as final states. The scattering rate depends therefore on the available phase space, and increases with increasing distance to the Fermi level. This means of course also a decreasing of the relaxation time τ_{ee} with higher energy.

Since the first description of the FLT, there were made many additional contributions to the original theory. As a small summary, the following table shows the predicted energy dependences of the relaxation time for different dimensions.

Dimensions	$(\tau_{ee})^{-1}$	**Authors**
1d	$\lvert E-E_F\rvert$	[Lut61]
2d	$(E-E_F)^2 \cdot \ln\lvert E-E_F\rvert$	[GQ82], [Cha71]
3d	$(E-E_F)^2$	[LP36], [Bab37], [QF58]

One can clearly see the strong dependence of the relaxation time on the dimensionality.

It is known and not further astonishing, that not only the dimensionality affects the relaxation time of excited electrons, but also the geometric structure via defect scattering, the material, the excitation energy, band structure, the spin polarisation, screening effects, etc.

2) 3d-Fermi-liquid theory

The following derivation of the 3d-Fermi-liquid theory (3d-FLT) follows mainly Quinn's article[57]. At the end, this theory will be applied to the special case: silver.

J. Quinn starts with the interaction energy of one single excited electron in the sea of conduction electrons of a metal. The only restriction to the system should be, that the energy uncertainty due to the finite lifetime is small compared to the real part of the energy of the excited particle. He considers then the *self-energy approximation*[58] of the interaction in a degenerated electron gas. The renormalised quasi particle energy is a complex function of the momentum[59]. The imaginary part is a consequence of the quasi particle state not being eigenstate of the system. The excited quasi particles may transfer energy and momentum to the electron gas. The transition rate of those real collisions is responsible for the imaginary part of the self-energy.

The wave function of a single excited electron has a time dependence of $exp\left(-iE(p)t/\hbar\right)$, where $\mathrm{E(p)=E_R(p)+i\cdot E_I(p)}$ describes the renormalised quasi particle energy. This time dependence leads to a decreasing probability for the electron to occupy a given state; expressed by $exp\left(-2|E_I|t/\hbar\right)$. The factor $2|E_I|/\hbar$ may be taken as a *transition rate*, and its *inverse* term may be interpreted as *lifetime*.

The *imaginary part of the self-energy* becomes after R.A. Ferell[60]:

$$E_I(p)=\mathrm{Im}\frac{e^2}{2\pi^2}\int\frac{d^3k}{k^2\varepsilon\left(k,E(p)-E(\vec{p}-\vec{k})+i\delta\right)} \qquad \textbf{(I.1.37)}$$

$$\text{for } E_F<E(\vec{p}-\vec{k})<E(p)$$

$\varepsilon(k,\omega)$ is the Lindhard dielectric constant[61], δ is a positive infinitesimal, E_F is the Fermi energy, and $E(\vec{p}-\vec{k})$ is an energy in the surrounding of E_F. Lindhard described this dielectric constant by a term, which mainly uses the plasma frequency ω_p and the Fermi velocity of the electron gas. This $\varepsilon(k,\omega)$ has a real and an imaginary part $\varepsilon(k,\omega)= \varepsilon_1(k,\omega) + i\cdot\varepsilon_2(k,\omega)$. The imaginary part ε_2 is simply a measure of the number of states available for real transitions involving a given energy $\hbar\omega$ and momentum transfer $\hbar k$.

---

[57] [Qui62]
[58] Also called: quasi particle approximation
[59] In this chapter the momentum of an electron is labelled as "k", "p" and "q"
[60] [Fer56]
[61] [Lin54]

For an excited electron, lying close to the Fermi energy (E(p) ≈ E_F), the energy E(p)-E($\vec{p}-\vec{k}$) is always small. Therefore, the equation above can be rewritten as

$$E_I(p) = -\frac{e^2}{2\pi^2}\int \frac{d^3k}{k^2}\frac{\varepsilon_2\left(k,\Delta E(\vec{k})\right)}{\left|\varepsilon\left(k,\Delta E(\vec{k})\right)\right|^2} \qquad \textbf{(I.1.38)}$$

$$\text{for } E_F < E(\vec{p}-\vec{k}) < E(p)$$
$$\text{with } \Delta E(\vec{k}) = E(p) - E(\vec{p}-\vec{k})$$

Since considering the case where ΔE is always very small, $\left|\varepsilon(k,\Delta E)\right|^2$ in the denominator can be replaced by $\left|\varepsilon(k,0)\right|^2$. Now, it is easier to integrate for p ≈ p_F, and it results in:

$$E_I(p) \approx -\frac{e^2}{2a_0}\frac{\pi^{1/2}}{32(\alpha\cdot r_s)^{3/2}}\times\left[\tan^{-1}\left(\frac{\pi}{\alpha\cdot r_s}\right)^{1/2} + \frac{(\alpha\cdot r_s/\pi)^{1/2}}{1+\alpha\cdot r_s/\pi}\right]\frac{(x^2-1)^2}{x} \qquad \textbf{(I.1.39)}$$

Where $\alpha=(4/9\pi)^{1/3}$, r_s is the radius[62] of a sphere equal in volume to the volume per electron, $x=p/p_F$ is the reduced momentum of the excited electron, and p_F describes the momentum of the electron at the Fermi level. This equation is in such form only valid for $p/p_F < 1.3$, resp. $E/E_F < 1.7$.

It should be pointed out that incidentally the mean energy lost by an excited electron, which does suffer a collision, is not small compared to its initial excitation energy. In fact, for the present case of low-energy excitation one can easily show that an excited electron loses 2/3 of its excitation energy in a typical collision.

By applying those results to the special case *silver*[63] (E_F=5.49eV, r_s=3.02), the range of validity become $E_{exc} < E_F$ +3.8eV. This energy range is well fulfilled by using blue (~3eV) excitation light.

After combining the equations above, one finally gets the important result of the Fermi-Liquid theory in 3d:

$$\tau = \tau_0 \cdot \left[\frac{1}{E-E_F}\right]^2 \qquad \textbf{(I.1.40)}$$

which describes the *lifetime of excited electrons in a free electron gas* between Fermi level E_F and $1.7\cdot E_F$, under the influence of electron-electron scattering.

[62] Measured in units of the Bohr radius a_0
[63] Values from [AM76]

This energy dependence has been proven quite often with huge accuracy. Especially for silver, with its low d-band (~4eV) and therefore without interaction of sp-electrons with d-electrons or d-holes, this equation fits very well[64].

The material constant (τ_0) is actually only a constant over the regarded energy range, but apart from that, it depends on different effects (see also page 38). The upper calculations show that τ_0 primarily depends on the electron mass, electron density and the electron charge.

For *silver* one gets: $$\tau \approx 18 \cdot \left[\frac{1}{E - E_F} \right]^2 \text{ (fs)} \qquad \textbf{(I.1.41)}$$

In the early years of the research with TR-2PPE, many corrections for this bulk-formula (I.1.40) were published. Mainly the influences of Auger-electrons, cascade electrons, or d-band electrons caused to an expansion of that formula. For further reading, see e.g. [EP78], [Paw98], [Bau97] and [Kno97].

3) The situation in 2d

Beside all interesting and important effects in a thick bulk material, there is huge interest in the behaviour of electrons in thin and ultra-thin structures. Especially, the industries of semiconductors and integrated circuits need to know the dynamics in adlayers and in interlayers.

As it is well known, there are a lot of changes in a two-dimensional electron gas, compared to a three-dimensional one. In particular, one expects *energy independent* behaviour in the density of states:

2d: $$\rho(E) = \frac{m^*}{\pi \cdot \hbar^2}$$

3d: $$\rho(E) = \frac{\sqrt{2} \cdot (m^*)^{3/2}}{\pi^{2} \cdot \hbar^3} \cdot \sqrt{E}$$

Further anomalies are expected in the electrical conductivity, the Hall effect, the magnetoresistance, and most important to us, in the dynamics and relaxation of optically excited electrons.

The independence of the density of states to the energy, leads to the fact that, in comparison to the 3d case, the holes have as much states as the

[64] [Por98]

electrons. That changes the phase-space argument, which is often used at the Fermi-liquid theory[65].

The following text gives a close, but brief look on the theoretically predicted behaviour and relaxation of excited electrons in a two dimensional Fermi gas. The description based on the article of Giuliani and Quinn[66]. They broadened the theory of Chaplik[67], Uren et al.[68] and Abrahams et al.[69]

The article can be described as following. Look at a degenerated Fermi gas with N electrons in the ground state. This is known as the Fermi sea. One gets a quasi particle by adding an extra electron, which settles down at an unoccupied state with wave vector $\vec{p}$ and spin projection σ. In analogy, removing an electron from an occupied state may create a quasi hole. With p_F the Fermi wave vector, it has to be $p \geq p_F$ for a quasi particle, and $p \leq p_F$ for a quasi hole[70]. The ground state for that $N \pm 1$ electron configuration is again a Fermi sea. Without a relaxation mechanism, states of quasi particles and quasi holes are stationary. However, the Coulomb interaction offers a way to distribute energy and momentum between the electrons, and leads therefore to a decay of a quasi particle state or a quasi hole state, and to an inelastic lifetime $1/\tau_{ee}$ for these electronic states. For *T = 0K*, $1/\tau_{ee}$ is determined by the decay rate of the intrinsic plane wave state. For *finite temperatures*, $1/\tau_{ee}$ is defined by the relaxation rate of the occupation number $n_{\vec{p},\sigma}$, which becomes available by a transport equation ansatz. In both cases $1/\tau_{ee}$ can be calculated with means of perturbation theory, which uses the Fermi Golden Rule:

$$\begin{aligned} \tau_{ee}^{-1} &= \frac{2\pi}{\hbar} \sum_{\vec{k},\vec{p},\vec{\sigma}} n^0_{\vec{k},\sigma'} (1 - n^0_{\vec{k}-\vec{q},\sigma'})(1 - n^0_{\vec{k}+\vec{q},\sigma'}) \\ &\times \left|V_c(\vec{p},\vec{q})\right|^2 \delta\left(E_{\vec{p}+\vec{q}} + E_{\vec{k}-\vec{q}} - E_{\vec{p}} - E_{\vec{k}}\right) \end{aligned} \qquad \textbf{(I.1.42)}$$

with $n^0_{\vec{p},\sigma'}$ the distribution function in equilibrium and $V_c(\vec{p},\vec{q})$ the matrix element of the electron-electron interaction potential. In the so-called *random-phase approximation* (RPA) is:

$$V_c(\vec{p},\vec{q}) = \frac{v(q)}{\varepsilon(q, \frac{1}{\hbar}(E_{\vec{p}} - E_{\vec{p}+\vec{q}}))} \qquad \textbf{(I.1.43)}$$

[65] See e.g. [LP36, Paw98]
[66] [GQ82]
[67] [Cha71]
[68] [UDKP81]
[69] [AALR81]
[70] At T = 0K

with the dielectric function $\varepsilon(q,\omega)$ of a two-dimensional electron gas, and the usual matrix element v(q) of the Coulomb potential.

After some calculations, eq. (I.1.42) results in:

$$\frac{1}{\tau_{ee}} \cong -\frac{E_F}{4\pi\hbar}\left[\frac{E-E_F}{E_F}\right]^2 \times \left[ln\left[\frac{E-E_F}{E_F}\right]-\frac{1}{2}-ln\left[\frac{2q_{TF}^{(2d)}}{p_F}\right]\right] \qquad \textbf{(I.1.44)}$$

for T=0K and $E << \frac{\hbar^2 p_F q_{TF}^{(2d)}}{m}$

Where E is the excitation energy of the electrons, $q_{TF}^{(2d)} = 2me^2/\hbar^2$ is the Thomas-Fermi screening wave vector in 2d, and $E_F = \hbar^2 p_F^2/2m$ is the normal Fermi energy of the system.

This final result is only valid for T=0K. For *finite temperatures* it is not possible to write down a close analytic equation, but the authors mentioned that also for higher temperatures the *same principal dependence* exists.

It is not possible and suitable to apply the equation above to the real system: *silver*. However, a trial can be seen in [Por98]. For this current work the *form* of the equation above is central. It shows a lifetime dependence for a *2d-system*, which is quite different from that in a 3d-system, seen in eq. (I.1.40):

$$\frac{1}{\tau_{ee}} \propto (E-E_F)^2 \ln|E-E_F| \qquad \textbf{(I.1.45)}$$

In a 2d-system, τ_{ee} shows an *additional logarithmic factor*. The authors G. Giuliani and J. Quinn comment that as a competition effect of the planar geometry and the conservation of energy and momentum during the electronic collision processes. As a supplement, they point out the interesting fact, that τ_{ee} *does not* depend at all on the electric charge. This is a consequence of the screening by the Coulomb potential. In a 3d-system, τ_{ee} *does* depend on the electric charge e, see e.g. [Paw98].

4) The 1d-behaviour

As it has been mentioned above, the quasi-particle behaviour in 1d, especially its inelastic lifetime, was explained by M. Luttinger[71] in 1961. He found a relatively simple form for the electron-electron scattering rate:

[71] [Lut61]

$$(\tau_{ee})^{-1} \propto |E\text{-}E_F| \qquad \textbf{(I.1.46)}$$

This means, the scattering rate depends linearly on the energy. Therefore, the inelastic lifetime of the quasi-particles in a one-dimensional surrounding, follows a hyperbolic $1/|E\text{-}E_F|$ curve.

Even though this 1d performance is quite important to the physics of nano-tubes and nano-wires, and thus more and more for technical applications, for example in the semiconductor industries, it did not have much influence on the measurements in this work, and hence was not followed up any further.

5) Small particles[72]

In structures having diameters below about 200nm the dynamical properties of optically excited electrons are not only altered due to reduced phase space for scattering events, but rather by how the light is absorbed in the system. In metal nanoparticles the excitation of electrons by light happens generally by means of Mie-plasmons. It is still a subject discussed controversially, but during the last five to ten years, most involved researchers agree on this opinion. The concept of plasmons have been discussed earlier in chapter I.e. Many even agree with the hypothesis, that generally in all structures of silver – 3d, 2d or smaller – an excitation takes place via plasmons and interband transitions, and subsequent decay into electron-hole pairs.

It is also important to mention, that the concept of plasmons is - in principle - not needed. Plasmons describe the behaviour of a collective excitation of charge carriers. It is therefore also possible to just consider the charge carriers in their excited states, and to mind of the correlation they have. Then, there will arise e.g. a resonance feature in a spectrum, which may be called "plasmon" but this is not necessary. A. Liebsch and many others follow this concept. By this, they avoid having to explain, what a plasmon really is.

It is still not clear, how the process of photo-excitation in silver really happens. However, it is clear, that a dephasing is needed to occupy an intermediate state. And this dephasing happens in between few fs[73].

[72] Note: The term "particles" means here the same as "clusters, islands, small structures", and not "electrons etc." as above.
[73] [Sch02]

6) Excitation of electron-hole-pairs

Up to now the assumption was made that the excitation of a Fermi-sea-electron via a photon brings a single electron to an energy above E_F. However, by the incident photon, not only an electron is excited, but an electron-hole-pair (eh-pair), which oscillates with the electro-magnetic field of the photon. Additionally, there is also a so-called *polarisation* created, between the photon, the electron and the hole. By exciting, the eh-pair does not yet populate any new energy level (except if there happened an interband transition). It needs a dephasing process, i.e. a scattering event with a phonon to get the right momentum (k-vector), in order to populate a real existing state. This is equal to a loss of the polarisation between photon, electron and hole. Having occupied that new state[74], the electron might relax to a lower lying energy level by scattering for example with another electron. If it did not yet relax, a second photon can let this electron oscillate again, and by another dephasing process, it could occupy an even higher energy level. It should be said, that the intermediate state might also be *virtual*. That happens if the second photon may couple directly to the *not yet* dephased electron[75]. The probability for such an event is quite low (but may not be neglected for some systems).

[74] It will be called *intermediate state* in the following text
[75] Still existing polarisation

II. The two-photon photoemission spectroscopy

a. Introduction

Photoemission[76] stands for the emission of electrons caused by illumination with light. A. Einstein could explain - on the basis of many contributions of other researchers (like W. Hallwachs, H. Hertz and P. Lenard) - in the year 1905, the outer photoelectron effect, by postulating the particle character of light, following M. Planck's idea.

By illuminating a surface with photons of a certain energy $E=\hbar\omega$, there is a non-vanishing probability of the photons to get absorbed. Caused by this supply of energy, electrons become excited from a band below the Fermi level to a higher band above Fermi level (in general). If this excitation level lies above the vacuum level, the electron may exit into the vacuum. The kinetic energy of the emitted electrons may be measured, and thus this principle led quite fast to the discipline of photoemission spectroscopy (PES), with its main advantage to depict the density of states of the occupied energy bands[77]. Additionally, it is also a versatile technique to study electronic states in solids and at surfaces as well as of adsorbates on surfaces. As an illustration of an UPS[78]-spectrum, take a look at Fig. 15, where such a spectrum is shown for the case of silver. The Fermi energy lies at the binding energy of 0eV. Below 0eV the 5s conduction band follows. The maximum below 3eV comes from 4d valence band electrons.

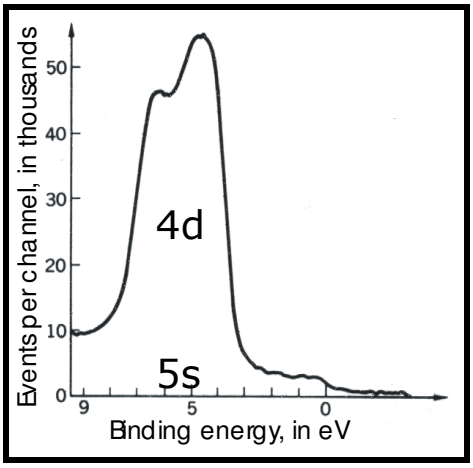

Fig. 15: UPS-spectrum of the bands of silver. From [Kit96], after Siegbahn et al.

[76] Photoemission spectroscopy and photoelectron emission spectroscopy are taken as synonyms

[77] To be more precise, one measures the "joint density of states", i.e. the combination of the density of states of all energy levels, involved.

[78] Ultra-Violet Photoelectron Spectroscopy. See appendix VIII.3

A real and instructive example of the power of photoemission as a tool, is the set of spectra from Cu(111) showing a surface state dispersion (Fig. 1) that can exactly be compared with the theoretical band structure.

The photoemission spectroscopy is not limited to *visible light*. Much progress could be made by using different regions of the e. m. spectrum (see the list in appendix VIII.3). One of the most important developments was the angle- and energy resolved photoemission spectroscopy, which enables to measure E($\vec{k}$)-dispersion relations (=bands) of the electrons. This method uses the principle that the excited electrons located at the final state, carry the information ($\vec{k}$, E) of their origin, the initial state.

The benefit of angle-resolved photoemission is, that one gets not only the energy but also the momentum $\vec{k}$ of the outcoming electrons. In this connection, it is important to point out, that there is a restriction to the gathering of information about the observed system. The momentum $\vec{k}$ is *not* fully determined. Let $E_{kin} = \hbar^2 \cdot (k_\parallel^2 + k_\perp^2)/2 \cdot m$, where $k_{||}$ and $k_\perp$ denote the components of the escaping photoelectron's momentum in the vacuum, parallel and perpendicular to the surface plane, respectively. Each plane wave $|\psi_{fi}>$ of the excited electron can match onto a vacuum plane wave at z = 0 having exactly the same $k_{||}$ (modulo a surface reciprocal lattice vector G_s). The $k_{||}$ conservation determines uniquely the direction and length of $k_{||}$ within the solid, because of $k_\parallel^{vac} = k_\parallel^{solid} + G_s$ and according to the equation

$$\left|k_{||}\right| = \sqrt{\frac{2 \cdot m \cdot E_{kin}}{\hbar^2}} \cdot sin(\theta) \qquad \textbf{(II.1.47)}$$

Where θ is the angle between the surface normal and the detector. However, one cannot determine $k_\perp$ within the solid, *assumptions-free*. In fact there is no simple, exact relationship between $k_\perp^{solid}$ and $k_\perp^{vac}$, because $k_\perp^{vac}$ is modified by the potential barrier at the surface. By given $k_{||}$, the ejected electron could originate from any value of $k_\perp$ along the reciprocal lattice rod perpendicular to the surface Brillouin zone at $k_{||}$. Some adequate methods have been developed to determine $k_\perp$ indirectly. The details are written e.g. in [Kit96].

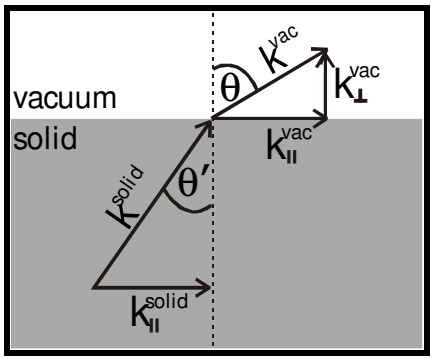

Fig. 16: Conservation of the parallel component of the momentum during electron emission

As a last example of how powerful photoemission is, at Fig. 17 an UPS-spectrum of a semiconductor is shown, before and after the deposition of an adsorbate (only little amount of adatoms). Without going too far into details (it will be referred in many contexts of this work), one can clearly

recognize, that changes of the Fermi level (E_F), of the band bending ($e\Delta V_s$) and of the surface dipole layer ($\Delta\chi$) become visible.

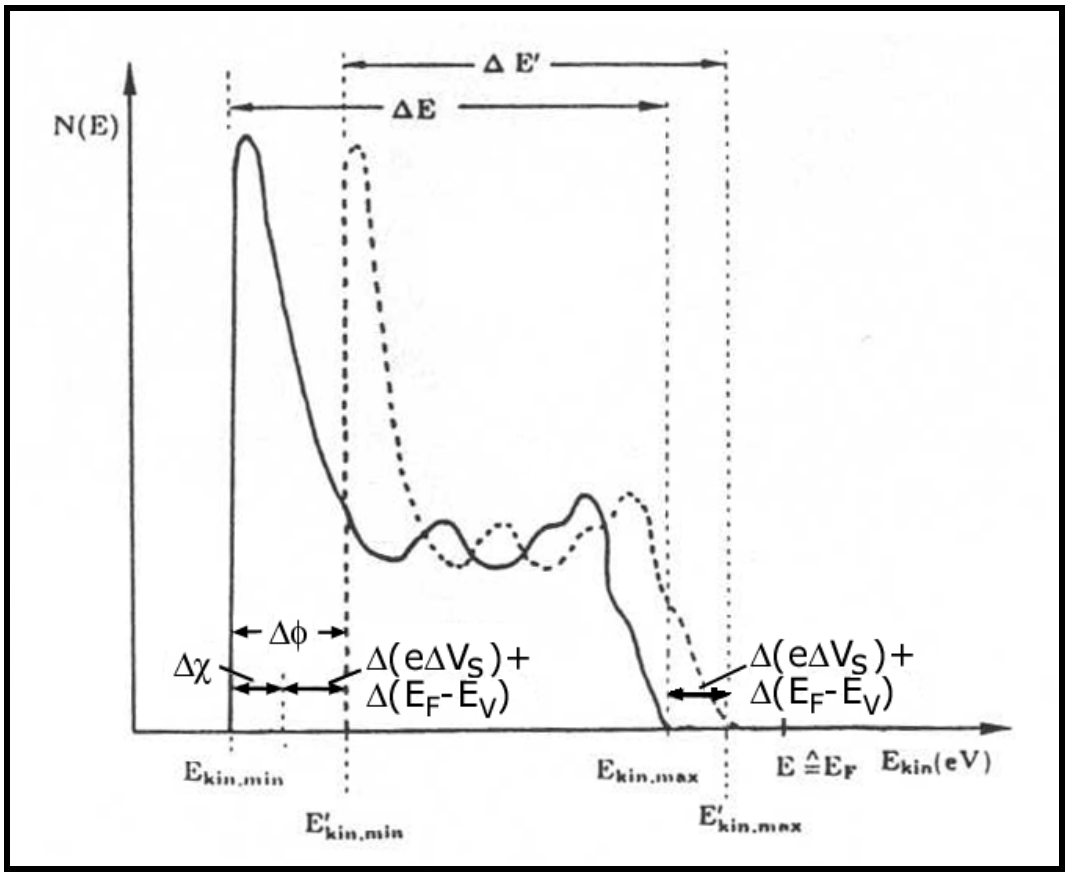

Fig. 17: UPS-spectrum of a semiconductor before and after the treatment of deposition. The curves show the amount N(E) of emitted electrons as a function of their energy. The left edge of the spectrum is being called *cut-off*, and the right edge determines the *Fermi edge*. From [GZ94]

b. Theory of photoemission

This theory has already been described quite often; lately e.g. by H. Ueba and T. Mii[79]. The main arguments – at least phenomenological – should be described here, in order to understand the remainder of this work.

The photoemission of electrons can be depicted either in a three-step model or in a one-step process. The most commonly used model for the interpretation of photoemission spectra in solids is the three-step model, developed by Berglund and Spicer[80]. It is a purely phenomenological approach, which has nonetheless proved to be quite successful. It breaks up the complicated photoemission process into three steps: the excitation of the photoelectron, its passage through the solid to the surface and its penetration through the surface into the vacuum, where it is detectable.

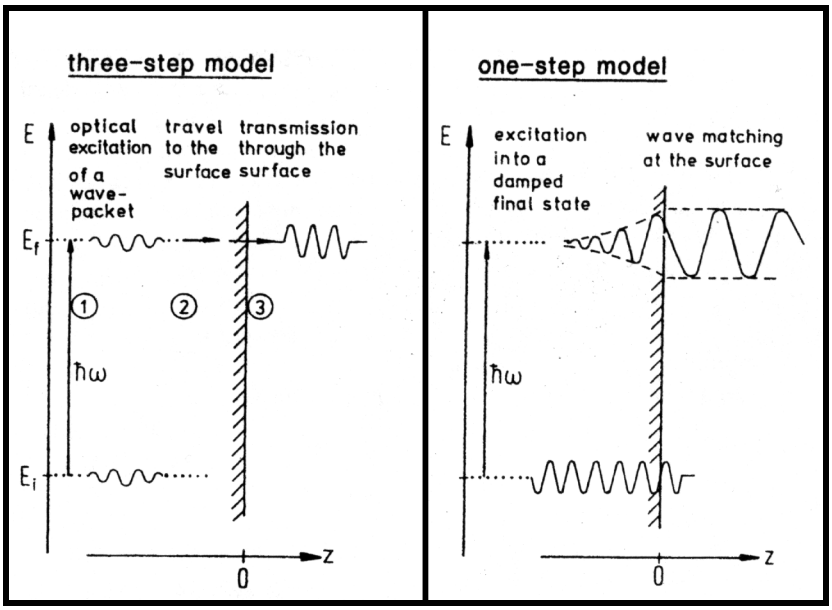

Fig. 18: Illustration of the three-step and the one-step model in PES. The three-step model consists of (1) photoexcitation of an electron, (2) its travel to the surface, and (3) its transmission through the surface into the vacuum. In the one-step model a Bloch wave electron is excited into a wave that propagates freely in the vacuum, but decays away from the surface into the solid. From S. Hüfner [Hüf95].

The *three-step model* and its relation to the correct *one-step model* are sketched in Fig. 18. In the *one-step model* the excitation is considered from an initial state (Bloch wave in the crystal) into a damped final state near the surface. The damping takes care of the short mean free path of the electrons in the solid (see below).

[79] [UM01]
[80] [BP64]

1) The three-step process in detail

A schematic picture of the energy levels, involved in a photoemission excitation process, is shown in Fig. 19.

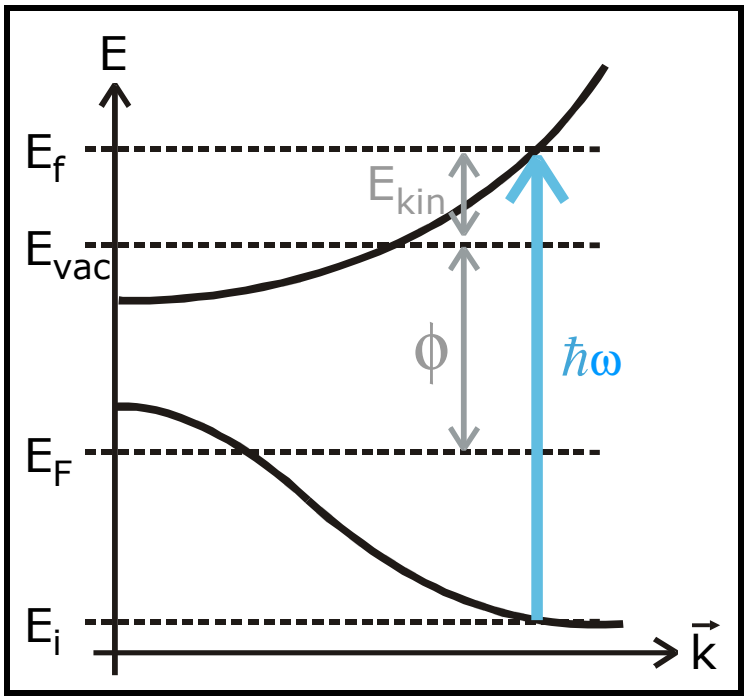

Fig. 19: A simple picture of the energy levels, involved in photoemission spectroscopy. With a photon energy of E=ħω, an electron at the initial state E_i (< E_F) becomes excited (1st step) to the final state E_f. If this final state lies above the vacuum level E_{vac}, and if the electron is near the surface (2nd step), it can leave the solid (3rd step) having a kinetic energy of $E_{kin} = \hbar\omega - (E_F - E_i) - \phi$.

Step 1: The absorption of a photon and thus the optical excitation of an electron in the solid

Neglecting the momentum of the photon, an optical excitation of an electron is a direct transition[81] in the reduced zone scheme.

The interaction of an electron with a time-dependent vector field[82] $\vec{A}(\vec{r},t)$ is given by the Schrödinger equation[83]

$$i\hbar\frac{\partial}{\partial t}\psi(\vec{r},t) = H\psi(\vec{r},t) = \left[\frac{1}{2m}\left(\frac{\hbar}{i}\vec{\nabla} - \frac{e}{c}\vec{A}(\vec{r},t)\right)^2 + V(\vec{r})\right]\psi(\vec{r},t) \qquad \textbf{(II.1.48)}$$

---

[81] Also called: momentum conserving or vertical transition

[82] $\vec{E} = -\frac{1}{c}\frac{\partial\vec{A}}{\partial t}$ i.e. $\vec{B} = rot(\vec{A})$

[83] In the non-relativistic case

with the electron's wave function $\psi(\vec{r},t)$, and the undisturbed potential $V(\vec{r})$.

It is possible to separate the Hamiltonian H into an undisturbed part H_0, and an interaction part H_{int}

$$\begin{aligned} H_0\psi &= \left(-\frac{\hbar^2}{2m}\Delta + V(\vec{r})\right)\psi \\ H_{int}\psi &= \frac{1}{2m}\left[-2\frac{e\hbar}{ic}\vec{A}\cdot\vec{\nabla} - \frac{e\hbar}{ic}\left(div\vec{A}\right) + \frac{e^2}{c^2}\left|\vec{A}\right|^2\right]\psi \end{aligned} \qquad \textbf{(II.1.49)}$$

In the case of weak electromagnetic fields, the last term of the operator of interaction may be neglected. The part including $div\vec{A}$ may not be suppressed by an appropriate gauge with means of a surface potential. It may even become relevant to describe surface effects. However, it is rather small in the bulk and thus being neglected in the following.

Thus the resulting Hamiltonian of interaction[84]:

$$H_{int} = -\frac{e\hbar}{imc}\vec{A}\cdot\vec{\nabla} = -\frac{e}{mc}\vec{A}\cdot\vec{p} \qquad \textbf{(II.1.50)}$$

The transition rate W_{fi} from an initial state $|\mathrm{i},\mathrm{k_i}\rangle$ to a final state $|\mathrm{f},\mathrm{k_f}\rangle$ resolves, by using time-dependent 1st-order perturbation theory, in[85]

$$W_{fi} \propto \frac{2\pi}{\hbar}\left|\langle f|H_{\mathrm{int}}^{'}|i\rangle\right|^2 \cdot \delta\left(E_f - E_i - \hbar\omega\right) \qquad \textbf{(II.1.51)}$$

Where the conservation of energy is ensured by the δ-function. By neglecting the momentum $\vec{q}$ of the photon[86] (dipole approximation) the assumed plane wave $\vec{A}(\vec{r},t) = A_0 \cdot exp(-i\omega t + i\vec{q}\vec{r})$ becomes spatially constant, and it is possible to show that eq. (II.1.51) transforms to

$$W_{fi} \propto \left|\vec{A}_0\langle f|\nabla V|i\rangle\right|^2 \cdot \delta\left(E_f - E_i - \hbar\omega\right) \qquad \textbf{(II.1.52)}$$

This optical transition rate is only relevant, if ∇V is large. However, in a free electron gas, V is constant, therefore ∇V = 0, and there is no possible transition: the conservation of energy and momentum may not be fulfilled simultaneously. It turns out that for an optical transition the lattice potential needs to provide the desired momentum.

---

[84] $\vec{p}$ is the momentum operator of the electron

[85] Fermi Golden Rule

[86] It is much smaller than the momentum of the electrons in the crystal

Step 2: The transport of this excited electron to the surface

The transport of an electron from its excited position to the surface is being disturbed by possible relaxation processes of this electron. The dominant scattering mechanism that reduces the number of photoexcited electrons reaching the surface with E_f is the electron-electron interaction. Other possible processes may be the excitation of plasmons, the inelastic scattering with phonons or the elastic scattering on defects and impurities. Only the unscattered (ballistic) electrons with conserved energy and momentum are simple to describe, all other electrons produce signals that are not directly correlated to the energy and/or momentum. The inelastic scattering processes determine the escape depth to about some tenth of Å. Photoemission spectroscopy might be quite surface sensitive.

Step 3: The transmission of that electron into the vacuum

The transmission into the vacuum is feasible for all electrons which possess a momentum with a component directed to the surface ($\Rightarrow k_{\perp}^{vac} > 0$), and an energy that is enough to surmount the barrier[87]. Apart from that, the facts stated on page 47, concerning the components of the momentum perpendicular and parallel to the surface, describe this third step.

The three-step model consists of some shortcoming, which are just phenomenological. It does not, for example, consider of the quantum mechanical uncertainty relation in the location of energy and momentum. However, Feibelman and Eastman[88] demonstrated, that for weak damping in the near UV, the three-step model is still usable.

2) The one-step process

The description of the one-step process does not need to use phenomenological considerations, like those at the three-step process. For an excitation from one band to another, normally there has to exist a real and unoccupied state at the final energy, with the exception at the surface, where an electron may be excited to a so-called *inverse LEED-state*. This inverse LEED-state is a special state, which *has not* to lie in a band: The plane wave in vacuum has an exponential decay tail in the solid, an excited electron at the surface may couple to this tail and thus to the vacuum.[89] (Fig. 18).

---

[87] $E_{\perp} = \frac{\hbar^2 k_{\perp}^2}{2m} > \phi$

[88] [FE74]

[89] Further details on the inverse LEED theory of photoemission spectroscopy are written in [Mah70], [FE74] and [Pen76]

c. The two-photon photoemission (2PPE)

The occupied energy states, i.e. core and valence electrons of a solid, can be analysed by using photoemission spectroscopy with different photon energies. To observe the unoccupied states above the Fermi level, there is - among others – a well known technique, called inverse photoemission spectroscopy (IPE). Via impinging of slow electrons (some eV) onto the surface, one generates outcoming photons, which can then be measured. However, inverse photoemission spectroscopy has at least two disadvantages. First, it is limited to unoccupied states[90], and second the poor energy resolution makes it difficult to obtain dynamical information of ultrafast electronic relaxations of excited states from the linewidth measurements of an IPE spectrum. Those limitations vanish by using the two-photon photoemission spectroscopy (2PPE) used for this work. It combines both advantages of traditional one-photon photoemission and of inverse photoemission spectroscopy, by providing an opportunity, which allows a simultaneous observation of occupied and unoccupied excited states.

For the following, it is important to define the polarisation of incident light, as how it is used in this work (Fig. 20). Hereby the usual conventions are taken, using the abbreviation *s-polarisation* for light that has the $\vec{E}$ vector perpendicular to the plane of incidence, and *p-polarisation* for light with $\vec{E}$ parallel to the plane of incidence.

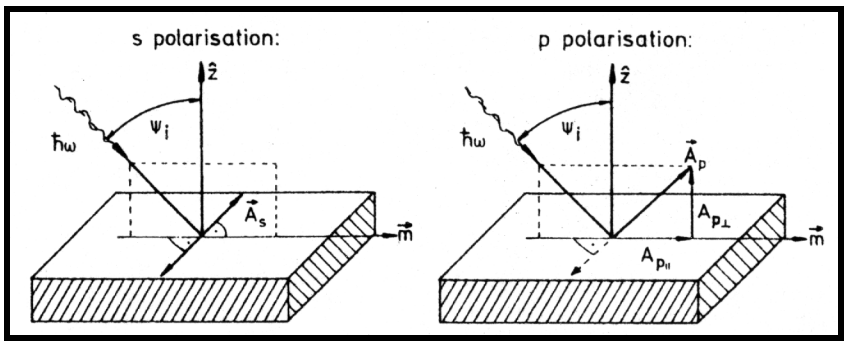

Fig. 20: Definition of directions used in photoemission experiment with polarised light. The incident light and detected electrons are in a mirror plane. From [Hüf95].

Photoemission may occur not only by absorbing a single photon, which has an energy that exceeds the work function ϕ, but also by successive absorption of two photons. Those photons may be called[91] "pump" and "probe", and their energies $\hbar\omega_{pump}$ and $\hbar\omega_{probe}$ fulfil the conditions

[90] This limitation can also be an advantage in some cases
[91] Shortly the advantage of such a differentiation of both photons will become evident

$$\begin{aligned} \hbar\omega_{pump} &< \phi \\ \hbar\omega_{pump} + \hbar\omega_{probe} &> \phi. \end{aligned} \qquad \textbf{(II.1.53)}$$

Those photons may of course be different in *energy* and *polarisation*. In case of two different energies, it is called a *two-colour experiment*.

The 2PPE excitation consists of two steps: The excitation of an electron to an intermediate level (step 1), from where a second excitation may lift the electron above the vacuum level (step 2). Therefore, the 2PPE procedure is a *non-linear process*. For this, the 2nd-order perturbation theory leads to the transition probability:

$$W_{f,i} \propto \frac{I_1 \cdot I_2}{(\omega_f - \omega_i - \omega_1 - \omega_2)^2} \cdot \left| \sum_k \frac{\mu_{k,i} \cdot \mu_{f,k}}{(\omega_k - \omega_i - \omega_1)} + \frac{\mu_{k,i} \cdot \mu_{f,k}}{(\omega_k - \omega_i - \omega_2)} \right|^2 \qquad \textbf{(II.1.54)}$$

where $I_{1,2} = \left|\vec{E}_{1,2}\right|^2$ are the intensities of the pulses, and $\vec{\mu}_{x,y} = \left\langle \psi_x \middle| \vec{r} \middle| \psi_y \right\rangle$ stand for the dipole transition moments. The measured signal is proportional to $\mathbf{S \propto I_1(\hbar\omega_1) \cdot I_2(\hbar\omega_2)}$.

A 2PPE spectrum represents the energy distribution curve of the photoelectrons, measured as a function of the kinetic energy. As already mentioned above, 2PPE spectroscopy enables to study occupied initial states, unoccupied intermediate states, and unoccupied final states. It gives the invaluable possibility to analyse the time-resolved evolution of states above the Fermi level. The spectral feature of the 2PPE spectra depends not only on the electronic properties of the initial and intermediate states but also on the excitation photon energy. It has been well established that a feature in a 2PPE spectrum may be easily assigned to an initial, intermediate or final state, depending on the peak shift with pump and probe photon energy (see Fig. 21).

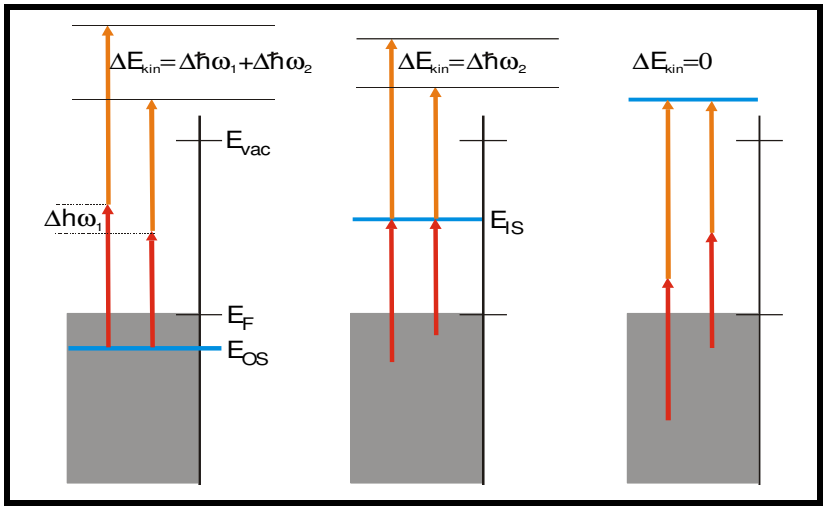

Fig. 21: The shift of a feature in a 2PPE spectrum depends on the photon energy changes and on the position of the probed electron state E_{os}.
a) Constant initial state spectroscopy (CIS)
b) Probing of an intermediate state and
c) Constant final state spectroscopy (CFS).

a) If coherent two-photon excitation from an occupied state E_{os} below Fermi level brings an electron above vacuum level, the photoelectron kinetic energy E_{kin} shifts to $E_{kin} = \hbar\omega_{pump} + \hbar\omega_{probe} + E_{OS}$.

b) If it is due to two independent processes, i.e. transient population in an intermediate state E_{is} by $\hbar\omega_{pump}$ and a subsequent excitation above E_{vac} by $\hbar\omega_{probe}$, it varies with $\hbar\omega_{probe}$ according to $E_{kin} = \hbar\omega_{probe} + E_{IS}$.

c) If an unoccupied state lies above E_{vac}, the final state $E_f > E_{vac}$, populated by two-photon excitation, couples to a continuum of free photoelectrons, so that E_{kin} is independent of photon energy $E_{kin} = E_f$.

It should be noted here that these simple shift relations hold only when there is no dispersion of the relevant electronic states along the normal component of the electron wave vector to the surface. This has been well demonstrated by S. Pawlik et al.[92] comparing 1PPE and 2PPE spectra on Ag(111).

In Fig. 22, the energy levels are summarised as how they appear in the measurement of this work. Here a *negative* bias V_{bias} applied between the sample and ground is assumed, as well as a sample work function ϕ_{sample}, and an analyser having a work function $\phi_{analyser}$. Then, the highest (E_{kin}^{max}), and the lowest kinetic energy (E_{kin}^{min}) detectable lie at

[92] [PBBA98]

$$\begin{aligned} E_{kin}^{max} &= \hbar\cdot(\omega_1+\omega_2)-(\phi_{analyser}+eV_{bias}) \\ E_{kin}^{min} &= \phi_{sample}-(\phi_{analyser}+eV_{bias}) \end{aligned} \qquad \textbf{(II.1.55)}$$

Therefore, the range of detectable energy is: $\Delta E_{kin} = \hbar\cdot(\omega_1+\omega_2)-\phi_{sample}$.

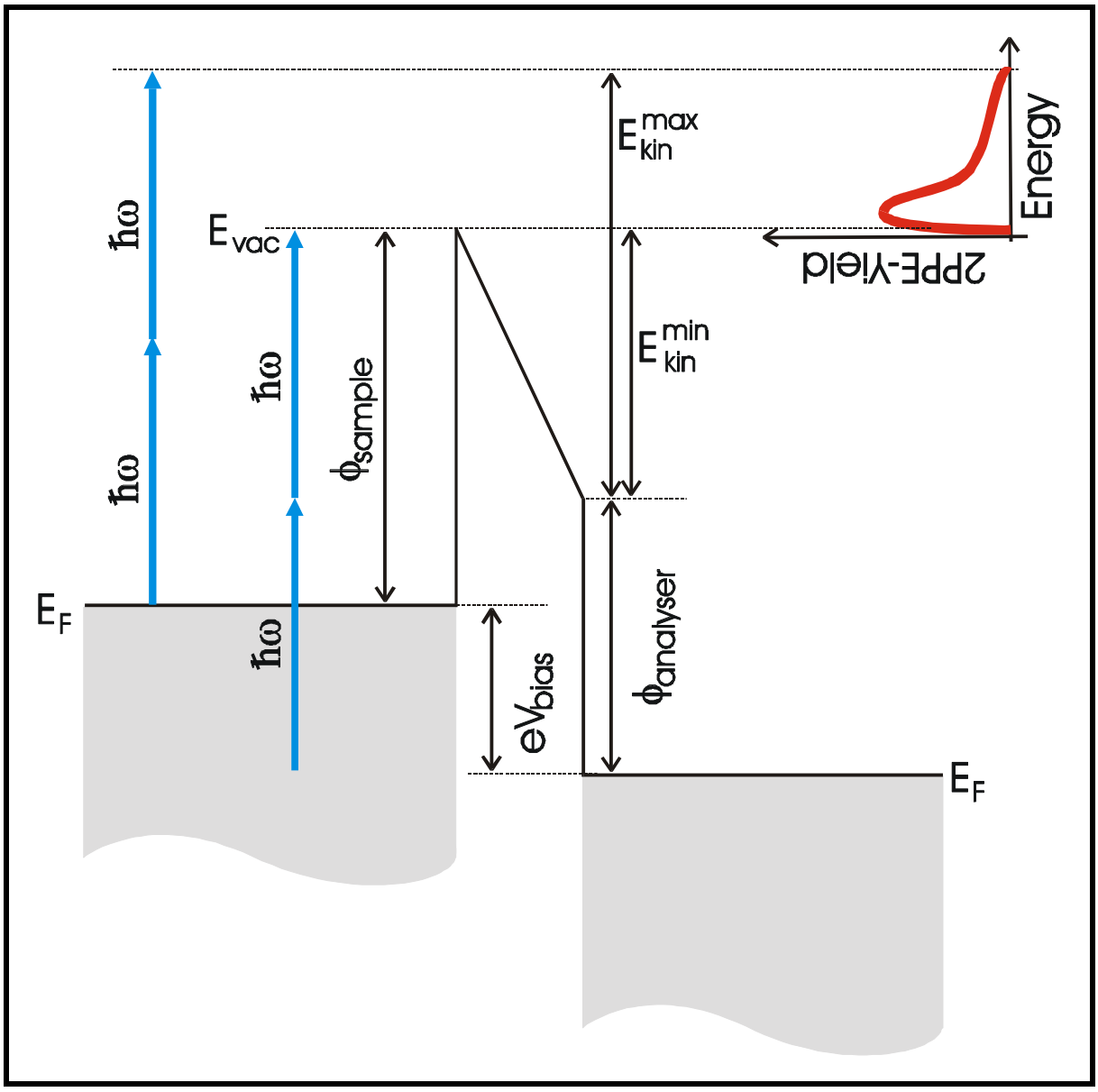

Fig. 22: A schematic picture of the energy levels in the experiment. With this, one can easily determine the highest and the lowest kinetic energy that are able to be measured. Also depicted is a schematic 2PPE spectrum.

d. The time-resolved two-photon photoemission (TR-2PPE)

Thanks to intensive and fruitful research and progress of generating ultrafast laser pulses in the last decade, one has the chance to get direct access to dynamical electronic properties in the time domain down to femtoseconds. This led to very interesting and important knowledge in many contexts. By means of those short laser pulses and some more equipment (chapter III.3), it is possible to perform time-resolved two-photon photoemission (TR-2PPE).

The principle of TR-2PPE is based on a pump-probe method, sketched in Fig. 23.

With the photons of the *first pulse*, electrons are being excited into an intermediate state above the Fermi level. A time-delayed *second pulse* excites the electrons above the vacuum level, where they can couple to vacuum wave functions, and be registered in the analyser. Until the second pulse affects, the electrons undergo different processes[93], which lead to a depopulation[94] of this intermediate state.

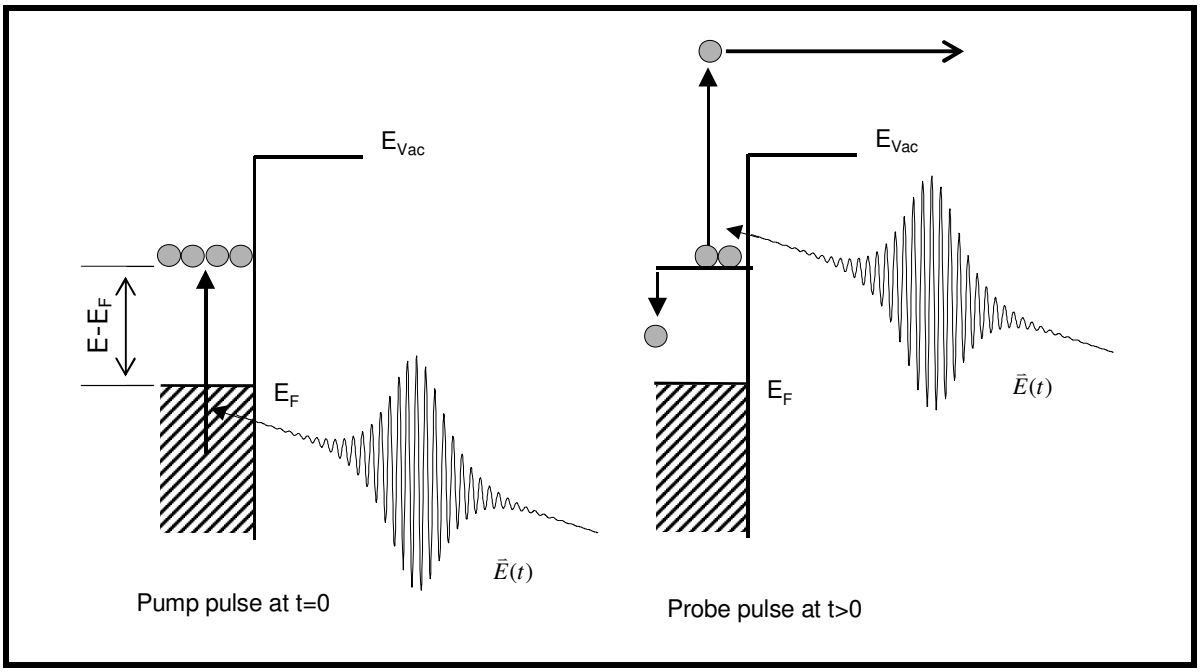

Fig. 23: Pump-Probe principle. A short laser pulse excites electrons to intermediate states. Until the second pulse probes the excited population, the electrons may suffer relaxation processes. The amount of the remaining population at the intermediate state is a mass for the relaxation process.

[93] For example: electron-electron, electron-phonon, electron-plasmon, …
[94] Energetically or by loss of their phases

By changing the delay between the two pulses, the evolution of a populated energy level can be measured. Because of many different relaxation mechanisms, there will be a time dependent population, which is a unique property of this intermediate energy level and of the observed system.

Important to stress is that the dynamics of the intermediate state[95] is studied not of the final state. That is the reason, for most of the considered energies in this work to be described by the difference to the Fermi level ($E-E_F$).

The use of two short laser pulses impinging onto a material (as described above) produces time-dependent electron distributions (=2PPE-Yield) that show the superposition of both pulses (*autocorrelation curve*, see also appendix VIII.4).

$$S = \Phi_1 \times \Phi_2 = \int_{-\infty}^{\infty} \Phi_1(t) \cdot \Phi_2(t-\tau) dt \qquad \textbf{(II.1.56)}$$

where $\Phi_{1,2}$ represents the pulse intensity shapes, and S is the measured signal.

A signal S like this is only detectable in systems with infinitely fast relaxation[96] processes. A (non-vanishing) lifetime of excited electrons in the intermediate state broadens this laser autocorrelation curve. In a first-order approximation, one may assume having *only one relaxation process* (electron-electron scattering) that reduces the considered population *exponentially* from the observed state. The longer the relaxation time τ, the wider the autocorrelation curve becomes (Fig. 24).

$$S = \Phi_1 \times \mathrm{e}^{-t/\tau} \times \Phi_2 \qquad \textbf{(II.1.57)}$$

As long as one measures *phase-averaged*[97], most information about the relaxation mechanisms is included in that expansion of the curve. In a *phase-conserving* experiment, one can learn much more by analysing the change of the fast oscillating parts of the interference measurement (appendix VIII.4 and Fig. 73).

[95] Determined by the energy of the *first* photon
[96] Instantaneous
[97] I.e. the phase of the electromagnetic wave packet is averaged

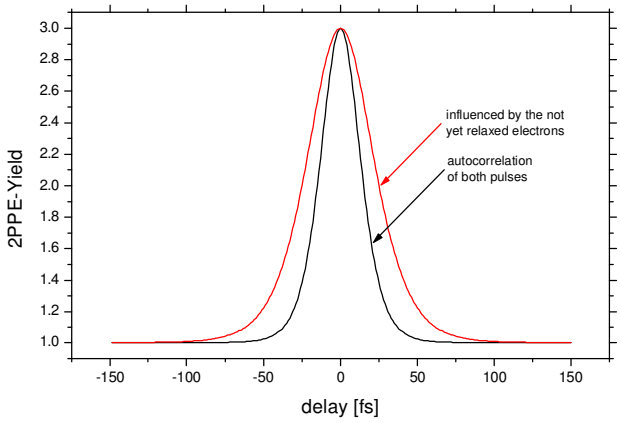

Fig. 24: The autocorrelation curve of two short laser pulses described by the time dependent population of electrons excited by two pulses; and the influence of delayed relaxation of excited electrons.

As shown above, one distinguishes in the two-photon photoemission spectroscopy between *two principle sorts* of electron excitation. The excitation with two photons having the *same* energy $\hbar\omega_1 = \hbar\omega_2$, ("one-colour experiment") and the excitation with two photons having *different* energies $\hbar\omega_1 \neq \hbar\omega_2$ ("two-colour experiment").

Due to the detection of two different intermediate states[98] (E_1, E_2), (Fig. 25b) with usually different relaxation times ($\tau_1 \neq \tau_2$), the autocorrelation curve becomes *asymmetric* in a *two-colour experiment* (Fig. 25a). It shows at *negative* delays[99] the influence of the population at one energy level, and at *positive* delays[100] that of the other energy level. This leads usually to a more difficult analysis of the involved relaxation processes, and to a more difficult determination of the time-zero point. However, the advantages of a two-colour experiment compensate some disadvantages: One has the possibility of measuring a larger energy range, there arise fewer problems caused by coherence, and the result is a function of two different energies, simultaneously.

As mentioned already, usually many relaxation processes take part in a TR-2PPE experiment, namely sorts of inelastic and elastic relaxations. The shape of a measured autocorrelation curve in a TR-2PPE experiment is therefore rarely described only by a *relaxation time* τ, but rather by at least *two parameters*: one for the *inelastic* relaxation, another for the *elastic*.

[98] Both pulses act as "pump" pulse only at different delays
[99] Pulse "red" before pulse "blue"
[100] Pulse "blue" before pulse "red"

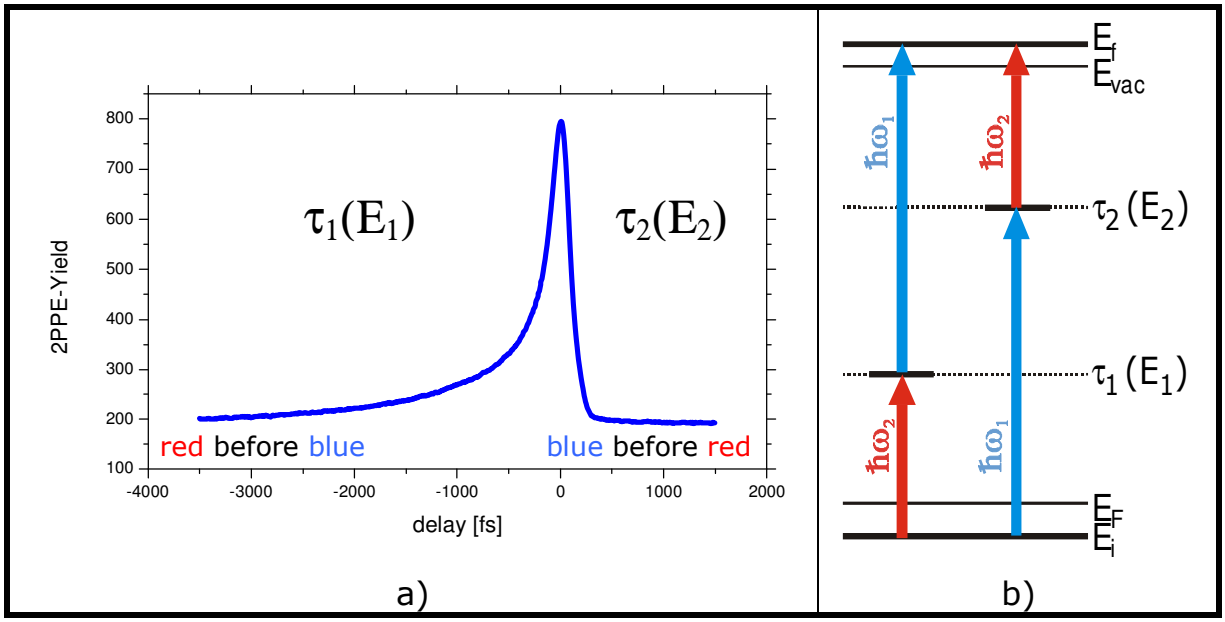

Fig. 25: Two-colour TR-2PPE
a) The time-evolution of two excited states (at GaAs)
b) Two-colour experiment enables to measure two different relaxation times at different energies. In addition, it expands the range of detectable energies.

From various research topics, like NMR or atom scattering, the following equation has been adopted to photoemission spectroscopy and to TR-2PPE, with great success. It combines the linewidth Γ in a spectrum, with the inelastic lifetime (T_1), the elastic lifetime[101] (T_2^*), and with the dephasing time[102] (T_2).

$$\frac{\Gamma}{2} = \frac{1}{T_2} = \frac{1}{2 \cdot T_1} + \frac{1}{T_2^*} \qquad \textbf{(II.1.58)}$$

where

T_1 : Inelastic lifetime
T_2^* : Elastic lifetime (pure dephasing)
T_2 : Dephasing time
Γ : FWHM of the linewidth in the spectrum

TR-2PPE gives the possibility to observe both relevant times (T_1, T_2^*), whereas purely optical investigations like second harmonic generation (SHG) may only detect a combination of them.

There were many attempts to get a fitting-tool for the determination of T_1, T_2 and T_2^*, in order to analyse the TR-2PPE-data more adequately. A useful one is the simulation of the autocorrelation curves with means of the Liouville-von Neumann – equations (LvN). Normally, the data are fitted with those coupled differential equations. For further information please see appendix VIII.4 and e.g. in [Bau97].

[101] Also called *pure dephasing*,
[102] Thus the term *dephasing time* stands not only for a phase-change, but rather for *any* change (inelastic and/or elastic) of the quantum mechanical state.

III. The experimental requirements

The measurements shown here demand a sophisticated set-up in order to fulfil the required conditions that are:

a) Ultra-high vacuum chamber:
It should be measured exactly the considered system, this means to avoid exciting electrons from impurities on the surface like carbon, nitrogen or oxygen, but only electrons from the surface or the bulk of the investigated material; for example of silver. This condition, and the need for long mean free paths of the electrons, leads to the requirement of an ultra-high vacuum chamber (UHV). With that apparatus, it is possible to produce clean surfaces, free them from impurities, and hold them in a vacuum to let them stay clean.

b) Ultra-short laser pulses:
Second necessity is as important as the first one above. The main goal was to detect optically excited electrons and the dynamics of them by means of a real time experiment. The energy decay lasts only some femtoseconds to tens of femtoseconds. That is the reason for the need of an excitation source, which produces pulses in the same time region. The source was a Ti:sapphire-Laser, which generates pulses of about 25fs to 50fs.

c) E-beam evaporator:
A quite essential part in this work is the production of thin films of material with a thickness of a few monolayers[103] up to some hundreds. Indifferently, whether those layers have to be grown epitaxially or not, a material source is needed, which evaporates clean materials. That is reached by using a 3-fold e-beam evaporator.

The used set-up for the experiments is depicted schematically in Fig. 26. In the following sections, the main parts will be described in more detail.

[103] A "monolayers" is an arrangement of some films, having the height of one atom each, and lying one above the other. Another term for it is "multilayer". If the growth mode of the multilayer show a layer-by-layer arrangement, one can speak of a coverage of "x monolayers", otherwise it is better to speak of "nominal x monolayers", this means, there is the same amount of adatoms, as if there were flat layers.

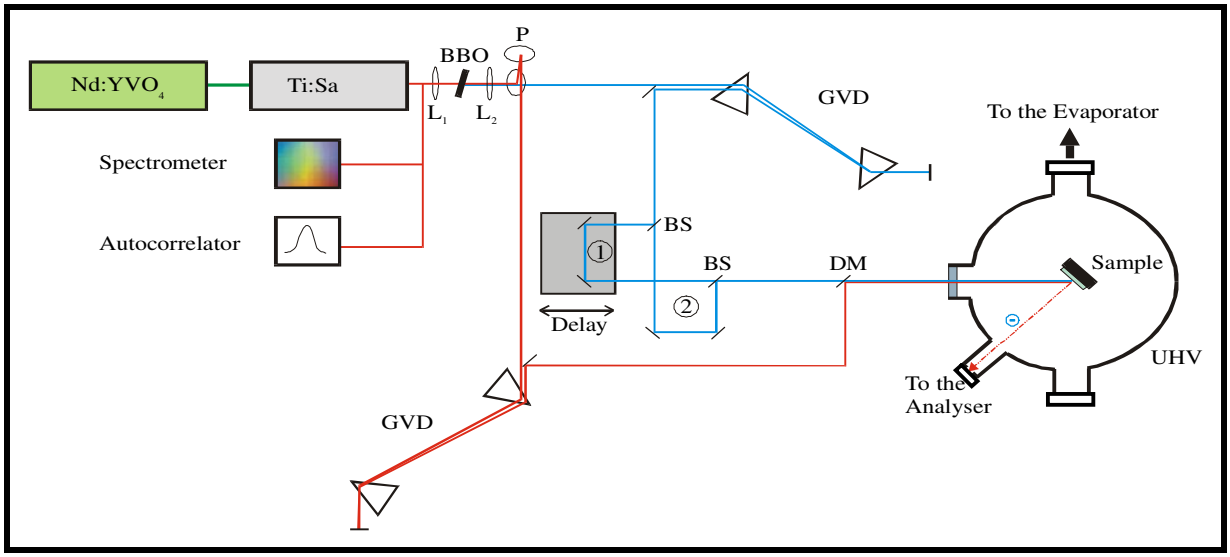

Fig. 26: Schematic plot of the used set-up. Possible are two-colour experiments (blue/red) as well as one-colour (blue/blue). (L=Lens, GVD=Group velocity dispersion, BBO=β-barium borate, BS=Beamsplitter, DM=Dichroid mirror, P=Periscope, Ti:Sa=Ti:Sapphire-Laser)

Some details of the following description were already explained at different places[104]. Hence, it will be illustrated here only briefly.

1. The ultra-high vacuum system

a. The main chamber

The investigations were carried out in a µ-metal screened stainless steel chamber, at a base pressure of about $1x10^{-10}$ mbar. This could be achieved by a three level pump system. The first raw vacuum has been attained by pumping with an oil-driven fore pump[105]. Therewith one gets 10^{-3} mbar. After that, a turbo molecular pump[106] of 520l/s followed. In combination with the following 210l/s ion-getter pump, a pressure in the region of 10^{-10} mbar has been made. Due to the bad efficiency of the turbo- and the ion-getter pump to reduce atomic hydrogen, a titanium sublimation pump was used. In this way $1x10^{-10}$ mbar became reachable.

Besides the pumping system, more instruments have been applied. Some were used to characterize the surface geometry (LEED[107]) or the cleanness of the material (Auger-spectroscopy using an e-gun[107] and a

[104] [Aes96], [Bau97], [Paw98], [Bur98], [Ohm02], [Sch02]
[105] From Edwards and Pfeiffer
[106] From Pfeiffer
[107] From Omicron

mass spectrometer[108] QMA) of the investigated sample. An argon ion sputter gun[107] has been utilised to bombard the surface, and in combination with the sample heating possibility up to 1200 K (resistive heater mounted on the manipulator behind the sample[107]), it was feasible to treat the sample by sputtering/annealing cycles, and therefore to remove impurities like carbon and oxygen. Furthermore, it was possible to cool the sample with liquid nitrogen.

The sample could have been transferred by a linear transfer stage[109] to a manipulator[107,109], where it has been held, and could be rotated (both angles) as well as moved up and down.

To measure the emitted photoelectrons, the use of an energy analyser in the form of a so-called cylindrical sector analyser[110] (CSA300) has been made. Whenever needed, there was the option to change the original set-up to measure also the spin, or to have five detectors at the same time. This analyser has an in-build electromagnetic lens; nevertheless, a negative bias on the sample was used, to attenuate the stray field, and to direct the electrons to the analyser's entrance slit.

b. The evaporator chamber

It was a special interest to grow atomically thin films with only a few monolayers in height. This has been carried out in an additional UHV chamber, connected to the main investigating chamber. A base pressure of $1x10^{-10}$ mbar and a pressure while preparing the film (=evaporation) of $< 8x10^{-9}$ mbar is produced again by a fore pump[106] and a turbo pump[106] of 70l/s.

Mounted on the main 6-way-cross there is, beside others, a multifunctional, self-designed device (from Hositrad) to hold the sample at a fixed position, to cool the sample with liquid nitrogen, to measure the sample's temperature, and to hold the quartz of a microbalance next to the sample. This microbalance is used to determine the frequency change caused by the additional mass while evaporating material. It stands exactly opposite to the main device, the evaporator itself.

That 3-fold e-beam evaporator[111] enables to evaporate three different materials, sequentially. It has an inbuilt flux tube to quantify and cross-calibrate the adsorbed amount of atoms and monolayers. To cross-calibrate, an atomic force microscope was used. Normal flux rates, as used for silver, were about I_{Flux} = 1µA, which gives a deposition rate of about 1ML/30sec or 1Å/15sec.

[108] From Balzers
[109] From VG
[110] Form Focus
[111] From Omicron

2. The preparation of the samples

While those measurements were carried out, many different samples were investigated. Usually, the (generally known) preparation method was adapted to the observed material. Some had to be etched with acids (GaAs[112]), others were made clean by removing the contamination with scotch-tape (graphite HOPG). Furthermore, many samples needed a daily maintenance like heating (HOPG, GaAs, MgO), cooling/annealing (GaAs) or sputtering.

Equal for all samples was, that they were cut and prepared in air, and mounted on a sample holder[113]. They became attached with conducting silver, in order to fix them and to make sure other electrons may replace the missing photoelectrons via conductance. Without such a connection, charging problems could arise. A routinely task was to check the surface quality with LEED and Auger, and often with STM/AFM also.

Whenever necessary to deposit material (Ag, Fe, Ta) on a substrate, the evaporating flux was controlled via the quartz microbalance and the in-build flux control. As soon as have had stable state, i.e. no fluctuations in the flux, in the vacuum's pressure and in the substrate temperature for 1 minute, the sample was moved to the evaporator. During the deposition process, the flux control device managed the power, in order to have the same flux during the whole process.

At the early phase of the investigations, an e-beam evaporator was used in combination with a quartz microbalance, which led to produce layers with an accuracy of about ±7%. That means, that all thickness values given in the chapter about silver on HOPG (see later) have also an accuracy of about ±7%. The following depositions had an accuracy of about ±5%.

Usually, the silver adsorption happened at room temperature, and the substrate was also at room temperature. The deposition of silver on GaAs was carried out at T < -150°C, and subsequent annealing to room temperature.

[112] The procedure is described in [Ohm02]
[113] From Omicron

3. The laser system

To generate the needed short pulses, a tuneable (λ=700nm–900nm), mode-locked Ti:sapphire laser (Tsunami[114]) was used. It usually ran at λ=790nm, where the laser's optimum lies. The wavelength could be adjusted to the specific requirements. This laser was first pumped by a 10W-Argon-ion laser (BeamLok[114]) and later by a 10W-Nd:YVO_4 solid-state-laser (Millennia[114]). The pulses have a length of 25fs to 50fs, an energy of about 10nJ/pulse, and a sech²-shape. They follow with a rate of ν=80MHz. The integrated power reaches about 1W. An autocorrelator[115] and a SPIDER[115] control their shape and FWHM (full width at half maximum). The laser beam is, after transmitted through the output Brewster window, linearly s-polarised (= vertical to the table).

In order to have the possibility to utilize not only the origin wavelength, the ability of a thin (0.2mm) BBO-crystal (β-barium borate) to produce the second harmonic of the laser light was used. It has a rate conversion of 5-10%, and generates photon energies of $E_\gamma \approx 3$eV from $E_\gamma \approx 1.5$eV. The polarisation of the beam changes thereby from s to p.

Normally, all optical elements, like mirrors, lenses, windows, etc., cause a higher order dispersion of the group velocity (GVD) of the laser pulse. In order to have transform-limited (= time bandwidth-limited) pulses, without chirp, one has to pre-compensate this dispersion. This can be achieved by using a prism set-up developed by R.L. Fork[116]. The laser beam is being directed through two prisms and back. They allow the red part and the blue part of the light to reach the sample, after going through all optical elements, at the same time.

In order to have the possibility of measuring with p-polarised as well as with s-polarised light, one may use either a half-wave plate or a construction with four mirrors, which also changes the polarisation. The latter method should be preferred, because of less group velocity dispersion.

The laser beam is sent trough a Michelson-interferometer, where it is divided into two equal parts[117], using a 50%-beamsplitter. One of them is being directed to a mirror pair on the delay-stage, and the other part is reflected on two or on four unmoveable mirrors, having same polarisation or being cross-polarised at the end, respectively. They remerge (time-delayed) in a second 50%-beamsplitter and are then collinearly focussed (f=200mm) through an input UHV-window (fused silica) to the sample in

[114] From Spectra-Physics
[115] From APE
[116] [FMG84]
[117] Seen in Fig. 26 named by (1) and (2)

the UHV chamber, where the spot has a diameter of about 50µm-100µm. See Fig. 26.

One of the central elements on the optic part is the linearly moveable, computer-controlled, positioning stage (Compumotor[118] PC21), which delays the branch (1) compared to branch (2) in the interferometer. It has a stepper motor, with a repeatability of about 50nm, which corresponds to about a tenth of femtosecond. It is moveable in the range of about 15cm, with an accuracy of 25nm. Using this "delay-stage", one gets rid of controlling electronically femtoseconds, which is not possible, and come to the opportunity, to control µm and nm, which is not really a problem anymore. That delay-stage carries two mirrors, which therefore can delay the pulses.

[118] From Parker

IV. The results

In this main chapter, some new effects and characteristics of the electronic system in small metallic structures will be shown. The used time- and energy-resolved two-photon photoemission technique is known to be adequate for studies of occupied and unoccupied states of metals, semiconductors and insulators.

The main way followed in the measurements, was to approach - from many different sites - the final goal: the understanding of the dynamics of optically excited electrons in small-extended configurations.

Experimentally, the transition from an already known 3d behaviour of the electrons, via a 2d performance to that of small clusters was tested. It is essential to understand the ongoing process while reducing the crystal's dimensions. It is also imperative to explain it for next coming techniques in the semiconductor industry, for example.

Measurements of *silver on graphite*, which show an enormous thickness-dependence in the lifetime of optically excited electrons will be firstly indicated. Then the system of *silver on the semiconductor GaAs* follows, in which the influence of small amount of silver, the time-resolved arising and refilling of a silver state in the gap of GaAs as well as the fortunate success of inverse spin injection will be demonstrated. Afterwards, the configuration of *silver on the insulator MgO* will be regarded in details, in which the influence of the substrate shall be neglected. Thereby, a huge increase of the lifetime of optically excited electrons, in a confinement of a thin film will be observed.

1. State of the art

The decision to use silver as the investigated material had some reasons. From earlier measurements[119], it became fact that optically excited electrons in silver behave quite well as predicted by Fermi-liquid theory. Despite the fact that aluminum, which seems on a first thought to be more adequate, because of having only sp-bands and no d-bands in the region around Fermi energy.

[119] [Aes96], [Bau97], [Paw98]

It was heavily debated for long time, why aluminum, known to be a nearly perfect free electron material, does not show a simple behaviour. One was surprised about the pre-factor of "$\tau_0 = 17fs \cdot eV^2$", needed to fit to FLT ($\tau = \tau_0 \cdot (E-E_F)^{-2}$), instead of the predicted "$\tau_0 = 70fs \cdot eV^2$". Its analyses have delivered two possible reasons. One explanation predicts an unexpected strong influence of transport[120] (transport time T_{trans}=23fs), which has to be taken into account[121]. Another possible reason is based on the polyvalent structure of aluminum, which leads to a degeneracy of the different valence bands, resulting in parallel bands, which open an additional decay channel.

Although noble metals (Ag, Au, Cu) seem to be less suitable as model system for FLT, due to their mono-valence[122] and localised d-electrons, the electron dynamics cannot be influenced by a parallel band effect in the investigated energy range, as in the case of aluminum. However, one must be aware of possible deviations from free electron behaviour due to the d-bands located well below the Fermi edge, but still within the conducting band. Enhanced screening[123] as well as additional decay channels, e.g. by interband transitions due to the excitation of electrons from the d-band into the sp-band, may be the result of this additional electronic structure.

The onset of the d-bands of *silver* at 4eV below E_F makes this electron system the most suitable Fermi liquid system in the row of noble metals. One can be sure of not exciting electrons via direct interband transition paths, because of the smaller excitation energy used (E_γ=3.1eV). It could be demonstrated, that silver behaves quite perfectly like a FLT system; over the full accessible energy range (see Fig. 27b). This is to be seen in comparison with gold and copper, both showing different additional relaxation paths, caused by the higher lying d-bands, leading to secondary electrons (Auger-like decay of longer living d-band holes).

[120] The meaning and influence of transport will be explained on the next page
[121] [Bau97]
[122] One conducting electron per crystal atom
[123] [Qui63]

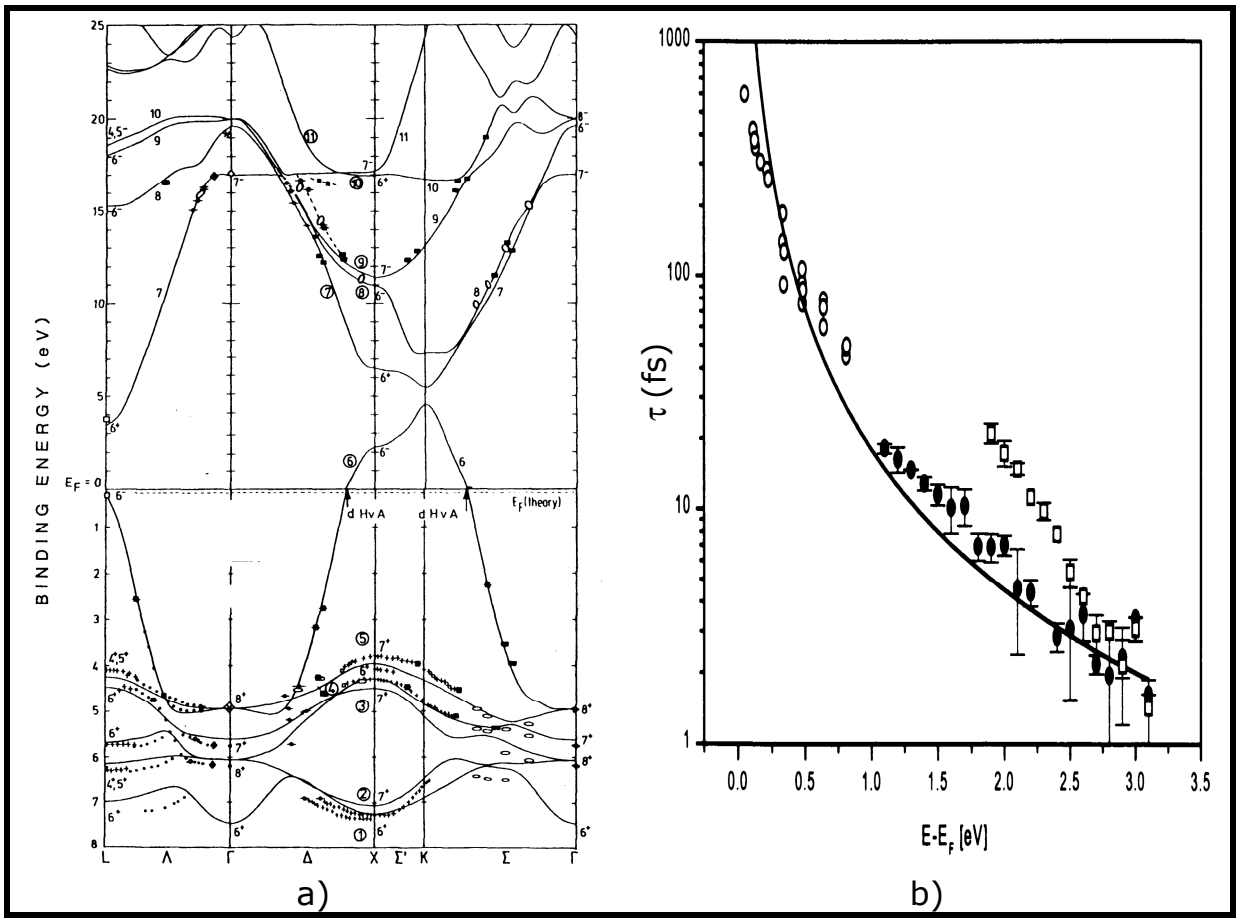

Fig. 27: Band structure and lifetime of silver

a) Band structure of Ag. Indicated are calculated lines ([EFN84]), and measured points ([WCLH85]).

b) The measured lifetime of Ag. Full circles come from polycrystalline silver ([Bau97]), open circles were determined on Ag(110) ([Kno97]), and the open squares show polycrystalline gold ([Bau97]). The solid line represents the behaviour expected from Fermi liquid theory for silver.

The results in Fig. 27b) are hampered by transport effects. Whenever electrons in a bulk material become optically excited[124], they emerge in a ballistic movement away from the illuminated and investigated area. Ballistic transport model calculations were made[125], based on the fact that excited electrons are free to move with equal probability in all directions without suffering any collision within the mean free path; and at the surface, they undergo a total elastic reflection. Those calculations led to absolute values of τ_{trans}, which could then be included[126] for the measured lifetime:

$$\frac{1}{\tau_{measure}} = \frac{1}{\tau_{decay}} + \frac{1}{\tau_{trans}} \qquad \textbf{(IV.1.1)}$$

[124] So-called: hot-electrons
[125] [Aes96], [Kno97]
[126] Matthiessen's rule

Hereby, refilling processes (cascade and Auger electrons) are neglected and it is assumed, within a 1st-order approximation, separate mechanisms for decay and transport. This leads to a seeming lifetime, which is smaller than the real relaxation time τ_{decay} (Fig. 28b). Hence, the depletion of an excited-state population in the probed surface region, as a function of the time delay between the two pulses, depends on the intrinsic decay of the excited energetic state and of the transport of the electrons.

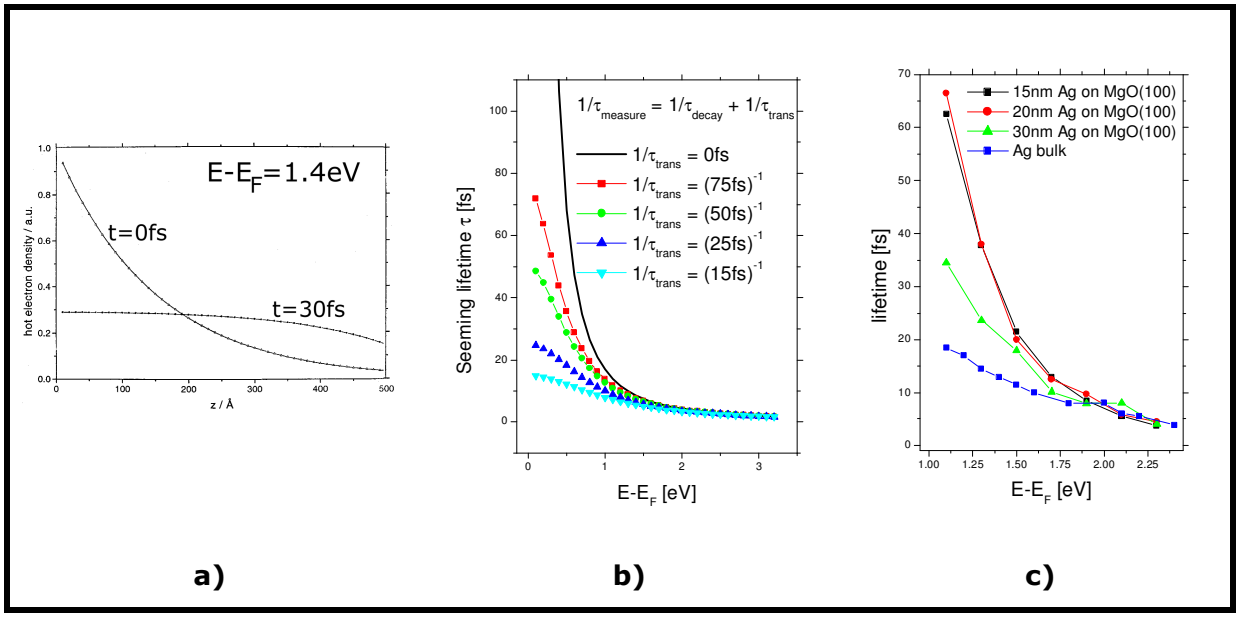

Fig. 28: The influence of the transport effect to the measured lifetime.

a) Calculation showing the influence of ballistic transport of excited electrons in metals. It is clearly visible, that the more time passed since the excitation, the fewer electrons are in the examined volume (assumption for the penetration depth[127] ~ 150Å). From [Aes96].

b) Reduction of the seeming lifetime caused by the diffusion of electrons into the bulk. Hereby, one assumes a transport time for the electrons to disappear from examined area. Assumption: τ_{delay}=17fs·eV². After [ABP+00].

c) Measured lifetimes of excited electrons plotted versus the energy above Fermi level for three different Ag film thicknesses. For comparison, also the bulk value of Ag is shown. After [ABP+00].

According to the simple model described, it should be possible to reduce or even eliminate the transport effect by using films as thin as the penetration depth of the laser light in the used material. Then, all excited electrons will stay within the probed area until the second pulse arrives. However, it has to be stressed that this simple rule is only valid, if the secondary-electron contribution or any other strong effect can be neglected.

[127] see page 18.

Interestingly, Cao et al.[128] could not find any thickness dependence at all in single-crystal Au(111) films using thicknesses in the range of 15nm to 300nm (penetration depth λ_{opt}=16.8nm in gold). In their unexpected results, they explained that electron transport is a much slower dynamical process in the near-surface region, than expected from bulk properties.

In contrast to this, however, pump-probe reflectivity measurements on gold films show a significant effect of transport at excited electrons[129].

Hohlfeld et al.[130] showed that a two-temperature model could only explain their reflectivity measurements, if the effect of ballistic transport is taken into account. They found out that a significant carrier redistribution due to transport takes place within the first 100fs. At least for the lower range of excitation energies (range of longer inelastic lifetime) this effect should be visible.

Aeschlimann et al.[131] had compared theoretical analyses, which included several relevant processes (Boltzmann equation in the random-k approximation, secondary-electron generation, transport, and electron-phonon scattering) with measured lifetimes of excited electrons in silver of different thicknesses on MgO(100) (Fig. 28, page 70) as well as in gold films on NaCl. They found a good agreement between experiment and theory, and could develop the theory of the influence of ballistic transport to an accepted model.

The goal in this work was therefore (among others) to eliminate the influence of transport, in order to investigate the relaxation dynamics of optically excited electrons in smaller structures as the only acting path.

From the context above, it became clear how to eliminate the transport effect (see Fig. 29 on page 72). In a simple model, one just had to hinder the electrons from vanishing from the probed area. This can be achieved by probing metals on an insulator or a semiconductor (Fig. 29b). Because of their band gap, the excited electrons may not take a quantum mechanical state in the substrate's gap, and therefore the moving electrons become reflected on the interface between metal and insulator. In a 2d metal film, the electrons may still travel away, parallel to the surface, but the transport time becomes clearly longer, and the electrons stay for a longer time in the area of the laser spot. Best method to eliminate transport is of course the limitation to a metal cluster with the same size as the probed volume[132] (Fig. 29c).

---

[128] [CGE+98]
[129] [BFI87, SBJ95, HMWM97]
[130] [HMWM97]
[131] [ABP+00]
[132] However, it has been told in previous chapter, that in such clusters the electron dynamics is strongly influenced by Mie-plasmons and the absorption of light

One should not disregard, that this model is quite simple, even too simple. It is helpful as illustration, but the data to follow will show, that it is not possible to just eliminate the transport effect, without having other influences.

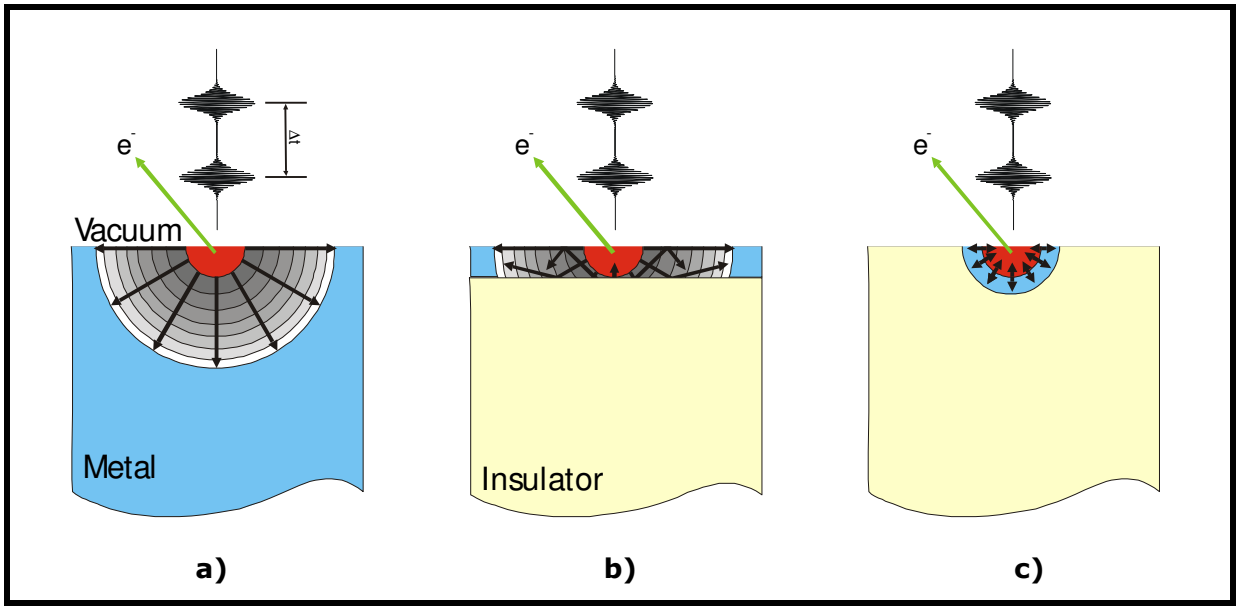

Fig. 29: A simple model, how to eliminate the transport effect. The probed volume has been coloured red, blue represents a metal, and yellow describes an insulator or semiconductor.

a) The situation in a bulk metal. Many excited electrons travel away from the probed area, leading to less measured population.

b) By taking an insulator as a substrate for thin metal films, most electrons remain in the probed area.

c) In a cluster with dimension comparable to the probed volume, no electron may vanish.

To complete this discussion it is necessary to mention a theoretical paper of Ekardt et al.[133]. They refuse this theory of the transport effect, and have two arguments against it. Firstly, they stated, that quantum mechanically seen, excited electrons are not located at the surface, but in the whole bulk, and may therefore catch a photon at all time. Secondly, excited electrons, which have a momentum k not in the direction perpendicular to the surface, would not be detected by an analyser, and should therefore not be considered. Thus, all detectable electrons have a direction from bulk to surface, and do not vanish. Despite their arguments, the authors did not describe the measured results by an adequate explanation. The investigations of Knösel[134] and of Aeschlimann et al.[135] do support the theory of transport.

[133] [ESK00]
[134] [Kno97]
[135] [ABP+00]

2. Layer-thickness dependence of silver on HOPG

One main goal of this thesis was to look for the experimental evidence of the predicted behaviour of optical excited electrons in a 2d system ($1/\tau_{ee} \propto (E\text{-}E_F)^2 \cdot \ln|E\text{-}E_F|$) and in smaller structures. For that it was necessary to use the method illustrated in Fig. 29b). Therefore, in order to measure the thickness-dependence[136] of the electronic dynamics in a metal, the following conditions had to be fulfilled by a substrate:

1. As the method is photoemission, the substrate has to deliver and compensate the emitted electrons, to avoid charging effects.

2. The influence coming from the substrate should vanish, so that the only detected lifetime signal originated from the overlayers. This implies a band gap at least in the transition's direction and energy. One knows, that the electron's Bloch wave is vanishing exponentially in a gap of the substrate.

3. It should be made possible to deposit metal layers on that substrate, best would be a flat and epitaxial growth mode (Frank - Van der Merwe).

The first attempt for this thesis was to deposit *silver atoms on highly oriented pyrolytic graphite* (HOPG). Graphite seemed to be best suited. The graphite's crystal structure, its corresponding Brillouin zone, and an XPS-spectrum, showing its approximate DOS, are displayed in Fig. 30.

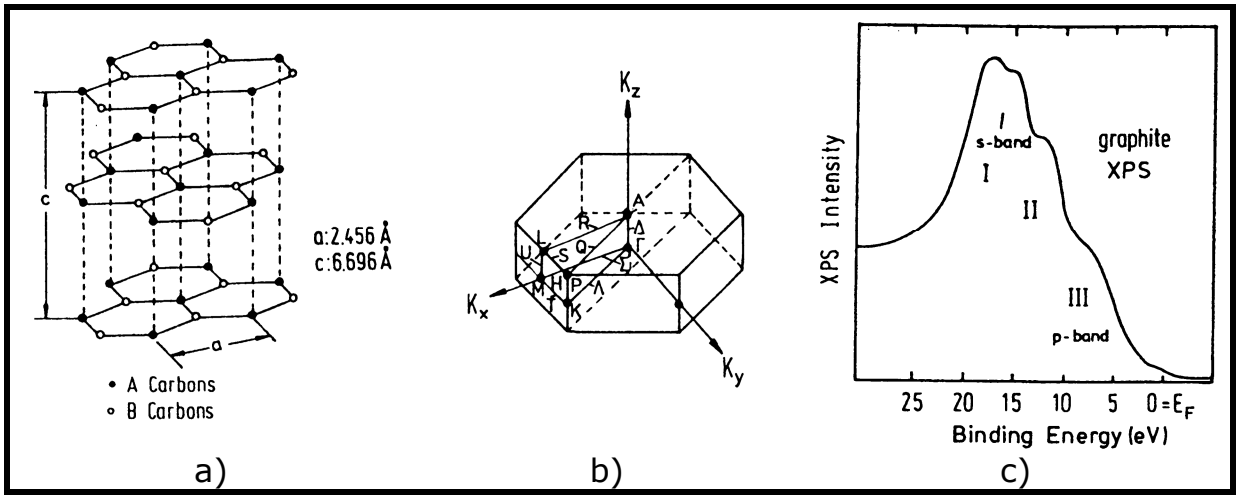

Fig. 30: a) Crystal structure, b) Brillouin zone, and c) XPS-spectrum of graphite. The crystal structure shows the two-dimensional sheets separated by c/2. The direction Γ-A, in the Brillouin zone, declares the track of the photoelectrons. As the XPS-spectra depicts, there is a vanishing amount of occupied states near E_F.

[136] Thus, the transition from 3d to 2d

The reasons for the usefulness of HOPG are firstly, the high mobility of the electrons in the a-b plane[137], which helps compensating charging, secondly the large[138] (3.6eV) band gap in the Γ-A direction, which is the direction normal to the surface and thus in the direction the used analyser measures the photoelectrons, and thirdly the ability of being easily prepared, by air-cleaving. Removing the top layers with a scotch tape, followed by heating and/or sputtering, could do this preparation.

Only the capability of becoming covered with silver, leading to epitaxial layers is not well known. There are a few articles showing an unepitaxial, dendritic growth mode[139], and others, which are demonstrating the generation of silver nanoparticles and clusters[140].

The experiences made for this work seem to indicate a *dentritic Volmer-Weber* growth mode, as non-fully covered HOPG-surface is observed (using AFM/STM), even with nominally 70ML of silver. However, there are also some signs[141], which lead to the assumption that the deposited silver on HOPG is polycrystalline but flat, while being in UHV, and continuously covering the substrate. Only whilst taking it into air (which was desired to take a STM picture), it becomes destroyed and agglomerated in dentritic clusters (Fig. 31).

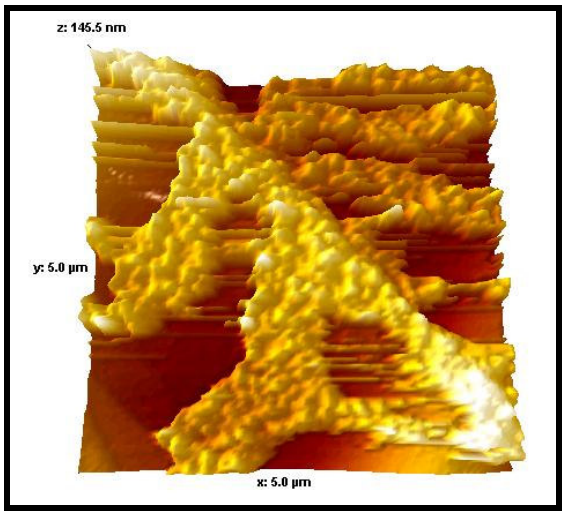

Fig. 31: A STM picture of 70ML Ag on graphite, after exposing it to air. The dendritic structure is probably a rearranging while bringing the sample from vacuum into air. Area dimensions: 5µm x 5µm. Picture by J. Beesley, University of Essen / Germany

Sputtering of HOPG, or any other damaging procedure has been avoided, because this would prefer a non-continuous, cluster-like growth mode.

[137] [Hüf95, TR82]
[138] [Hüf95, PBFW84]
[139] [AS98]
[140] [MPT+00]
[141] [Bee02]

Small quantities of silver were deposited, using an e-beam evaporator at a rate between[142] 0.1 - 0.4ML/s (note: one monolayer (1ML) silver is equal to a height of 2.045Å). The processing way was to evaporate increasingly, from 1ML up to 80ML. Because of the doubts pointed out above, both situations are to be taken into account: flat silver layers as well as silver clusters agglomerating to dendritic fingers.

What may be expected, while analysing the lifetime of optically excited electrons in silver layers, starting at 80ML and ending at 1ML? It should become visible, that the influence of transport vanishes more and more (levelling off), and one can suppose a change, as soon as the transition from 3d-bulk to a 2d-system happens.

This is exactly what could be seen in Fig. 32. The picture shows the fitted lifetime of optically excited electrons at an arbitrary energy of $E\text{-}E_F$ = 1.24eV. The black coloured points indicate the levelling off. One sees (from 80ML to 25ML) an increasing lifetime, which tends to saturation with vanishing transport influence. The value of saturation (25fs) is almost reached at 60ML, although the penetration depth for blue light (E_γ = 3.1eV) is about 150Å (~70ML) in silver[143]. This confirms the postulations about transport. As comparison: the seeming lifetime at the same energy but in a film thickness of 500ML (~bulk), is 12fs.

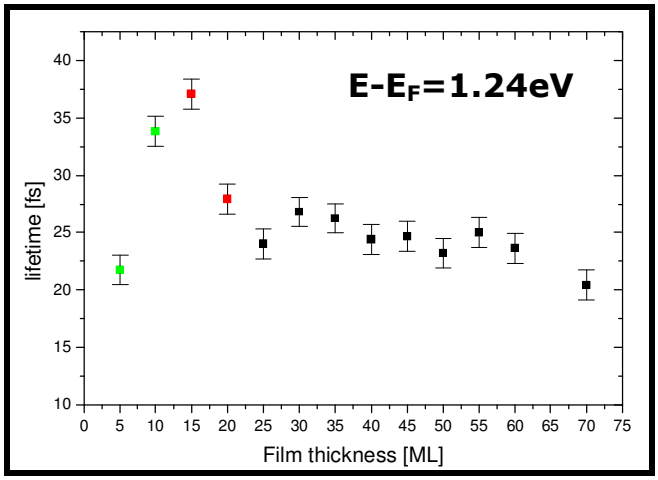

Fig. 32: Film thickness dependence of silver on HOPG, at $E\text{-}E_F$=1.24eV. It is clearly visible, that there is a levelling off, and a dramatic change in the region, where the system alter from 3d to 2d

Looking at the red coloured points in Fig. 32, one identifies an enormous rise in the lifetime compared with that of thicker layers. The lifetime changes from about *25fs* at 20ML to almost *38fs* at 15ML Ag. This rising spreads over the full accessible energy range[144], indicating a dramatic

[142] The deposition rate stayed constant, while evaporation. However, the rate had been changed a few times from sample to sample, in order to find good configurations.
[143] Calculated using tabulated function of the complex index of refraction. See page 18
[144] About: 1eV ≤ $E\text{-}E_F$ ≤ 3eV

change in the intrinsic relaxation probability in those small dimensions at 15ML.

The question arises hereby, whether this is a first indication for Mie-plasmon excitation, caused by a non-continuous Ag film, or rather surface plasmons or even interface plasmons in these silver films. It is also necessary to check, whether it is the expected contraction of the phase space in 2d, which would lead to longer living states.

A polarisation dependence of the photo-emitted electrons would give relevant information, whether plasmons are excited or not. It became clear in the last years, that an excitation of *surface plasmons* (and in some cases also Mie-plasmons) is much more effective with *p-polarised* light than with *s-polarised*[145]. Lehmann et al.[146] found out, that on a corrugated Ag film, grown on the HOPG surface, the observed polarisation dependence is much less pronounced, than on Ag nanoparticles embedded on HOPG, indicating that dipole moments with different surface orientations contribute to the total photoemission yield. The polarisation dependence is strongest for photoemission from Ag nanoparticles (even if they cover only 2% of the HOPG surface). There the electron yield with *p-polarised* light is about 25 times higher than with *s-polarised*[147].

Unfortunately, there is no unique evidence in the measured records of silver on HOPG, which prefer the *excitation of (surface) plasmons* to the effect of *phase space contraction* (from 3d to 2d, or vice versa). One may take the symmetric autocorrelation of the cross-polarised[148] measurements[149] of *Ag on HOPG* as a proof of not having a polarisation dependence. This seems to be a passable way, which led to good analyses at *Ag on GaAs* (chapter IV.3). It is therefore a confirmation for having probed the transition from a bulk system to a 2d system with confined electronic states.

The confinement of electronic states and the extreme decrease of the available free phase space in a 2d system, both lead to these *clear long lifetimes*.

Whilst looking for a proof for this view, one may compare the spectra of the different coverages of silver on graphite. In Fig. 33a) some characteristic spectra are plotted; one spectrum of the clean HOPG sample and a few spectra with different amounts of silver on HOPG. Note, the intensities may not be compared, because they are not normalised and depend on every day's laser intensity.

[145] [MPT+00], [SPO+01], and references therein
[146] [LMP+00]
[147] [MPT+00]
[148] One pulse is p-polarised, the other pulse is s-polarised
[149] Not shown here

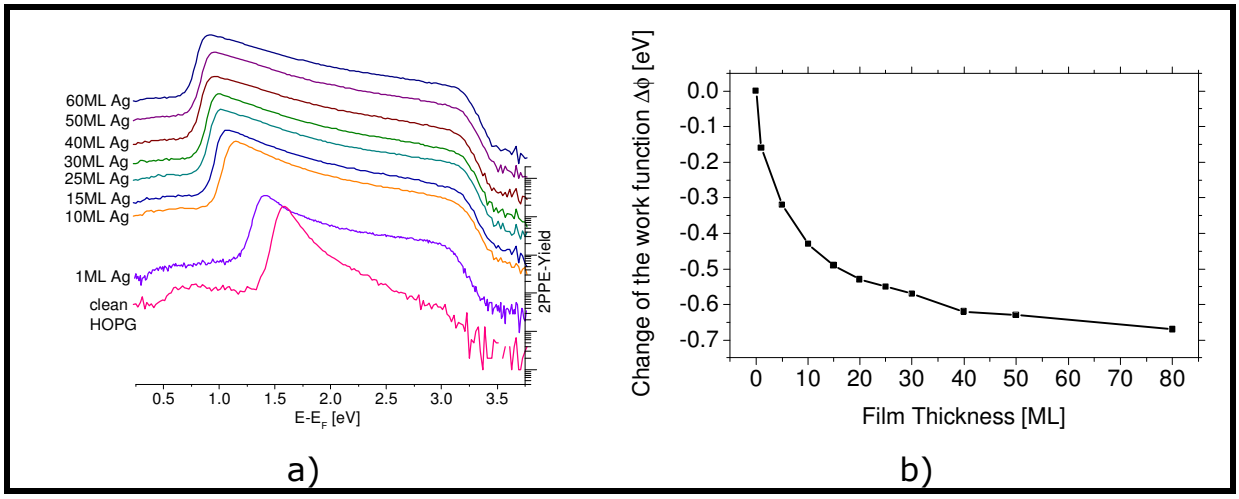

Fig. 33: Analyses of spectra of silver on graphite.

a) Some characteristic spectra have been plotted to compare them. It is clearly visible that the Fermi edges stay at the same energy, whereas the cut-off[150] energies change.

b) A plot of the cut-off energies vs. the film thickness.

Obviously, even with a deposition of one single monolayer of silver, the spectrum changes. One identifies easily the visible Fermi edge even at 1ML. This is an evidence for a strong increase in the density of states around the Fermi level. There is therefore already a "metallic" density of states at one monolayer of silver on graphite.

The fact that the Fermi edge does not change its energetic position with higher coverage shows that there was no charging problem, in spite of the reduced electric current between different graphite layers (Fig. 30, page 73).

It is not yet fully understood, why no modification of the 15ML silver spectrum may be seen. The lifetimes at 15ML show a remarkable evolution, but the corresponding spectrum does not. It may be explained it that way: With 2PPE one probes not only the DOS of the initial state or that of the final state, but a "joint density of states" from initial, intermediate and final state, at the same time. 2PPE smears most of the features out, in comparison with normal photoemission, except e.g. a strong interband transition or a stable surface state and image state.

Also noticeable is that the more silver is deposited the wider the spectrum is. It shows the change of the work function with different deposited amount of silver. The evolution of that variation is separately plotted in Fig. 33b). The supposed exponential decay of the curve indicates the increasing approach of the band structure from that of graphite to that of a silver bulk. At 80ML the saturation point of the work function is already reached, and it is exactly the same as of a thick (1000ML) bulk structure of silver on HOPG.

[150] This is the lowest detectable energy

From the difference (ΔE) between the Fermi edge and the cut-off in a spectrum, it is easy to calculate the exact value of the work function[151]: $\boldsymbol{\phi = (E_{\gamma 1}+E_{\gamma 2})-\Delta E}$. In the current case, the work function of the 1000ML polycrystalline silver layer on graphite is $\boldsymbol{\phi = 3.8 \pm 0.1eV}$, which is lower than the tabulated ϕ = 4.26eV (polycrystalline[152]). The reason for this difference is still not known.

Reconsidering Fig. 32 (page 75), the green points, which show a tendency to lower lifetimes with lower coverages, seem to be in contradiction to the idea of confined electronic states, as mentioned before. However, carefully analysed, it is rather an effect of the underlying substrate. Although the penetration possibility of an electron Bloch wave into the graphite's gap vanishes exponentially, there is still a probability of scatter with electrons in HOPG or even to excite electrons there, e.g. by multi-photon excitation or into virtual states in the gap. As noted by Merschdorf et al.[153], and as it could also be seen in Fig. 30c) (page 73), there is a (small) density of states around the Fermi edge in HOPG. The lifetime of optically excited electrons in clean HOPG have been measured for this work, and it came out a rapid (0-5fs) relaxation over the full accessible energy range. In view of band structure considerations this becomes reasonable, because of the existence of many decay channels in graphite, like e.g. interband transitions. This leads to the assumption, that the lifetimes of the lower coverage thicknesses (0-15ML of Ag) seem to be influenced by the fast graphite's relaxation paths. By examining Fig. 31 one recognizes that the area of not-yet covered HOPG depends on the amount of silver. Therefore, one may think of a measured lifetime:

$$\tau_{measure} = a \cdot \tau_{HOPG} + b \cdot \tau_{Ag} \qquad \textbf{(IV.2.1)}$$

where a and b are variables for the part of the full surface area[154]. The more area is covered, the more is $\tau_{measure} = \tau_{Ag}$.

It is very likely, that measuring much longer lifetimes at these low thicknesses would have been possible, if there were no influence from the substrate. For that reason a substrate with a real band gap was needed: gallium-arsenide (GaAs), see next chapter. One less important, but not neglectable condition, was the relevance and applicability of the system to given industrial techniques. This is of course unquestionable in the case of silver on GaAs.

[151] See also eq. (II.1.55) on page 56
[152] [Lid95]
[153] [MPT+00]
[154] a+b=1. Thus b=1 would mean: the whole HOPG surface is covered by Ag

3. Metal atoms on a semiconductor: Ag on GaAs

Looking to reach the fixed goals, i.e. the relaxation dynamics of optically excited electrons in small structures, the system *silver on gallium-arsenide* was success-promising. The main reason for having taken GaAs is its direct band gap at the Γ-point. This band gap was useable in the experiments by measuring the photoelectrons in the ΓX-direction (=[100]), i.e. perpendicular to the surface. The used sample was a p-doped (10^{19} cm^{-3}, Zn) GaAs(100) in order to produce a Schottky-junction.

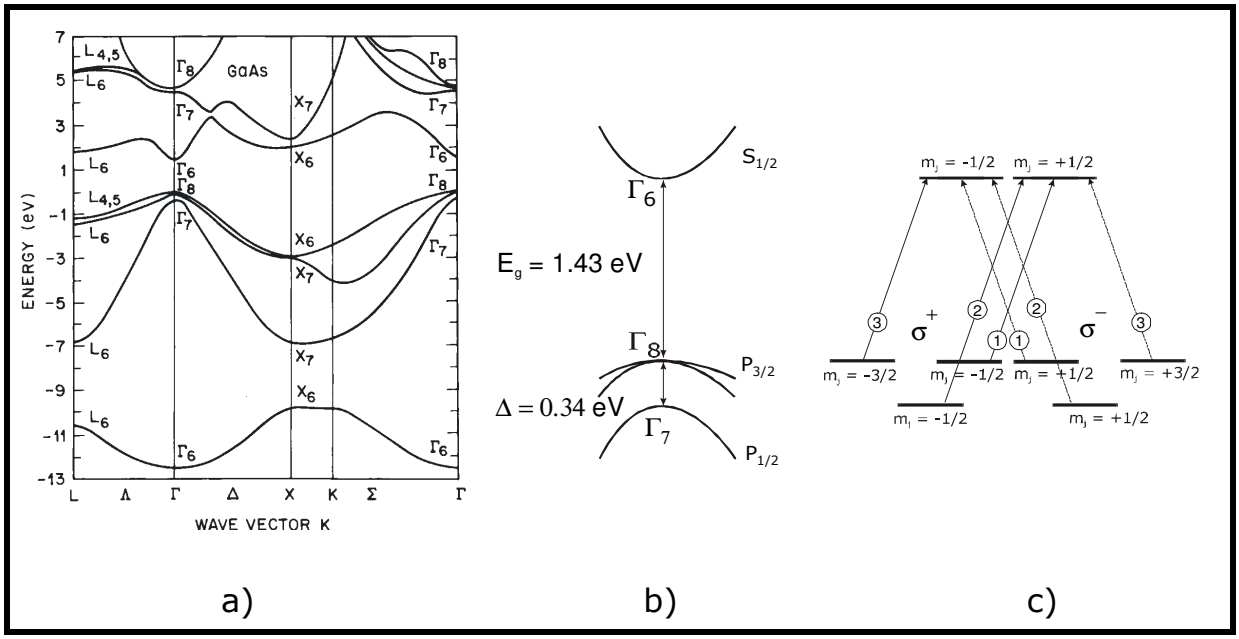

Fig. 34: Gallium-arsenide

a) Band structure of GaAs.

b) A small extract of the full band structure, containing the situation at the Γ-point around the direct band gap.

c) The optical selection rules for a transition from valence band edge to the conduction band edge at the Γ-point, which lead to spin-polarised electron populations (explanation in the text).

Gallium-arsenide is a direct III-V semiconductor (Fig. 34). The partially ionic compound GaAs possesses the crystalline structure of zincblende (ZnS), which is related to the diamond structure (e.g. Si). Further essential facts about GaAs can be found in the appendix on page 148. Besides silicon, GaAs is one of the best-investigated semiconductors, and led to many important applications, for example in microelectronics, but also in research.

One of these applications is the efficient method to produce spin-polarised electrons by taking advantage of the optical selection rules in GaAs (Fig. 34c). The band gap of GaAs at the Γ-point is about 1.43eV, at room temperature. Because of the spin-orbit splitting (~0.34eV) of the valence band, there are optical selection rules for the transition from valence band to the conduction band at the Γ-point. With circularly polarised light, only three transitions are allowed (indicated in the figure by three arrows for circularly-left light (σ^+) and three for circularly-right (σ^-)). The numbers in circles in Fig. 34c) show the relative intensities of the transitions. Restricting the photon energy to about 1.43eV reduces the number of possible transitions to two. These transitions carry electrons of opposite spins but are different in intensity. A maximum polarisation of 50% can be attained:

$$P = \left| \frac{n_\downarrow - n_\uparrow}{n_\downarrow + n_\uparrow} \right| = \left| \frac{1-3}{1+3} \right| = 0.5 \qquad \textbf{(IV.3.1)}$$

T. Ohms[155] used this method to study the dynamics of spin relaxation at the GaAs surface. The use of this technique in analysing the inverse spin-injection from a semiconductor through a metal will become clear in the later part of this chapter.

From previous treatises[156] the energetic relaxation mechanisms of optically excited carriers in semiconductors far from equilibrium is known. In a sample like the one used in this work, Collet[157] showed (Fig. 35) that for weak excitation (E_g + 0.4eV) the dominant process of relaxation at that high doping level, is scattering of electrons with holes, which transit from the heavy to the light hole band (LH). The corresponding intraband process in the heavy hole band (HH) is an order of magnitude lower in scattering rate. So are the scattering rates for LO-phonons (longitudinal optical) with electrons and that of mixed plasmon-phonon modes.

[155] [Ohm02]
[156] E.g. [Col93], [Hai95], [Ohm02], and references therein
[157] [Col93]

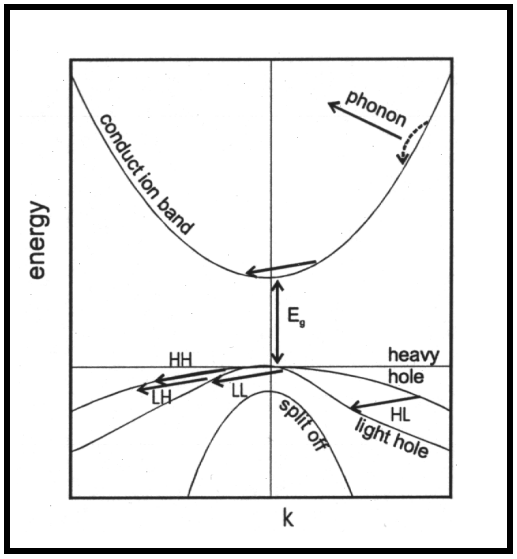

Fig. 35: Different scattering processes applying to electrons in GaAs. From [Col93]

In a recent work, T. Ohms[155] concluded from his observations with different excitation densities on the same type of GaAs sample that the electron-electron scattering processes are of minor relevance[158]. He discussed the importance of screening by the used high hole density. His investigations show that the lifetimes (tens of femtoseconds) are shorter than theoretically predicted. This points to the strong contribution of electron-hole scattering, because of that high doping level. He could even determine the step-by-step energy loss (0.3eV) of conduction electrons, which relax after scattering with interband holes.

So, the relaxation dynamics of optically excited electrons in *GaAs* is known. It can be included in the analyses of this work, which concerns about the relaxation dynamics of optically excited electrons in the system *silver on GaAs*.

[158] This is a strong contradiction to excited electrons in metals

For this thesis, silver adatoms were deposited on the pure GaAs, and it was tried to get some information about electrons in silver in spite of the underlying substrate. One thinks of an electron excitation in silver (Fig. 36), which leads to an intermediate state there, at an energy that lies in the gap of the semiconductor. The influence from the substrate to this intermediate state should then vanish, and one should be able to detect the relaxation of this metal-electron-state only.

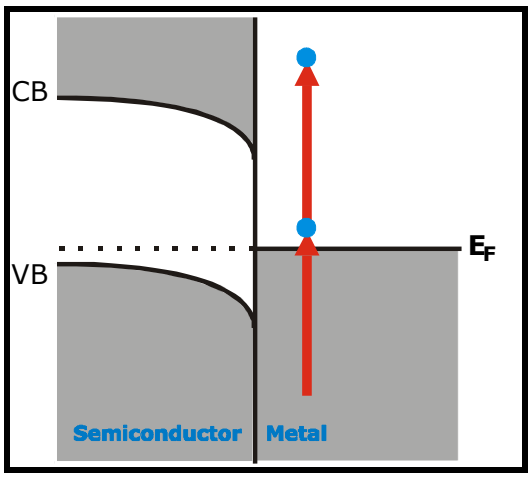

Fig. 36: A schematic diagram of the excitation process. It was expected to get no influence of the semiconductor to the excited intermediate state.

The deposition of silver on GaAs has often been reported. Smith et al.[159] saw a flat epitaxial silver film on a GaAs(110) surface, after deposition at 135K and annealing up to room temperature. They found this procedure to lead to atomically flat films with closed-packet (111) structure modulated by a quasi-periodic sequence. The growth of silver films on GaAs(110) by deposition at 100K and annealing up to RT, was investigated by Neuhold et al.[160]. They noted with increasing doses of Ag, first, ordered arranged islands (<5ML), then continuous open films with holes, (<8ML) and finally closed films with large atomically flat regions. Evans and Horn[161] reported that the deposition at RT leads to formation of islands. They even found islands forming due to the increased surface mobility of the adatoms, when a layer, deposited at low temperature is warmed up. This stays in contradiction to the investigations of the authors mentioned above, and therefore, it seems to be critical to the surrounding conditions, whether one gets islands or films.

Let us briefly look also at the investigations on thin Ag films on GaAs by Dubois et al.[162]. The Ag films were grown and studied at T=170K. They saw that the very thin silver films (<2ML) have a large resistivity (at 170K), comparable to those of liquid Ag. They argued that at low coverage there is a very low concentration of connected (and thus conducting) paths, because of the not-fully covered GaAs surface (Stranski-Krastanov growth). Thus, the high resistivity is caused by Drude damping (elastic scattering of electrons from lattice imperfections) and becomes similar to liquid Ag. When the low-temperature-deposited Ag films were slowly heated to room temperature, Dubois et al. noted the structure to become

[159] [SCNS96]
[160] [NBPH97]
[161] [EH93]
[162] [DSCM84]

of Volmer-Weber type. They interpreted this as the growth of metal islands separated by areas of almost uncovered GaAs.

The GaAs(100) sample used in this work has been cut and treated with wet chemical methods before bringing it to UHV. The chemical treatment includes mainly etching in sulphuric acid and rinsing afterwards[163]. In UHV (base pressure $4 \cdot 10^{-10}$mbar) it was cleaned in-situ each day by heating up to about 500°C for 30min, monitored by a mass spectrometer, in order to avoid structural changes[164].

The sample GaAs was hold at less than 120K during the slow deposition of the silver adatoms from an e-beam evaporator. The deposition rate of 0.03 - 0.04ML/s was controlled with a microbalance quartz.

Although, similar conditions have been used as reported by other groups, the AFM-analyses of the observed system (silver on GaAs) lead to the assumption that there has always occurred island growth (Stranski-Krastanov or even Volmer-Weber growth mode). Again, it is questionable, because this structure can be generated during the transfer of the sample to air. One has to assume having measured silver islands of dimensions between 10nm and 40nm, see Fig. 37.

Having such a deposition, F. Arciprete et al.[165] calculated the fraction of covered surface as a function of the Ag amounts: At 5ML, 42% of the GaAs surface is covered, at 10ML, 60%, and at 20ML, 80%.

All measurements were made at room temperature unless otherwise stated.

[163] See [Ohm02]
[164] There must not come any arsenic
[165] [ACF+96]

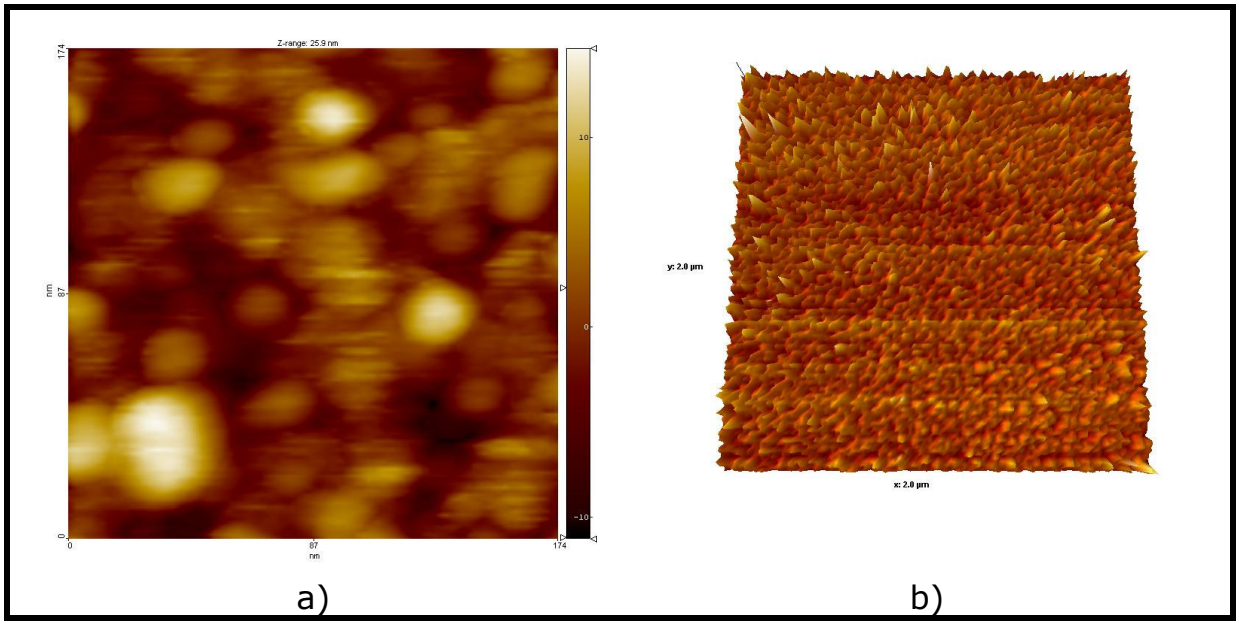

Fig. 37: AFM pictures of Ag[17ML]/GaAs[166]. Made by J. Seifritz in the group of Prof. Dr. R. Möller in Essen / Germany

a) An analysis of the sizes showed an average diameter of 24nm. The particles vary between 11nm and 39nm. Picture dimensions: 174nm x 174nm

b) The picture shows a Volmer-Weber growth mode. Dimensions: 2µm x 2µm.

The experiments started with an amount of nominal 1.5ML Ag on GaAs(100). As could be seen in Fig. 33 on page 77 there is already a significant change in the spectrum of Ag/HOPG at a coverage of 1ML Ag compared to the spectrum of the clean HOPG substrate. One may therefore also expect noticeable changes after deposition of Ag[1.5ML] on GaAs.

One important fact should be emphasised here: As described in previous chapters, there is a band bending at the interface between semiconductor and vacuum. This band bending is being changed as soon as the metal covers the surface, i.e. *before* deposition there exists a band bending because of dangling bonds and *after* deposition there exists another band bending because of the adsorbate. It is therefore build up a *changed* band bending for the interface between semiconductor and metal.

It may be learned from previous chapters that the Fermi level (E_F) stays pinned at the observed system. Because of the compensating charge flows, E_F lies at the surface at about 0.5eV above valence band edge[167], before and after the deposition. The band bending, caused by the Schottky barrier on the interface between the silver metal and the p-

[166] Note, in this work the simplified abbreviation Ag[xML]/GaAs(100) is used to describe a nominal deposited amount of xML of Ag on GaAs(100).

[167] Typical values lie around 0.6eV [Mön01]. T. Ohms [Ohm02] had extracted the value out of his work to 0.5eV at the same type of sample. In this work, this value of about 0.5eV had been determined many times from different measurements.

doped semiconductor could be determined (through analysing different transitions before deposition and after) to be about 0.4eV. This value agreed with the measurements of T. Ohms[168] on the same type of system, and could have been proofed by backward calculations from the further analyses of this system (see below).

Calculations made by van Schilfgaarde and Newman[169] show explicitly the formation of the silver density of states during deposition of silver on GaAs (Fig. 38). The DOS far from the interface (more than about 6ML) is essentially like those of the bulk metal. Tails of the metallic wave functions tunnelling into the semiconducting band gap are clearly shown at the interface, decaying in four monolayers. The magnitude of this interfacial DOS is large, showing that the metal Fermi level is strongly pinned, as have been discussed before.

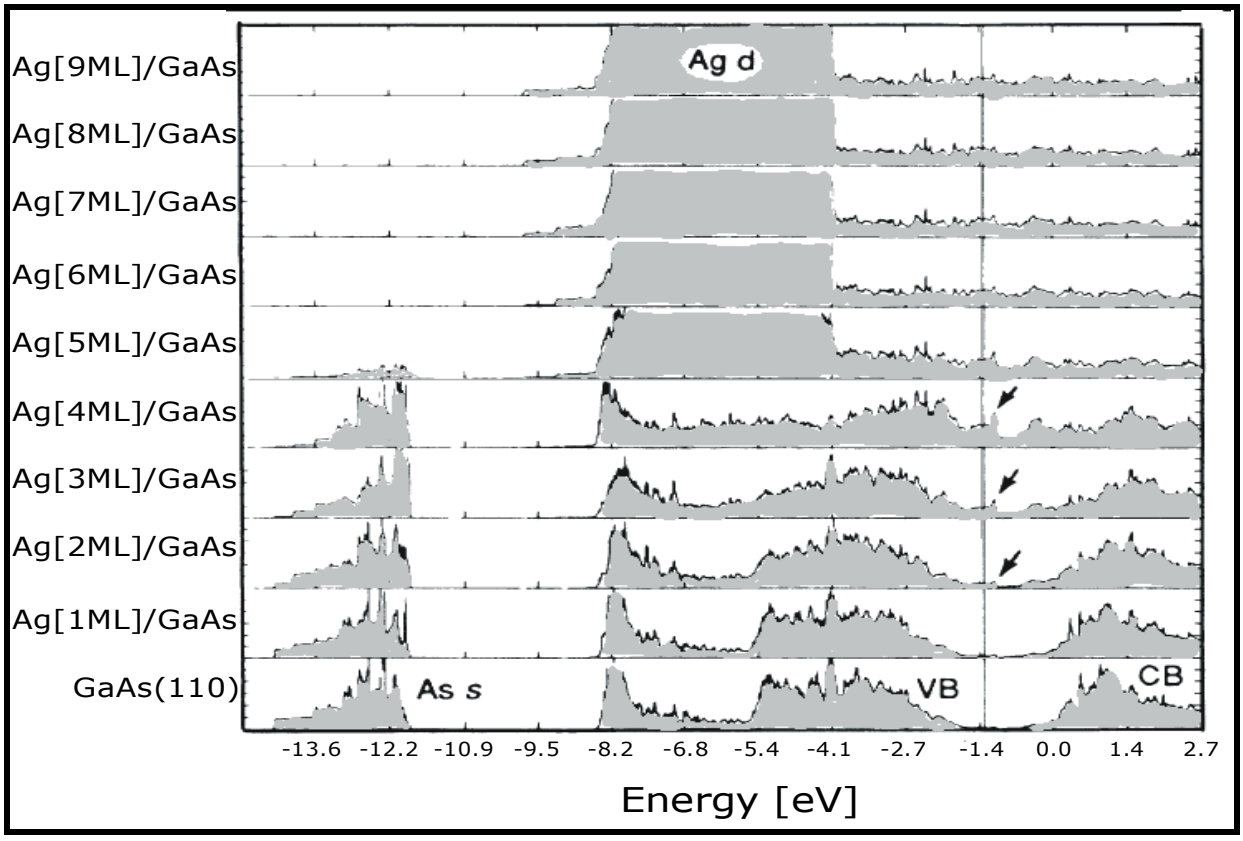

Fig. 38: Calculated DOS of increasing coverage of silver on GaAs, from [vSN90]. The vertical line marks the Fermi level.

The authors point also out, that at transition metals (like Fe) and at noble metals (like Ag) the Schottky-barrier height possess an additional contribution, which arises from charge transfer between the metal d-states and the semiconductor, raising the semiconductor bands with respect to the metal and lowering the pinning position within the gap.

[168] [Ohm02]
[169] [vSN90]

However, this contribution is quite small (0.15eV) at silver, because of the far (4eV) d-bands. It is however not surprising, that it should be possible to see it at spectra of gold or of iron.

a. Small amounts of silver on GaAs

The next steps are to discuss the dynamics of the optically excited electrons in the system Ag[1.5ML]/GaAs(100), and later of the thicker films. Again the questions: what may be expected from the measurements? An electron dynamics, which mainly shows that one of GaAs? An additional influence from silver to the data? Already the known pure silver dynamics, like in 3d?

It is certain, that the wave function of the excited electrons can penetrate into the gap of GaAs, at least an exponentially decaying tail. It is also known, that the impinging electromagnetic wave (light from laser) can enter into the GaAs through the silver. This may lead to transitions from GaAs as well as from silver.

It should be mentioned explicitly, that in this first section a) and also in the next section b) the considered intermediate states of the optically excited electrons lie *above* the band gap. And one has therefore to expect influences from the electrons of GaAs.

The first step to do, is to compare measurements from clean GaAs with those of Ag[1.5ML]/GaAs, see Fig. 39.

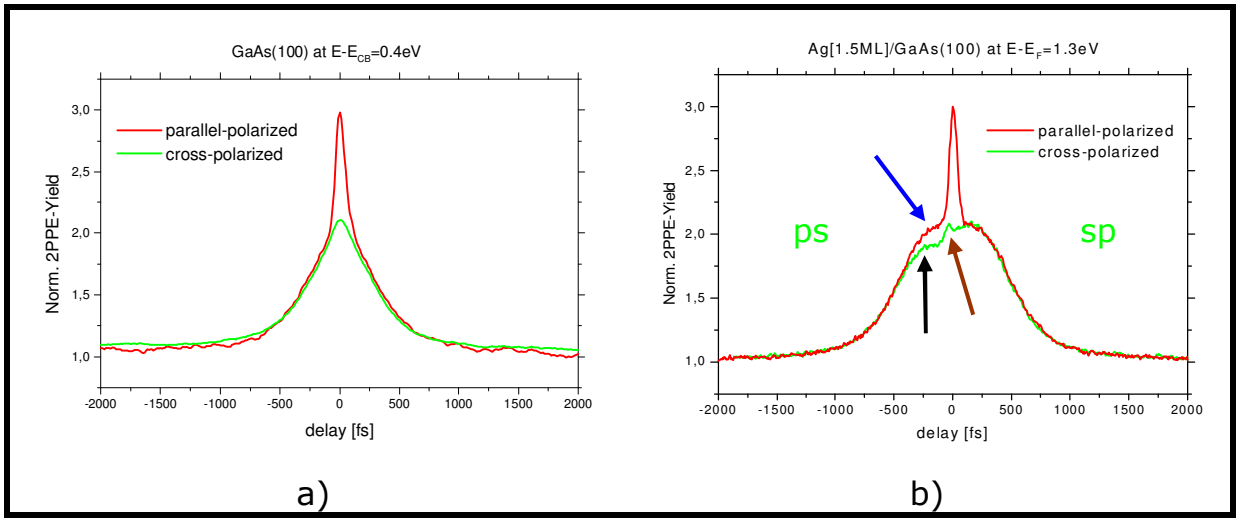

Fig. 39: Comparison of TR-2PPE-measurements, taken with blue (3.1eV) light between

a) clean GaAs(100)

b) Ag[1.5ML]/GaAs(100)

The *red* curves illustrate the *parallel-polarised* (pp) case, and the *green* curves represent the *cross-polarised* one (*p before s* left, and *s before p* right of zero delay). The tested energies are written at the top. They are related to Fermi energy and conduction band edge, as usual; but they correspond to one another (i.e. same E_{kin}) by taking into account the band bending.
The *blue* arrow indicates the "*shoulder*", the *brown* arrow indicates the "*additional peak*" and the *black* arrow indicates the "*dent*".

A few details are worth mentioning: at Fig. 39a) two curves are plotted, representing TR-2PPE measurements with *cross-polarised* (ps, green plot) and *parallel-polarised* (pp, red plot) pulses. The coherence peak in the pp-autocorrelation is clearly visible and will be explained in VIII.4; roughly spoken, it is an artefact of the used set-up, caused by the coherence between the first and the second pulse. It will not be considered further. Another fact is that the widths of the autocorrelations (neglecting the coherence peak) are almost the same at ps and pp. The small difference occurs because of changing pulse width day by day. The electron behaviour based on those curves has been analysed by T. Ohms[170] and shall not be subject here.

At Fig. 39b) one identifies a dramatic change caused by the small quantity of silver. At *both combinations of polarisation* (red = pp, green = sp and ps), there arises a noticeable *shoulder* (blue arrow) at small delays (about –250fs till +250fs). The *cross-polarised* case shows even more: there is a remarkable *dent* (black arrow) at the left side at about –300fs. A *p-polarised* pulse followed by a *s-polarised* one generates the left side until zero delay. From zero to higher delays, the *s-pulse* comes ahead of the *p-pulse*. That means the measurements show a *polarisation dependent dynamics*. Besides that dent, there is also an additional *peak* (brown arrow) at about –50fs. It is definitely *not* located at zero delay. Such a wide *shoulder*, a *dent* and an *extra peak* appears at least from $E-E_F = 1.3eV$ until $E-E_F = 2.0eV$.

As all effects discussed above are obviously correlated, it is thoughtful to gather all facts and discuss them comprehensively. Hence, before going on explaining the dynamics, firstly look at Fig. 40, where a kind of law has been tried to be recognised by analysing the location in time[171] of the start of that dent and the peaks' location. The positions of those blue and red marks were determined by computing the points of change in the slopes of the cross-correlation curves.

[170] [Ohm02]
[171] I.e. the time delay

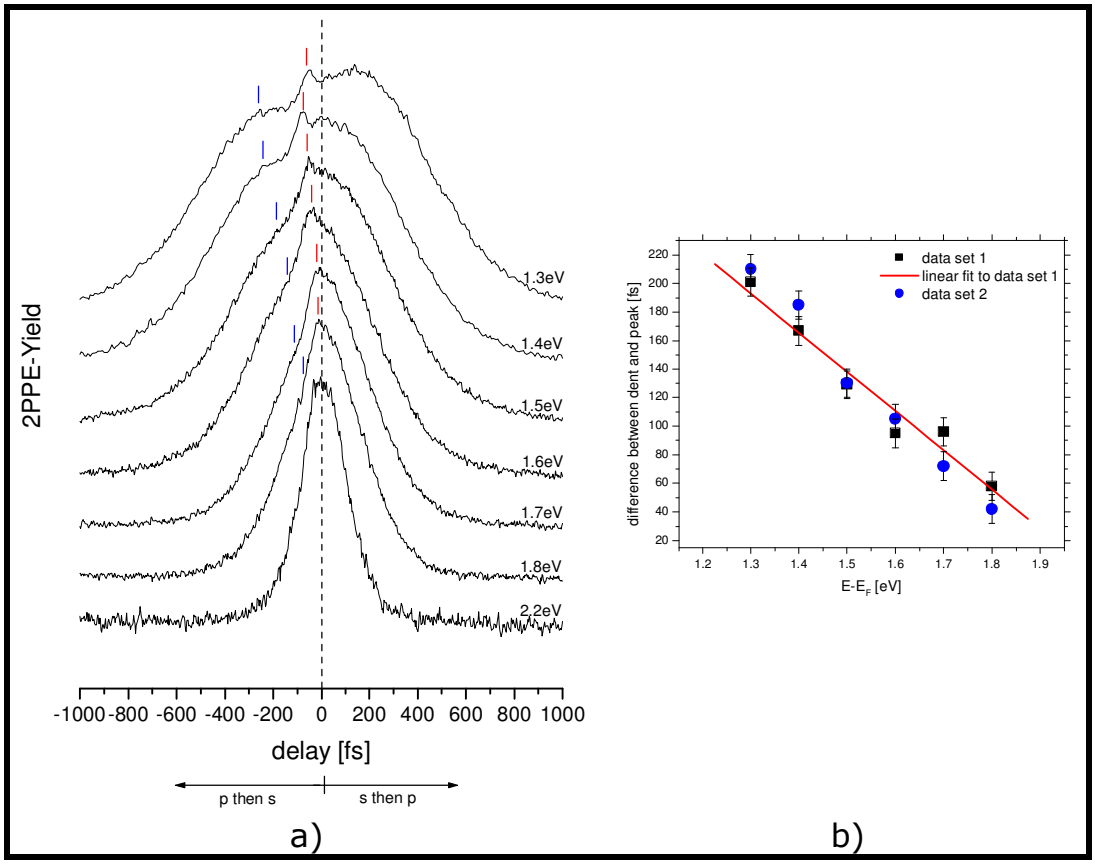

Fig. 40: Some autocorrelation curves of Ag[1.5ML]/GaAs(100), taken with cross-correlated pulses.

a) The start of the dent is indicated in *blue*, and in *red* the position of the additional peak. Those blue and red positions were determined by computing the points of change in the slopes of the curves.

b) Plot of the differences (in fs) between dent and peak against the intermediate state energies. Black squares and blue circles represent different datasets. The red line indicates a linear fit for the black dataset. It agrees well also with the second dataset.

At Fig. 41, a measure for the *shoulder* of the autocorrelation curves has been given. Thereby the pp-autocorrelation curves of *corresponding energies* at GaAs and at Ag[1.5ML]/GaAs were compared, by including the shift of the energies due to the band bending. Further, the surplus was calculated, by determining the difference between both yields. Note that even though silver is known to show fast relaxation times and thus should make the autocorrelation curve of Ag[1.5ML]/GaAs thinner, it does the opposite, the autocorrelation curve becomes wider with Ag.

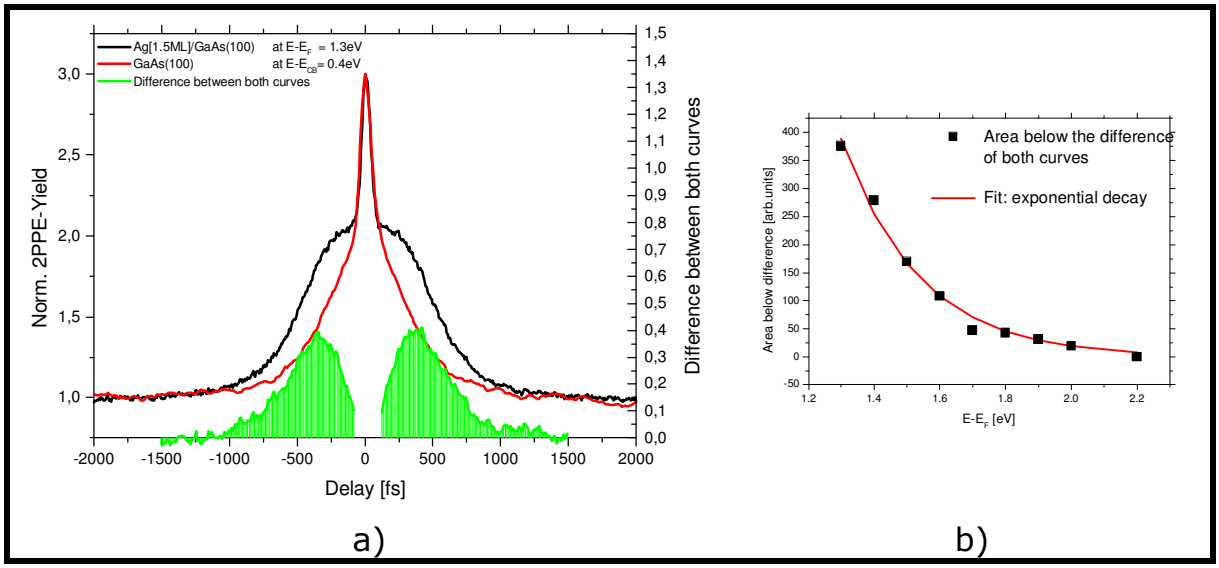

Fig. 41: Calculation concerning the additional shoulder at the (pp-) autocorrelation curves of Ag[1.5ML]/GaAs(100).

a) Black and red are the energetically corresponding TR-2PPE measurement data. Green is the difference between them. The green area is determined by integrating.

b) A plot of the determined green area for different energies. The red exponentially-decaying curve represents a fit through the data points.

The next three sections give a comprehensive explanation for such a dramatic behaviour of excited electrons in Ag[1.5ML]/GaAs.

1) Different lifetimes at the same energy?

At first sight, the curves in Fig. 39b) and Fig. 40a) seem to be built by the addition of two different curves, illustrated in Fig. 42.

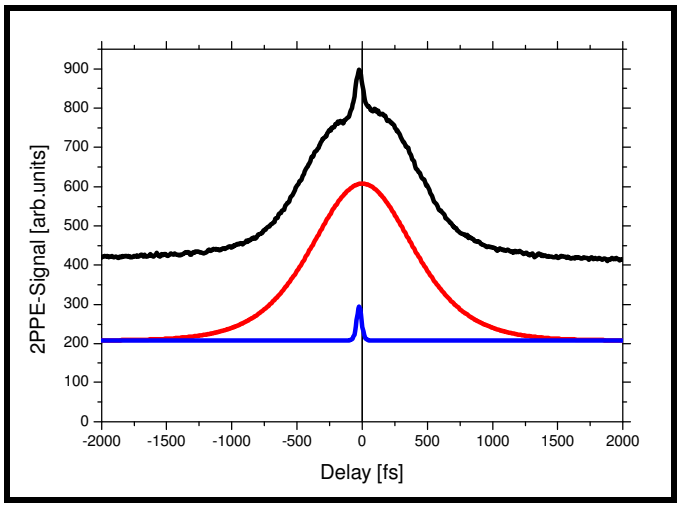

Fig. 42: The measured curve may only be built by two separate curves, having not the same relaxation time. Nevertheless, there is no reason for two different relaxation times at the same intermediate energy level.
The red curve demonstrates the p before s excitation, and the blue curve indicates the s before p excitation.

Even though, the intensities of the *ps-curve* and the *sp-curve* may be different, caused by the dissimilar transition probabilities of electron excitation with p-polarisation and with s-polarisation, there is no reasonable motive for two different relaxation times at the same energy level. No matter if the first pulse is p-polarised or s-polarised, the *intermediate state* of electrons originated from the same energy level is always the same. Thus, the relaxation probabilities are the same and so are the relaxation times the same. One can conclude therefore that the measured curves are not a combination of two curves.

2) Cascading electrons

This description is based on the hypothesis given by Leitenstorfer et al.[172] and T. Ohms[173]. They analysed the influence of electromagnetic fields on highly doped, band-bended GaAs, especially in the ultra-short time regime. They concluded that there are two different sources for *cascading electrons*[174], and both are always active, Fig. 43a) and Fig. 43b)[175]:

First source (Fig. 43a): The first incoming laser pulse excites e-h-pairs within the penetration depth of light[176]. The e-h-pairs inside the band bended area are immediately *projected to the surface of GaAs* by the internal electric field ($5x10^5$ V/cm). The transfer to the surface happens within a few femtoseconds. From there, they will suffer electron-phonon as well as electron-hole scatterings, which are main relaxation processes in this highly doped semiconductor. The electrons at the surface will also suffer electron-electron scatterings, caused by the high density of electrons at the surface. The second pulse excites then a wide distribution of electron energies.

Second source (Fig. 43b): Excited electrons *within the volume* of the semiconductor decay by electron-phonon and electron-hole scattering to lower lying states and become then probed from there.

[172] [LHS+99]
[173] [Ohm02]
[174] Cascading electrons lose a small part of their energy, and thus populate the energy region below.
[175] Both sources are active in GaAs with or even without silver, caused by band bending
[176] 14nm for blue in GaAs, see Appendix

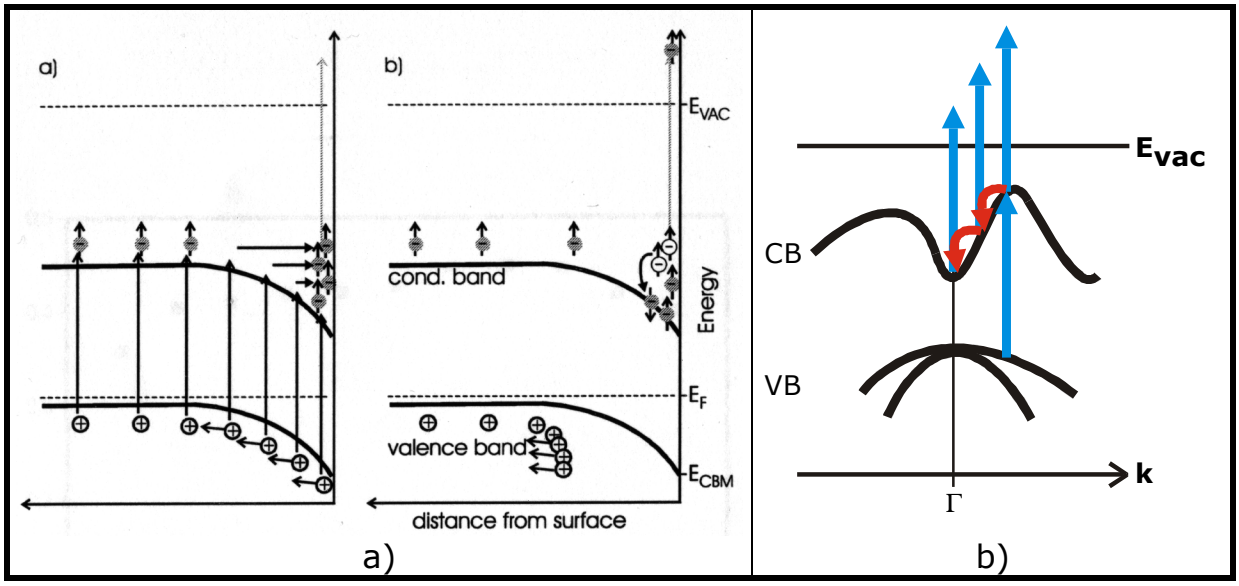

Fig. 43: The electron dynamics in GaAs(100) a few femtoseconds after being excited.

a) The electrons are being projected to the surface. There, they suffer electron-phonon scatterings, and populate lower lying energies.

b) Excited electrons decay (mainly) by electron-phonon scattering.

Is it likely, that both relaxation paths take place at the same time-scale? No, because the *second process* starts immediately after the excitation, whereas the *first process* starts also immediately, but cannot be detected until the electrons moved to the surface (2. step of photoemission). In addition, the cascading at the *first process* is probably faster, because of the strong electric field of the band bending, which increases the density of hot electrons and thus increases the contribution of electron-electron scattering.

Leitenstorfer et al. give a transport time[177] (to the surface) of up to a few hundreds of femtoseconds. Ohms declares the average decay time for scattering with LO-phonons to about 150fs, and the loss per cascade step to 0.3eV, which is an order of magnitude higher than expected, and is traced back to strong interband hole scattering, caused by the split off at valence band.

Both relaxation processes happen not only in GaAs, but also in Ag[1.5ML]/GaAs, because there is a similar band bending and the impinging light excited electrons in silver as well as in GaAs.

The autocorrelation curves in Ag[1.5ML]/GaAs are *broadened*, compared to GaAs, even if the metal silver is known to show fast relaxation times,

[177] The transport time has been determined at different GaAs samples (but similar to those in this work) using red light, which penetrates deeper in the material than blue light, which has been used here, see appendix. This transport time depends on the level of doping and on the Debye-length.

and thus actually the curves are supposed to be *narrower*. So, why do the TR-2PPE-signals of Ag[1.5ML]/GaAs not show the same autocorrelation curves as the clean GaAs sample?

The *exponential* decay of the surplus in counted electrons, seen in Fig. 41b), points to the *influence of cascading electrons*. The lower the intermediate energy the bigger is the difference[178] in counts in Fig. 41a), and thus the more cascade electrons take part. Nevertheless, besides the usual cascading electrons in GaAs, there must be an additional electron source at Ag[1.5ML]/GaAs, in order to populate those intermediate states in such a huge number. It seems that the cascading process becomes delayed in the system Ag[1.5ML]/GaAs. This occurs because of two reasons, which both are consequences of the structure of the deposited silver: hot electron temperature and plasmon excitations.

3) Hot electron temperature and plasmon excitation

Due to the not-fully covering structure of the silver surface and due to the potential (and weak connection) between silver and GaAs the optically excited electrons in silver may not thermalise as fast as usual in silver. The hot electron gas cannot cool down via electron-electron scattering, but only by electron-phonon scattering, which is known to last up to 4ps. Thus, this is the reason for the mentioned delay in Ag[1.5ML]/GaAs. However, there is another effect, which is important here:

In chapter I.e (page 28)[179] the excitation of plasmons in solids of different dimensions was dealt with. It has been showed that surface and interface plasmons may only be excited by p-polarised light, which has a component perpendicular to the surface. Also, the different plasmon modes in small nanoparticles, leading to different excitation frequencies have been explained.

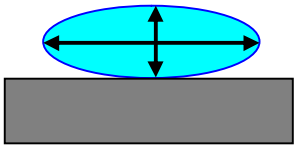

Unfortunately, the crystal structure of the deposited silver layer on GaAs is unknown. This turned out at the beginning of this chapter. As reported by Lehmann et al.[180], *silver nanoparticles on HOPG* could be excited about 25 times better[181] by *p-polarisation* than by *s-polarisation*. Therefore, the plasmon mode *parallel to the surface* could not be excited efficiently in their investigated particles. On the other hand, it is known[182], that for many rough surfaces *p-polarised* light may excite plasmons at thin metal layers and at metal-X interfaces[183] much better than *s-polarised* light. Therefore, this does not

[178] Seen as the green area
[179] And references therein
[180] [LMP+00]
[181] I.e. more photoemission yield
[182] E.g. from [Rae80]
[183] X=metal, semiconductor, insulator, vacuum

give additional knowledge helping to decide whether there is a smooth silver layer or nanoparticles in the observed system. Still, this is of minor importance now, because it is sufficient to know that *p-polarised* light excites plasmons more efficiently than *s-polarised*. In addition, the 2PPE-yield in the experiments was about 3.5-4.5 times higher with p than with s. One can therefore assume to excite any kind of plasmons.

Back to the explanation: besides the dynamics of cascading electrons, one excites with the p-pump pulse, plasmons in silver and at the interface. Those plasmons absorb even more energy than an electron gas. Thus, there is more energy, which cannot vanish via electron-electron scattering. The thermalisation and the cooling of the electron gas are hindered stronger.

The combination of *cascading electrons*, *hot electron temperature* and *plasmon excitation* explains well the shoulder of the autocorrelation curve of Ag[1.5ML]/GaAs.

But, what about the asymmetric cross-polarised autocorrelation curves (Fig. 40)?

Normally, there does not arise any asymmetry even with different laser intensities of both pulses[184]. In the experiments of this work, the ratio of laser intensity was always close to 1:1. Asymmetries in the cross-correlation curves of fs-time-resolved measurements like those reported in this work, has been published only once by Cao et al.[185]. They investigated the transport effect at Au(111), and saw a small dent at the side, where the *s-pulse is followed by the p-pulse* (opposite to measurements in this thesis). They argued that the *s-polarised* light results in an about six times smaller yield as with *p-polarised* light, and therefore causes the non-linear repopulation process to be weaker when the *s-beam* is the *pump* and the *p-beam* is the *probe*. They also found this asymmetry to become stronger as the intermediate levels get closer to the Fermi level, where the repopulation process makes a larger contribution to the dynamics. Put briefly to the point, they called this asymmetry a "fingerprint" for the repopulation process in the cross-polarised TR-2PPE experiment.

In the experiments of this work, electrons have been excited with *p* about 3.5 times better than with *s,* at the interesting energies. As in the observation of Cao et al. the dents in the measurements become stronger, closer to the Fermi level. However, there is not only a *dent*, but also an *additional peak*. This cannot be explained solely by the hypothesis of cascades, hot electron temperature and plasmon excitation. It has to be

[184] Laser intensity ratio up to 1:2 does usually not produce an asymmetric cross-correlation curve.
[185] [CGE+98]

connected to a *polarisation dependent* excitation. Up to now, there is no explanation for this behaviour. It is important to repeat those measurements with pp, ps/sp and ss. The latter one has never been measured, but may help to find a solution.

b. Thicker deposited silver layers on GaAs

At 1.5ML silver on GaAs the excitation of plasmons and the hot electron temperature are responsible for a delayed electron relaxation. Is there any change in the dynamics at a higher silver coverage?

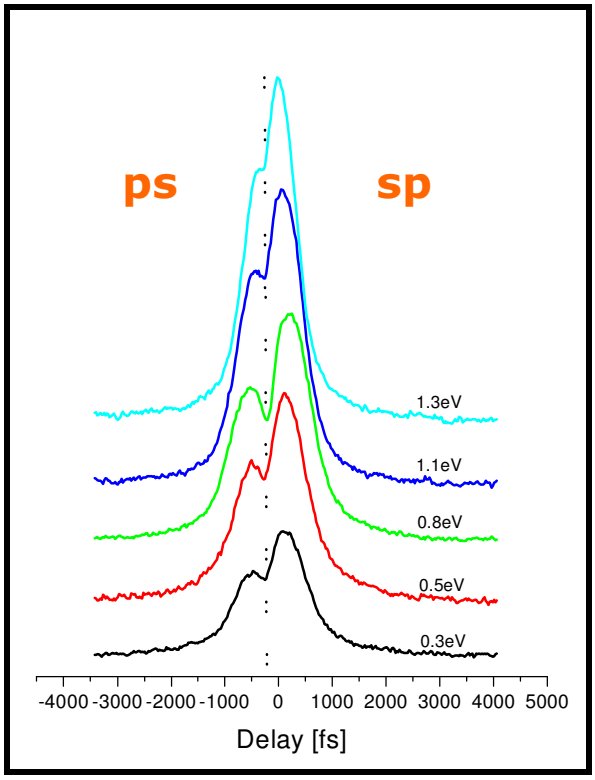

Fig. 44: Evolution of the dent in Ag[3.5ML]/GaAs. Shown are some TR-2PPE curves for different energies above Fermi edge.

From 1.5ML to 3.5ML silver, there is a work function change of about 0.2eV to lower energies. At an *electron-yield ratio* of about p:s=4:1, the autocorrelation curves of ps and pp show similar shapes, as at 1.5ML Ag. The difference between dent and peak at Ag[1.5ML]/GaAs seems to follow again a linear law with increasing energy. At an energy of about $E\text{-}E_F$ = 0.8eV there appears to be a resonance (Fig. 44). This is visible in a strongly developed dent, which not only forms the shape of a shoulder, but of a real dip. This is surely connected to the fact, that $E\text{-}E_F$ = 0.8eV is near to the conduction band minimum E_{CB}.

At 7.5ML Ag there is again a reduction of the work function by about 0.2eV. The autocorrelation and cross-correlation curves remain unchanged compared to smaller amounts of deposition. As before, the dependence seems to be linear between energy and time delay of the determined differences between dent start and additional peak.

It is interesting to visualise the slope of this linear law for different thicknesses:

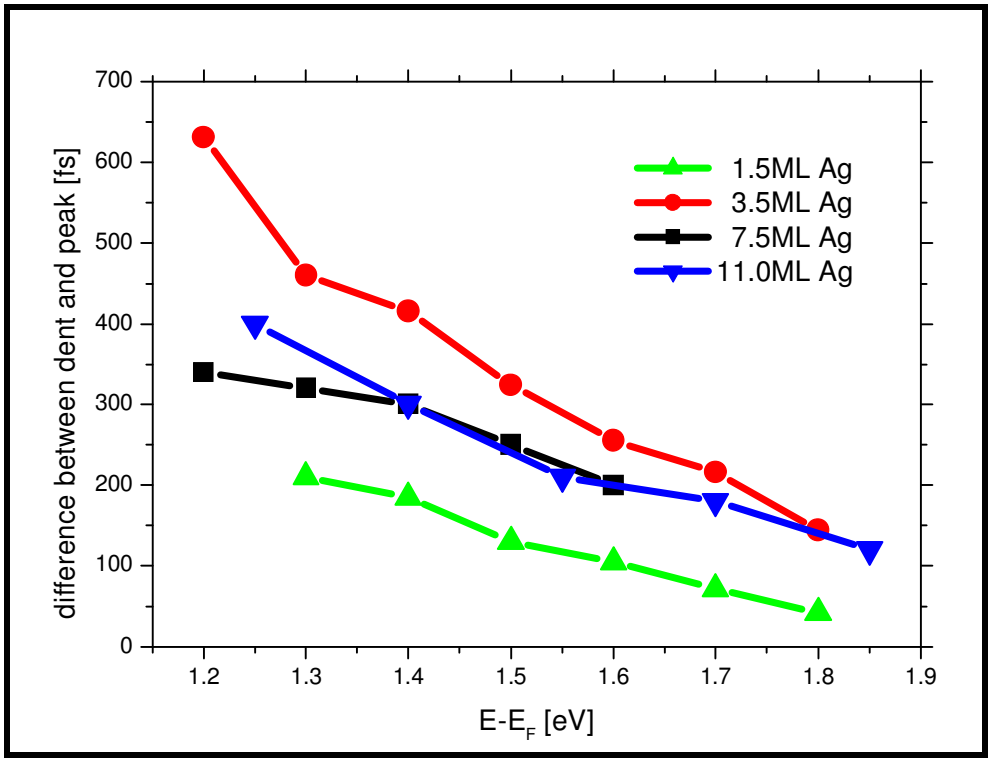

thickness [ML]:	1.5	3.5	7.5	11.0
slope [fs/eV]:	**-275**±10%	**-750**±10%	**-350**±10%	**-450**±10%

Fig. 45: The dependence between energy and time delay of the determined differences between dent start and additional peak, drawn for 4 different silver coverages. The table indicates the slopes of the linear fits to the curves.

The table show a continuous decrease of the slope value with increasing deposited material, except at the coverage of 3.5ML. This points again to the fact that the quantity of silver, which corresponds to 3.5ML, leads to a system with special dynamics (see above).

Dramatic changes like the ones seen in the last some figures, recalls the impressive increase of the electron lifetimes at about 15ML silver on graphite (Fig. 32 at page 75) and on the electron behaviour at Ag[3-6ML]/MgO(100) seen later (Fig. 56 and Fig. 57 on page 114).

c. Quantum well state in the gap of GaAs

In order to get more information about what is happening in the energy range of the gap of GaAs(100), where there should not be any influence of the electrons coming from GaAs, a two-colour experiment with a *red* (1.5eV) pulse and a *blue* (3.0eV) one have been performed.

The principle of a two-colour TR-2PPE experiment was explained upon Fig. 25 on page 60. There it was described that *two different* intermediate states are detected, depending on whether *red* comes first, or *blue*. Both states have usually different relaxation times. That makes the *autocorrelation curve become asymmetric in a two-colour experiment*. It shows on the left side (=negative delays) the influence of the population at one energy level, and on the right side (=positive delays) that of the other energy level. In the middle, the signal is a sum of both states.

In addition, a two-colour experiment enables to measure at energies, which lie in the gap of GaAs, because the red pulse enables ot excite electrons from the valence band just above or into the gap, and the sum (4.5eV) of red and blue is sufficient for many electrons to surmount the vacuum level.

In Fig. 46a) some representative spectra of Ag[11ML]/GaAs are plotted with the *red* pulse coming before the *blue* one. As mentioned above, the Fermi level at the surface lies in the gap of GaAs at about 0.5eV above valence band. Therefore, one may identify the semiconductor's gap at $E-E_F$=-0.5eV until 1.0eV.

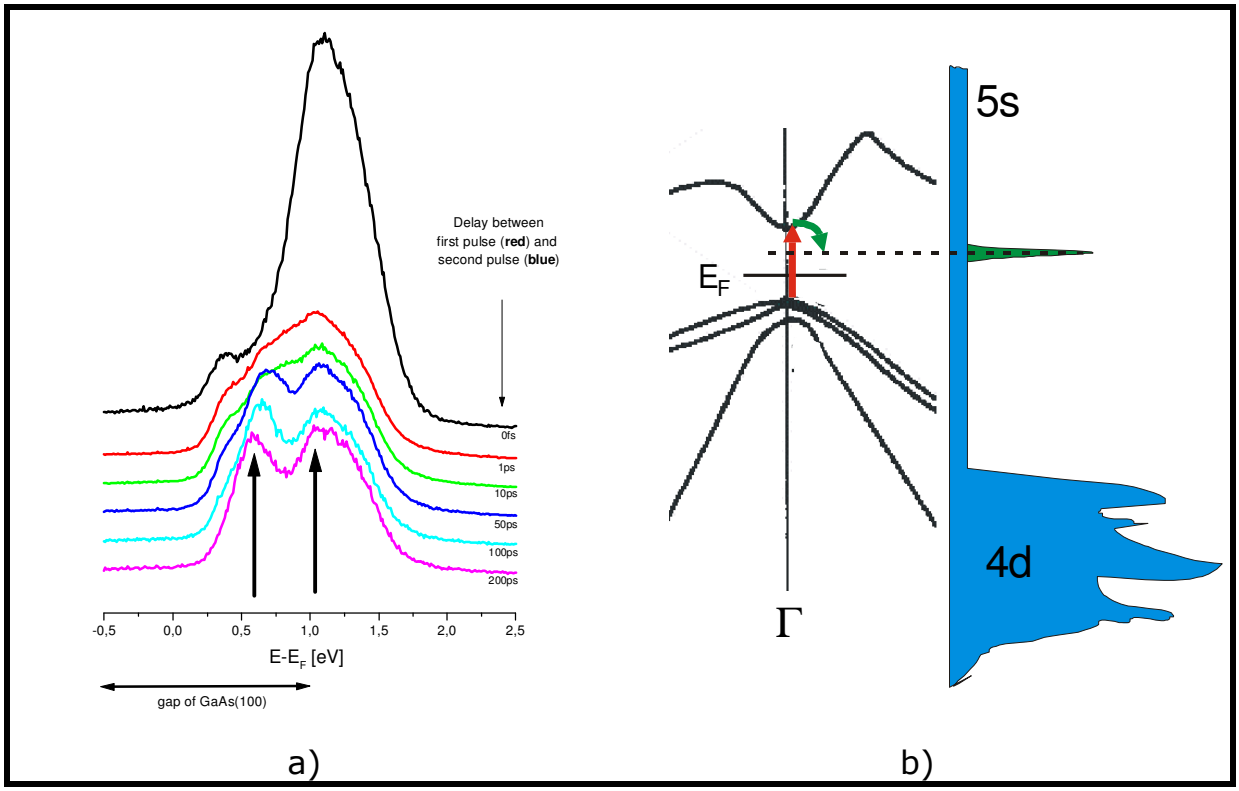

Fig. 46: Spectra of Ag[11ML]/GaAs taken within a two-colour experiment using red (1.5eV, s-polarisation) and blue (3.1eV, p) pulses.

a) Different spectra showing the time evolution with the *red* pulse *before* the *blue* one. The gap of GaAs(100) lies between E-E_F=–0.5eV and 1.0eV.

b) A symbiosis of two different views: a part of the band structure of GaAs around the Γ-point, and a schematic DOS of silver, with its 5s and 4d bands. The red arrow indicates the excitation above the gap, and the green arrow symbolizes the first approximation model for the decay into a quantum well state (green peak) of silver.

In the picture at 0fs delay (black curve) a strong but not sharp feature in the spectrum at E-E_F=1.1eV is clearly visible. This comes from a direct excitation of electrons from the valence band edge to the conduction band edge. Due to the dispersion and splitting of the valence band in GaAs, this feature is smeared out. Even though we excite electrons in silver, the spectrum is dominated by the electrons, which were excited in GaAs.

In the picture Fig. 46a), one recognizes two evolutions with increasing time delay, indicated by two black arrows.

At E-E_F = 1.1eV, right at the edge of the conduction band, the population of detectable electrons is more and more *decreasing*, as delay time becomes longer. This decrease is much faster[186], than if there were no deposited silver. Normally, the relaxation of electrons in GaAs from the conduction band edge into the valence band may only happen via photonic

[186] In the region of picoseconds

decay over the gap, and it is known to take up to nanoseconds[187]. Besides that, the reason for this peak to stop decreasing at time delays above a few picoseconds, are of course cascading electrons from higher levels of the conduction band, excited e.g. by the blue pulse.

Along with this feature at the conduction band level, increasingly a new peak arises, which lies in the gap of GaAs. It is hardly seen at 1ps time delay, but becomes stronger with increasing time delay. It does not show a dispersion (= any shift to lower or higher energies), indicating a *stable unoccupied state*. This *quantum well state* (QWS) is definitely positioned in the gap of GaAs(100) and may only be located at the interface and the silver side.

A QWS is a standing wave that extends over the full width of the silver layer, between both interfaces to vacuum and to the substrate. QW states are created by trapping the electrons in a thin film. The surface barrier on the vacuum side, and a band gap for propagating s-p states, on the substrate side, confine the s-p electrons within the film. When the film thickness is comparable to the electron wavelength, these states appear at discrete energies with quantised wave vectors *perpendicular* to the film. This makes them detectable only with p-polarised light.

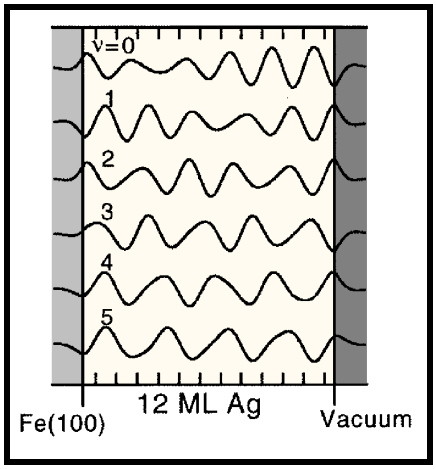

Fig. 47: The calculated QWS wave functions for Ag[12ML] on Fe(100). Outside the film, wave functions are assumed to decay exponentially. The indicted values (ν) correspond to Fig. 48. Picture from [ONP02]

The stable feature in Fig. 46a) shows an adsorbate state (QWS), which becomes continuously refilled by cascading electrons from higher levels. It opens a new relaxation path for the electrons at the conduction band edge, as depicted in Fig. 46b). Electrons excited or cascaded to the conduction band minimum may relax into this quantum well state. It can be given a rough relaxation time for this process to about 1ps.

Spectroscopic evidence of gap states has been found in GaAs interfaces with techniques such as catholuminescence[188], scanning tunnelling spectroscopy[189], photoemission spectroscopy[190], inverse photoemission[191],

[187] [Ohm02]
[188] [VSB86]
[189] [Fee98, Fee92]
[190] [SLSS80, KNMN95, HB86]
[191] [LSHG86]

and non-linear optical spectroscopy[192]. None of them had the possibility to describe the time-evolution of a population in those QWS.

Gap-states of silver on GaAs(110) were also reported by Arciprete et al.[193]. However, they had not had exactly the same situation as in this work. They observed interface states by high-resolution electron-energy-loss spectroscopy [HREELS] in metal-GaAs(110) junctions. Due to the impinging of electrons into the system, they observe mainly two additional peaks in their spectra. One, at 4eV above valence band, coming from the obvious plasmon loss of the Ag. The second, at 1.2eV above valence band, could – at first sight - be interpreted as a quantum well state, but it shows no energy dispersion with changing coverages, and it disappears with increasingly coverage. So, they assigned it to an interface plasmon mode. Of course, the used method in this thesis would not be sensitive to such an interface plasmon, due to the use of photons instead of electrons. This fact, and the appearance of coverage-dependence in the measurements of this work (see just below), confirms that in this thesis not interface plasmons were detected, but QWS.

The current measurements of this work might be more suitably compared to quantum well states in **Ag/Au** systems described by Pérez-Díaz and Muñoz[194], **Ag/Fe(100)** by Ogawa et al.[195], and **Ag/Si(001)** by Matsuda et al.[196]:

Pérez-Díaz and Muñoz[197] investigated theoretically the electronic structure of metallic-thin-film overlayers grown on a substrate, mainly *silver on gold* as well as *cobalt on copper*. They described it in terms of the overlayer *size-quantised* states and continuous substrate bands, and showed that the wave-vector component in the growth direction, $k_{\perp}$, of thin-film states is quantised due to its finite thickness. They also found, that the binding energy of the QW states is film-thickness dependent. Unfortunately, it is not possible to compare it directly with the current measurements, because in this thesis only usually unoccupied QW states in the gap of GaAs may be detected, whereas these authors have only depicted occupied states.

Ogawa et al.[198] examined QW states in Ag/Fe(100). They could show the QW states' energetic positions, and they were able to determine the QW states' lifetimes to 3.8fs and 9.2fs for 4ML and 18ML silver, respectively, using photoemission linewidths calculations. These lifetimes are clearly shorter than those of bulk single crystal. Ogawa et al. pointed out that

[192] [AYYT95]
[193] [ACF+96]
[194] [PM96]
[195] [ONP02]
[196] [MYT+01]
[197] [PM96]
[198] [ONP02]

such fast population decay could be due to both electron-electron scattering in the Ag film and reflection loss at the substrate and vacuum interfaces: Since the electron confinement by the hybridisation gap is not perfect, the reflectivity at the Fe(100) interface is less than unity. Scattering at the vacuum barrier may also reduce the lifetime.

In Fig. 48 the results by Ogawa et al.[198] on Ag/Fe(100) have been compared with those of Ag/GaAs(100) of this work. All *black* marks were produced by Ogawa et al., the *coloured* circles indicate the measurements on Ag/GaAs(100). This viewgraph shows calculated and measured QWS energy positions in dependence of the film thickness. The calculation has been developed originally by J.J. Paggel, T. Miller, and T.-C. Chiang[199], and it is based on the same terms as used in appendix VIII.2 for the description of surface states and image states.

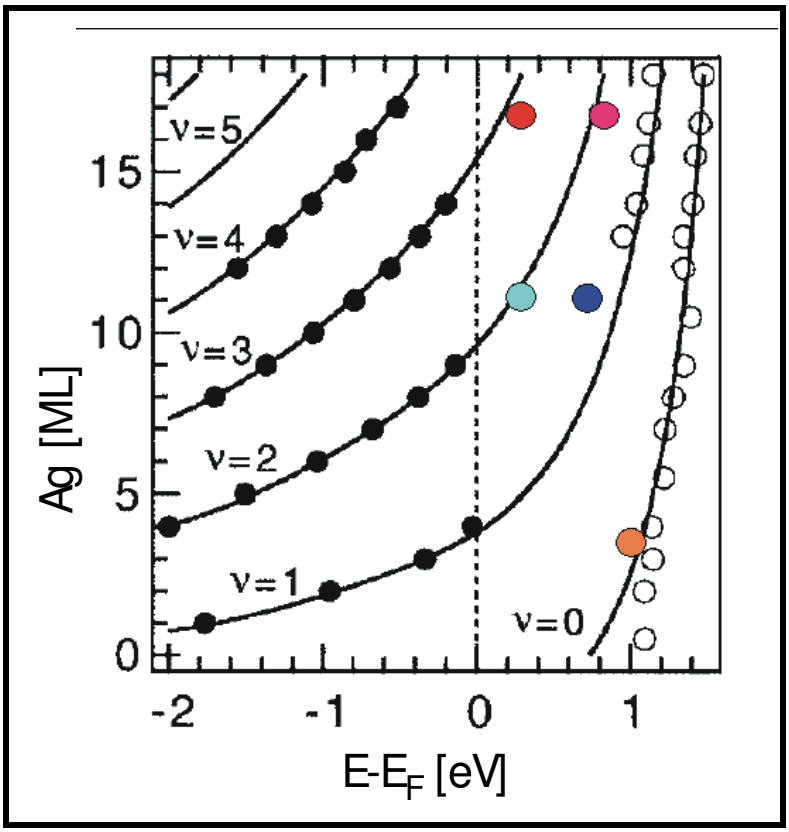

Fig. 48: Energetic locations of QWS in silver as a function of the layer thickness, adopted from [ONP02]. *Black* points and lines are occupied (filled circles), unoccupied (open circles), and calculated (lines) QW energies for different film thickness, produced by Ogawa et al. [ONP02]. The *coloured* circles indicate results of the current measurements, explained in this work.

One recognizes a quite good correspondence of the results of this work with the theory. One has to consider, that the current measurements were carried out at room temperature, and the fact that the deposition consists

[199] [PMC98]

of islands (Stranski-Krastanov mode), instead of epitaxial films. The effect of such an inhomogeneous film is, that the QWS smears out, because of measuring not only the n^{th} layer (thickness n), but also the $(n\pm1)^{th}$, $(n\pm2)^{th}$, … However, the advantage of the system used in this work is that there is no hybridisation between wave functions of the film and of the substrate.

The arising questions are: why is the measured relaxation time so short at the conduction band edge (Fig. 46), and how strong is the influence of refilling processes into the QWS?

To analyse both time evolutions, red/blue measurements at Ag[17ML]/GaAs(100) were performed, which can be seen in Fig. 49.

In Fig. 49a) three spectra were plotted; taken with *red* light only, with *blue* only and with *both*. The purple arrow indicates the position of a QWS, whereas the olive arrow points to the conduction band edge.

First, concentrating on the conduction band edge, i.e. the *olive* arrow in Fig. 49a) and the *olive* two-colour TR-2PPE curve in Fig. 49b).

Curves in a two-colour TR-2PPE show a combination of the evolutions of two populations at two different energies. So, one has to separate them carefully. Such a separation for the evolution of the QWS (*purple* arrow) is drawn in Fig. 49c). It will be discussed below.

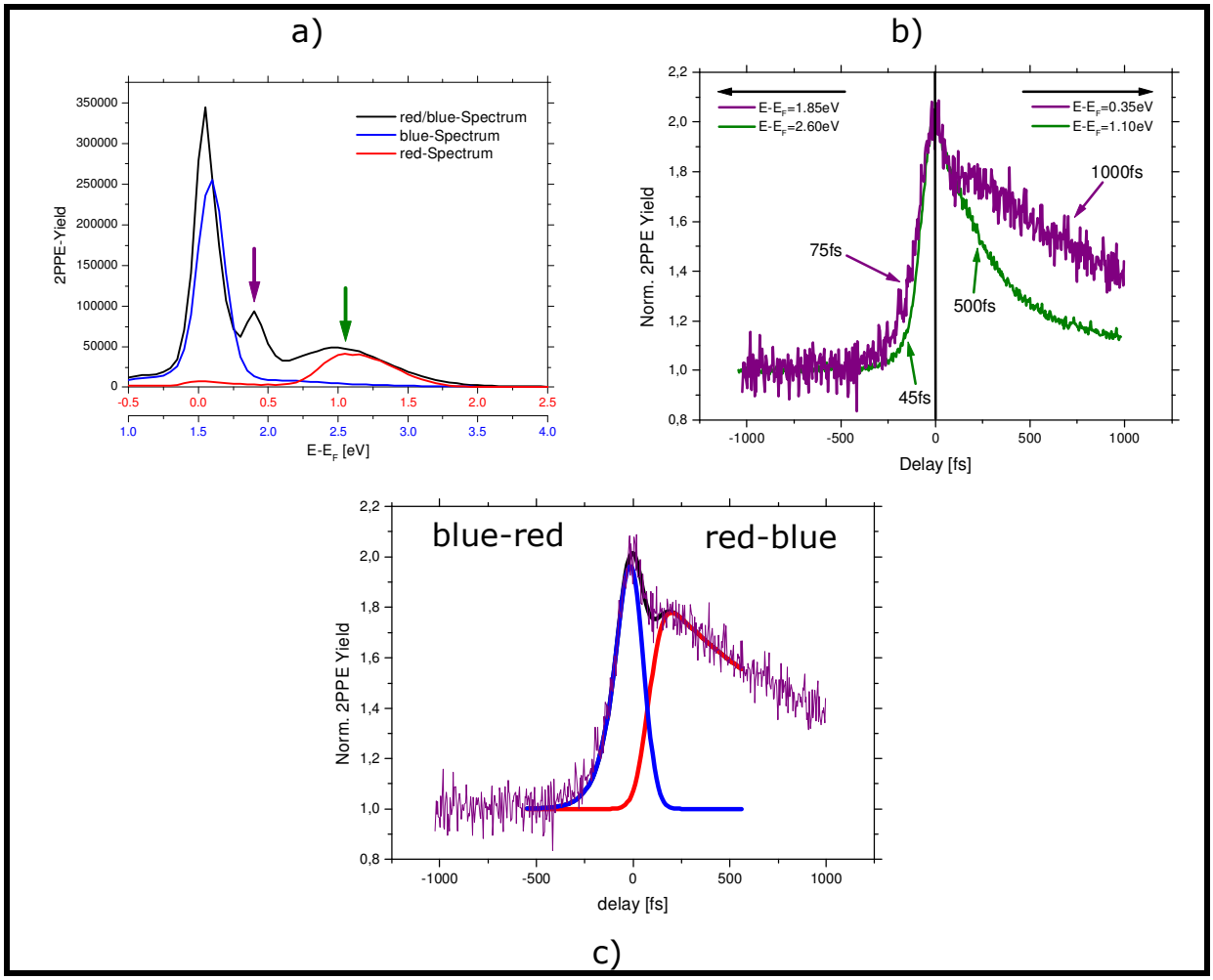

Fig. 49: Red/blue-TR-2PPE measurements on Ag[17ML]/GaAs(100).

a) Depicted are spectra taken with red ($\omega_1+\omega_1$), with blue ($\omega_2+\omega_2$), and with both ($\omega_1+\omega_2$). The *purple* arrow indicates the location of the probed QWS. The *olive* arrow points to the conduction band edge. At the bottom, two scales are drawn; one for the pump pulse being red, and one for it to be blue.

b) Both two-colour TR-2PPE curves are plotted; for the energies of the *purple* and the *olive* arrow. On the *left* side, the energy corresponds to excitation with blue as pump pulse, and the *right* side is the situation for excitation with red as pump pulse.

c) The separation of the time-evolutions of two different energy levels (exactly: the population at both energies). The colours (blue, red) indicate the excitation energy of the first pulse (blue: 3eV, red: 1.5eV). Note: the colours do not indicate the shape of the pulses, but the populations at those energies.

Roughly spoken, one sees at the *left* side of this *olive* curve (in Fig. 49b) the evolution of the population at energy $E\text{-}E_F$ = 2.6eV. This is far away from conduction band minimum, and exhibits an energy relaxation of about T_1 = 45fs, which agrees well with measurements of T. Ohms[200].

At the *right* side of Fig. 49b) (still looking at the *olive* curve), one sees the relaxation at the conduction band edge ($E\text{-}E_F$ = 1.1eV). The population there decays with about T_1 = 500fs, which is at least an order of

[200] [Ohm02]. He observed GaAs without silver deposition.

magnitude faster than at GaAs(100) without silver. The relaxation occurs mainly into unoccupied states in silver, as it will become visible below.

The *purple* arrow in Fig. 49a) points to the QWS. Its time evolution is drawn in Fig. 49b). However, it is necessary first to separate the populations of both energies out from the *purple* curve. The result of this separation is shown in Fig. 49c).

The blue curve in Fig. 49c) indicates the time-evolution of the population at **1.85eV above E_F**, which is populated with 3eV excitation energy. With about T_1 = 75fs is corresponds well to published values[200]. One may also recognize, that this energy level becomes populated immediately; there is no temporal shift between the exciting laser pulse maximum (not shown, but located at 0fs delay) and the population maximum at that energy.

The red curve in Fig. 49c) is a representation of the filling into, and the relaxation from the QWS. The *filling process* into this energy level at **$E-E_F$ = 0.35eV** may have *two* origins (Fig. 50): the excitation of electrons from lower lying occupied states in silver (at $E-E_F$ = -1.15eV), and the cascading of electrons from higher lying energy levels in silver and in GaAs. To be precise, the latter electrons mainly come from the conduction band minimum of GaAs, because the electron density there is much higher than at the silver side, and the ΔE = 0.3eV of the cascading process in GaAs[200] disables relaxation from levels higher than the conduction band minimum.

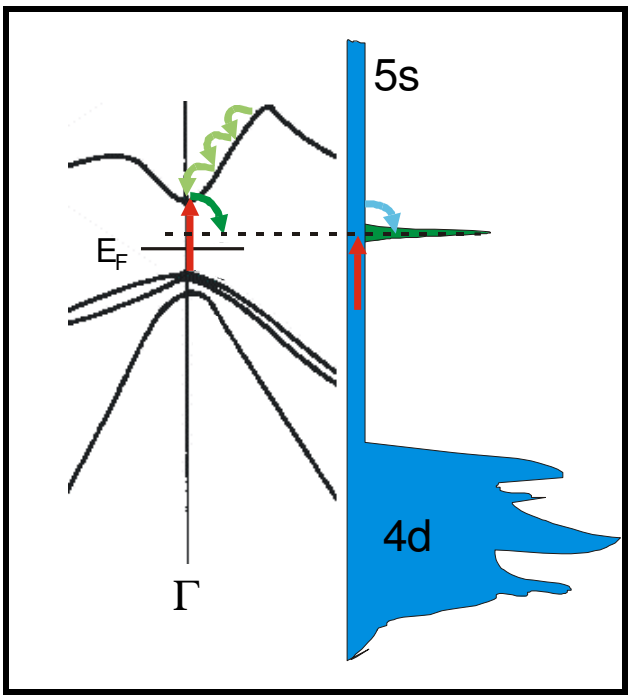

Fig. 50: Schematic view on the filling processes of the QWS.

The shape of the *red* curve in Fig. 49c) indicates a delayed occupation of the QWS by about 200fs, seen by a shift in the population's maximum. That fact *excludes* a strong contribution to this filling process by excitation of electrons from lower lying occupied states in silver, because this would start immediately. The origin of such a delayed occupation of this QWS may be estimated as following:

1. The relaxation of excited electrons from the conduction band minimum: This process must involve photons with wavelength of about λ=2000nm (ΔE=0.6eV). It is known, that such a fluorescence does not take place in just some tens of femtoseconds. The

fluorescence over the whole band gap, e.g., happens in nanoseconds. Therefore, one may exclude that process. This means: the dark green arrow in Fig. 50 *does not* show a probable relaxation path.

2. The filling via electrons, which relax from the conduction band minimum (and/or move) into unoccupied silver states, and then from there via cascading processes into the QWS: By assuming relaxation times in silver of 200fs up to 40fs[201] for electrons with energies between 0.35eV (QWS) < $E-E_F$ < 0.85eV (CBM), one comes without problems to a time delay between pulse maximum and population maximum of about 200fs. This seems therefore to be the *true* process.

The relaxation of electrons from the QWS is very slow. Although the measured curve (right tail of the red curve in Fig. 49c) contains both the relaxation from QWS and the refilling into the QWS, it is possible to give an approximation to the relaxation time of $T_1 = 1000\text{fs} \pm 10\%$. Further investigations will improve the accuracy of the relaxation process out of the QWS.

Comparing these times to those of Ogawa et al.[202], one recognizes much longer (two orders of magnitude) relaxation times. This is probably due to the much better reflection of the wave function at the substrate's gap in the current case, than at Fe(100), leading to less interface scattering, and thus to higher relaxation times. Ogawa et al. suggested, that the relaxation time increases with film thickness because of a reduced number on encounters with interfaces. The measurements of this thesis show this tendency. However, even these decay times in the current data are too low, because of the scattering at grain boundaries at the surfaces, which leads the electrons to dephase and relax earlier.

[201] E.g. [Por98]
[202] [ONP02]

d. Inverse spin injection

Apart from the investigations above, the system Ag[17ML]/GaAs(100) brought the opportunity to check also the so-called *inverse spin injection*. The deposition of metals on a semiconductor is a hot-topic, for its being used in spintronic device fabrication. For a long time, a question in this context could not have been answered yet: Is it possible to inject spin-polarised electrons from a ferromagnetic layer into a semiconductor (and vice versa)?

LaBelle et al.[203] has recently demonstrated some measurements of the spin-injection probability from a ferromagnetic metal tip into p-type GaAs(110) surface (Fig. 51a). They found a decrease of the bulk spin relaxation lifetime of a factor of 12 on step edges. This would lead to the assumption, that spin injection is limited to very few numbers of electrons, which survive the transition through the boundary.

The investigations of this work show a passable transfer of injected electrons from the GaAs(100) through the 17ML-layer of silver into the vacuum (Fig. 51b).

Spin injection Inverse spin injection

Fig. 51: Spin injection.

a) Spin injection from a ferromagnet into a semiconductor

b) Inverse spin injection from excited electrons in GaAs through a metal into the vacuum.

The measurements have been carried out within a two-colour experiment. The red pulse was circularly polarised using a quarter wave plate. As depicted in Fig. 34c) on page 79, the optical selection rules for transitions over the gap at the Γ-point of GaAs(100) lead to a spin polarisation at the conduction band edge, when using circularly polarised light. The spin-polarised electrons could be detected using a spin-analyser add-on mounted on top of the energy analyser (described on page 63).

[203] [LBD+01]

In Fig. 52 a typical spectrum (blue curve) of a red-blue two-colour experiment is drawn. The peak at about $E\text{-}E_F$ = 1.1eV is produced by red-red excitation, that one at $E\text{-}E_F$ = 2.6eV by blue-red excitation.

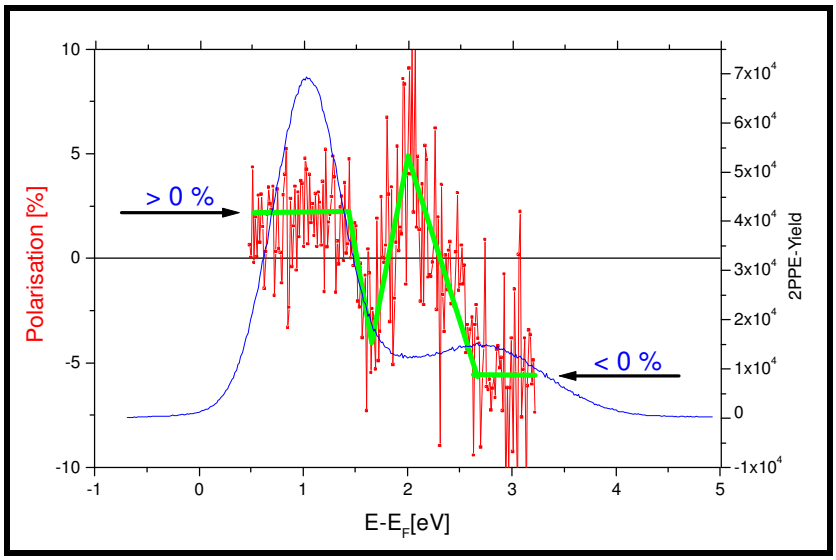

Fig. 52: Spectrum (blue curve) and spin polarisation (red curve) of inverse spin injected electron, which have been excited over the gap of GaAs, and emitted through the silver layer (17ML) into the vacuum. The green lines are eye guide-lines.

One can see a spin polarisation of excited electrons at $E\text{-}E_F$ = 1.1eV of more than 2%. This means, the emitted electrons, which had a spin polarisation of max. 50% at the conduction band edge could be transmitted through the 17ML thick silver layer into the vacuum. This is an evidence of the inverse spin injection.

The different polarisations in Fig. 52 (green lines) come from electrons, which were excited by both the red and the blue pulse at the same time. The spin polarisation at $E\text{-}E_F$ = 2.6eV is also a consequence of the selection rules. This can be explained easily: During the excitation of spin-polarised electrons from valence band into the conduction band (with 1.5eV), this process leaves in the probed volume electrons unexcited, which have a net spin-polarisation of opposite sign. Those spin-polarised, unexcited electrons are then excited by the blue-red pulses up to $E\text{-}E_F$=2.6eV, and show there of course a negative polarisation.

The used method is a proper tool to produce a spin-polarisation of desired polarity. It is only necessary to choose the energy in order to switch from positive to negative polarisation.

4. Metal atoms on an insulator: Ag on MgO

In the last sections, the dynamics of optically excited electrons in silver on HOPG and in silver on GaAs(100) have been described. Both substrates have a band gap (in the measured direction), which are smaller than the used excitation energies of 1.5eV (red) and 3.0eV (blue). That is the reason for not being able to totally eliminate the influence of the substrate. One always had to take excitations into account, which happened in the substrate.

The only chance to hinder any influence of the substrate to the excitation is to look for a system with a gap bigger than about 3.0eV. A second condition, however, is still the same: silver should grow epitaxially on it, or at least one should have the possibility of using known recipes for the uniform deposition of silver onto.

Magnesium-oxide MgO(100) produced by CrysTec became the observed system. MgO(100) has a band gap of 7.8eV, which would be sufficient even for two blue excitation steps. It is an ionic insulator with the rocksalt cubic structure with a lattice constant of 0.421nm, and is regarded as one of the better electrical insulators in refractory oxide materials. The in-plane mismatch of MgO(100) and fcc Ag(100) is below 4%.

Perry et al.[204] described the importance of such a system as following: "*The growth, resulting structure, and stability of metal thin films on metal oxide substrates represent critical elements in the production of modern microelectronics, solid oxide fuel cell devices, and many catalysis systems. Many of these technologies involve interfaces that must be understood and controlled on the atomic scale. As a result, a fundamental under-standing of the atomic-scale parameters controlling the structure of metal films on oxides or oxide surfaces is desired.*"

There is large knowledge about deposition of metals on MgO, even at neighbouring groups. Many publications describe recipes for the evaporation of silver on MgO.

Zhukovskii et al.[205] carried out theoretical analyses of the deposition of silver on MgO(100). For a coverage of more than 25% of the MgO surface, they found that the position above the oxide atoms are energetically preferred for the silver atoms (Fig. 53). The silver layer is expected to grow with the (100) plane parallel to the (100) surface of the MgO substrate[206].

[204] [PY01]
[205] [ZKJ+99]
[206] [DJ94]

The growth mode of silver thin films on MgO(100) is shown to strongly depend on the chemical purity of the oxide surface. On a carbon- and defect-free surface the silver deposit grows layer-by-layer, while the presence of any of these chemical defects prevents such a growth mode, and lead to three-dimensional islands[207]. At nominal 10ML silver on MgO, there is then only a coverage of[208] 35%±5% of the substrate.

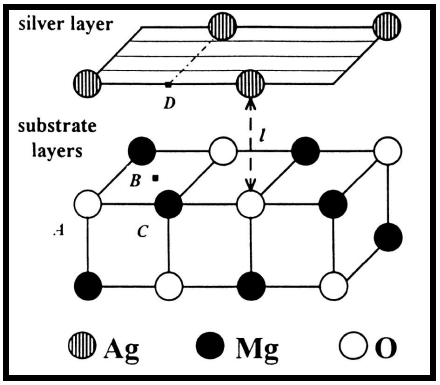

Fig. 53: Fragment of the Ag/MgO(100) interface where Ag atoms are placed at the distance *l* above the O atoms of the substrate surface

Li et al.[209] found the total energies of the system Ag/MgO to be 0.3eV/atom. This adsorption energy indicates, that Ag/MgO belongs to a physisorption class, which is expected, since there is no noticeable charge transfer and chemical bonding existing in this system. The Ag-Ag interaction is much stronger than that of the Ag-MgO[210].

Rickart et al.[211] report a layer-by-layer growth mode of silver on MgO using a new technique for the preparation of carbon-free MgO surfaces with the means of ion beam oxidation. This technique takes advantage of the high chemical activity of dissociated low energy oxygen atoms, which removes the carbon contamination from the MgO surface. They found an even simpler way to get epitaxial flat silver layers, by using a 1nm thick Fe seed layer between the MgO surface and the silver layer. This leads to the formation Ag(100)/Fe(110)/MgO(100).

The sample preparation for investigations of this thesis followed Rickart's recipe and consisted of heating the MgO to 650°C for 2-3 hours, partly under 10^{-6} mbar O_2. The cleanness was checked with Auger, LEED, and a mass spectrometer. The silver has been evaporated at 0.03ML/s, room temperature and $8 \cdot 10^{-9}$ mbar.

Eventually, the measurements with the system Ag/MgO led to some unexpected results. However, the interpretation of the time-resolved data is quite questionable, caused by the nonepitaxial growth of the silver layer.

[207] [DJ94 and references therein]
[208] [SPS98]
[209] [LWFF93]
[210] [SPS98]
[211] [RRM+01]

First, some information of the clean substrate: The insulator MgO has a band gap of 7.8eV, and an ionisation potential[212] of 6.7eV. As an ionic insulator, it has a tendency of showing F-centres (see page 12) at low-coordinated surface sites (such as steps, kinks, corners) and at surface vacancies. Moreover, exposure of the MgO surface to light can lead to ionisation of different sites and to the creation of electron-holes. F-centres may therefore, in conjunction with metal adsorbates, produce occupied and unoccupied states.

The exposure of the MgO surface to air, leads to the generation of hydroxides, therefore to a passivation of the oxides on the surface and thus to an approach to metallic Mg behaviour. This could be taken as a criterion, whether the sample is still hydroxide-free or not: whenever there was such a contamination, many photoelectrons were detected coming from the Magnesium on the surface. The clean and hydroxide-free surface showed very few photoelectrons, caused by surface defects. However, the LEED pattern showed sharp spots, at the contaminated as well as at the hydroxide-free surface.

a. Preliminary experiments

First thickness-dependent TR-2PPE measurements were performed on a rough MgO substrate that was passivated by hydroxides. Thanks to the surface configuration, there were no problems with charging effects; the photoelectrons were being replaced by conducting electrons via the Mg atoms on the surface. However, not thickness-dependence, but amount-dependence is the proper denomination. The layers were far from being flat; see Fig. 54. Nevertheless, the influence of the substrate's surface should vanish increasingly with higher silver coverage, and one gets the chance to test, if there is a dimension-dependence in the z-direction (perpendicular to the surface). The x- and y-directions (parallel to the surface) are affected by Mie-plasmons caused by the islands' dimensions of about 25nm - 85nm, which is exactly the regime of Mie-plasmons[213].

[212] Valence band to vacuum level
[213] [Lie93], [Sch02]

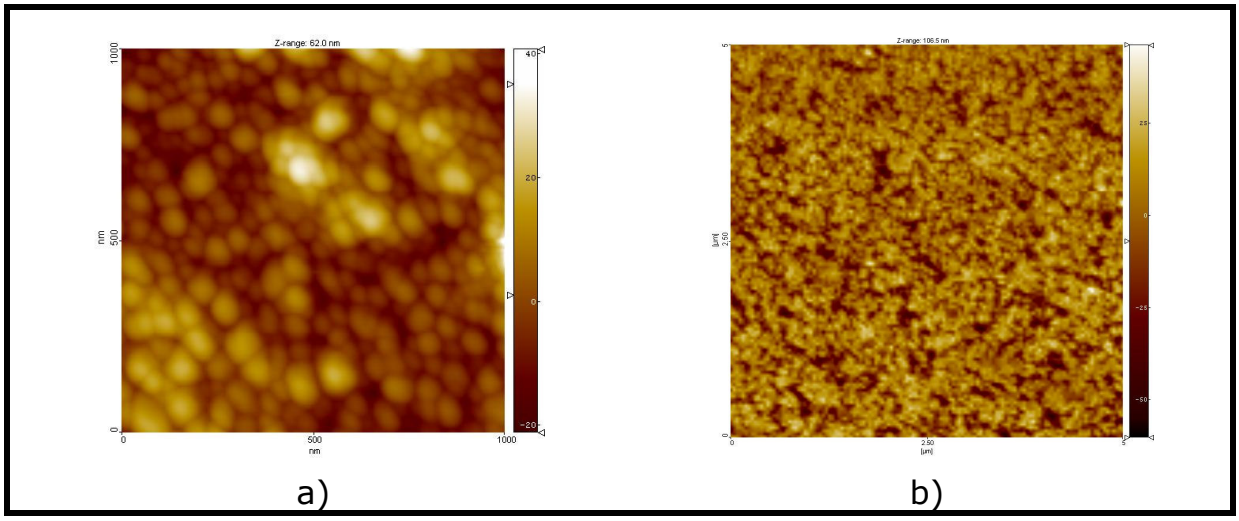

Fig. 54: AFM-picture of nominal 200ML silver on a rough MgO substrate. The MgO surface is almost completely covered by islands of diameters of 25nm - 85nm. Pictures made by M. Mondon in the group of Prof. Dr. Ch. Ziegler, Kaiserslautern / Germany.

a) 1µm x 1µm.

b) 5µm x 5µm.

Fig. 55 shows the (nominal) thickness-dependence of the electron's lifetime at an energy of $E\text{-}E_F$ = 1.55eV. Similar behaviour could be seen at the whole accessible energy range. The situation is comparable to that one at the system Ag/HOPG, discussed under chapter IV.2. At large coverages (bulk), the lifetime is influenced by ballistic transport effects, which reduces the population at the intermediate state, and thus leads to a reduced measured lifetime. The value of the lifetime seems to saturate at about 20fs, as can be seen between 380ML and 100ML, where the influence of transport vanishes increasingly.

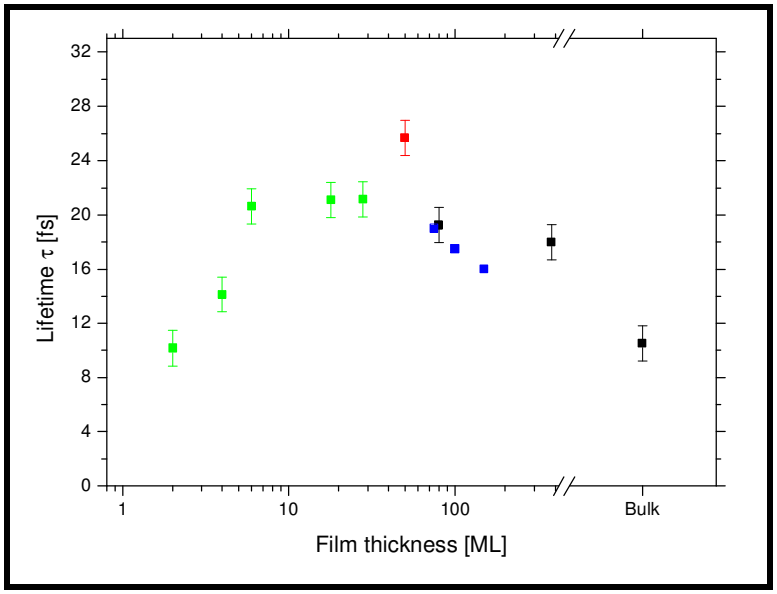

Fig. 55: Film thickness dependence of silver on a rough MgO surface, at $E\text{-}E_F$ = 1.55eV. The rise of lifetime at about 50ML is clearly visible. The blue points indicate results of [ABP+00] taken as a comparison.

By further reduction of the film thickness (~50ML, red point), again a *raise* (~5fs) of the lifetime is detectable. The peak appears at a higher coverage than at the system Ag/HOPG, where the maximum is at about 15ML. This difference has two different reasons. Firstly, the strong roughness of the underlying surface (RMS[214]: 6-8nm ≈ 30-40ML) leads to grain boundaries and large height distribution, which smears out any thickness-dependence of the lifetime. Secondly, the influence of the unpassivated Mg lying under the silver layer leads to undeterminable effects in conjunction with the silver.

The blue boxes depicted in Fig. 55 indicate results coming from preliminary TR-2PPE-experiments[215] at silver on MgO. The silver was prepared by wet-chemical deposition. In spite of the imprecisely determination of the layer's height at these used samples, the results corresponds quite well with those of this thesis.

In spite of the problems and limitations of the investigated subject, one recognizes - in this third system (**Ag/HOPG**, **Ag/GaAs**, **Ag/MgO**) - a change in the behaviour of the inelastic lifetime of optically excited electrons between bulk and a 2d-system.

[214] RMS (root-mean-square-roughness) is defined as the square root of the mean value of the squares of the points' distances from the image mean value:

$$\mathrm{RMS} = \sqrt{\frac{1}{N}\sum_{i=1}^{N}(Z_i - \bar{Z})^2}$$

[215] [ABP+00]

b. Long lifetimes at Ag[3-6ML]/MgO(100)

After those promising results using a rough MgO surface, experiments on smooth substrates were performed. The smoothness was certificated by CrysTec to RMS = 0.03nm, own verification resulted in RMS = 0.24nm, which corresponds to a height of only one atom. The surface was not only flat, but also free of hydroxides. This could be analysed with AFM and upon the very little excitation of photoelectrons (10^{-3}-10^{-4} times less than usual with blue light), assumed to come from F-centres. After heating to 650°C for 2h the surface was carbon-free, checked with Auger-spectroscopy. The LEED-pattern was sharp and without any superstructures.

The deposition of nominal 1ML silver on the clean MgO surface (at the same evaporation rate as before) raised the count-rate of emitting photoelectrons already by a factor of 100, despite the problem of focussing the laser beam on this thin layer (1ML = 0.2nm). Observed TR-2PPE curves showed unrealistic constant lifetimes (about 5-10fs), over the whole energy range ($E-E_F$ = 1.3eV - 2.9eV). This is caused by the separation of the deposited silver atoms, which did not fully covered the MgO surface, and thus the substrate is probed mainly.

At coverages between (nominal) 3ML and 6ML, there has been detected, reproducible at independent different samples, a lifetime of optically excited electrons of about **160fs ± 5%**, over the full accessible energy range ($E-E_F$ = 0.8 - 3.1eV), see Fig. 57. This is *an order of magnitude* longer than in bulk. One observed example is illustrated in Fig. 56 together with the cross-correlation curve of the laser pulses. Although the statistics is not perfect, one can see the broad cross-correlation curve of Ag[3ML]/MgO(100).

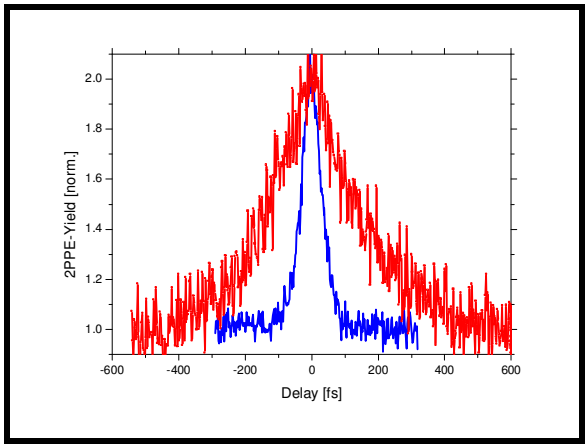

Fig. 56: The TR-2PPE curve of Ag[3ML]/MgO(100) at E-E_F = 0.9eV is shown together with a cross-correlation of the laser pulses (tantal used). It is impressive, how long the lifetime is: ~160fs.

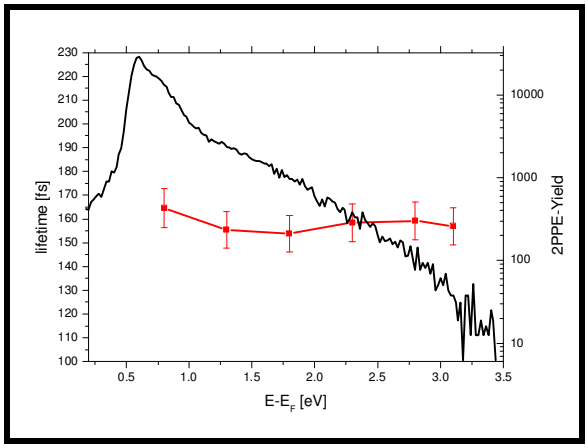

Fig. 57: The lifetime and spectrum of Ag[5ML]/MgO(100), versus E-E_F. The lifetime does only change weakly, there is almost no energy-dependence. The error-bars have been an estimate to ± 5%.

Those long lifetimes could only be detected at surfaces, which exhibit silver islands with heights between 3 - 6ML, diameter between 20 - 60nm, statistically distributed and almost all separated form each other (Fig. 58). One can assign this growth mode to the "Volmer-Weber"-type.

The question arises how such a long lifetime can be explained.

Up to now, there is no conclusive answer to this question. There are two different possible explanations. One having to do with plasmon excitation and one with generation of very hot electrons.

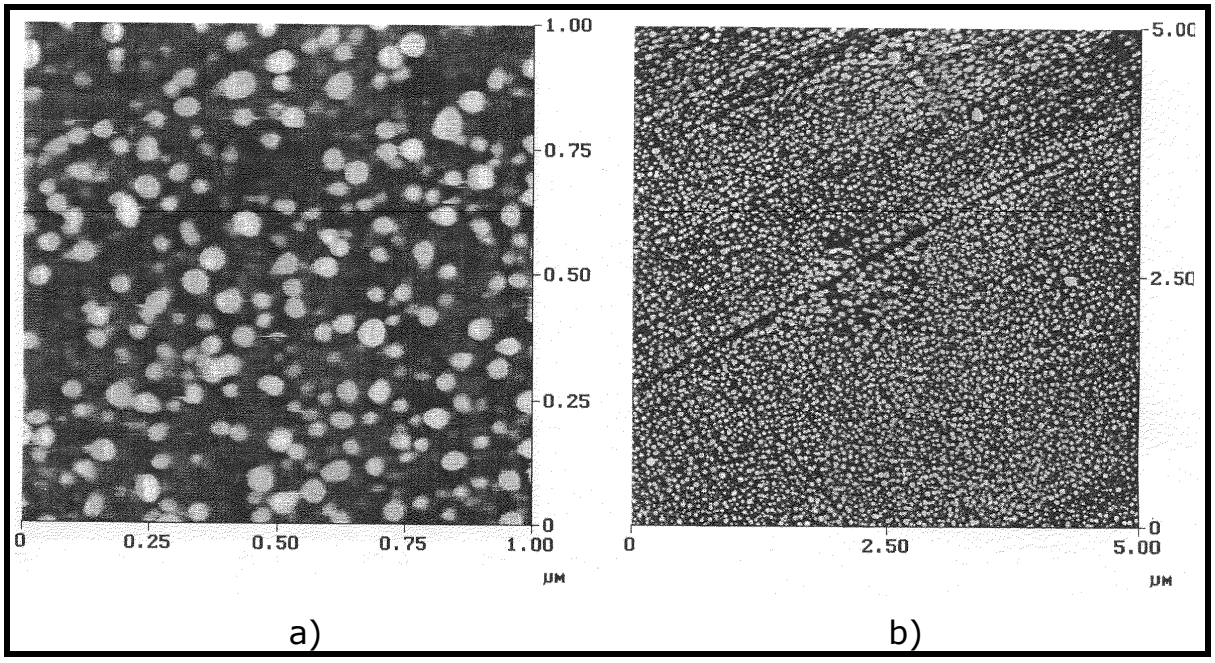

Fig. 58: AFM-picture of Ag[6ML]/MgO(100). Silver islands with heights of 2.7nm (Gauss-distribution with standard deviation: ~1nm), diameter between 20 - 60nm (average: 30nm), statistically distributed and almost all separated from each other. Excited electrons in those islands show very large (160fs ± 5%) lifetimes. Picture made by S. Berger in the group of Prof. Dr. Ch. Ziegler, Kaiserslautern / Germany.

1) Plasmon excitation

The fact that one does not detect long lifetimes (see later), whenever the surface does not show islands, implies an influence coming from those nano-particles. The diameter of 20-60nm (average: 30nm) links directly to the theory of Mie-plasmons. As mentioned on page 32, one of the most important values to change the Mie-resonance frequency – and therefore also the absorption frequency - is the ratio between surface und volume. In principle, this frequency increases with smaller volume. The present nano-particles possess large radii, but small heights, much smaller than the penetration depth of the blue light, and also smaller than the mean free path of the electrons[216]. One would therefore observe small volume-to-surface ratio leading to stronger surface scattering in z-direction, but the electrons may only travel parallel to the surface, and thus the surface scattering process should be suppressed.

The idea, having excited Mie-plasmons (particle-plasmons), could be quite easy checked by considering the statements made by H.-G. Rubahn[217]. The author has plotted an overview for relevant time scales appearing after excitation of small metallic islands (Fig. 59).

---

[216] The mean free path in metals is energy dependent, and lies in the order of $\bar{l}$ =10nm. It may be determined e.g. by resistivity measurement or be calculated using theories of Drude and Sommerfeld, which utilise the Fermi-velocity in metals: $v_F \approx 10^8$ cm/s.

[217] [Rub99]

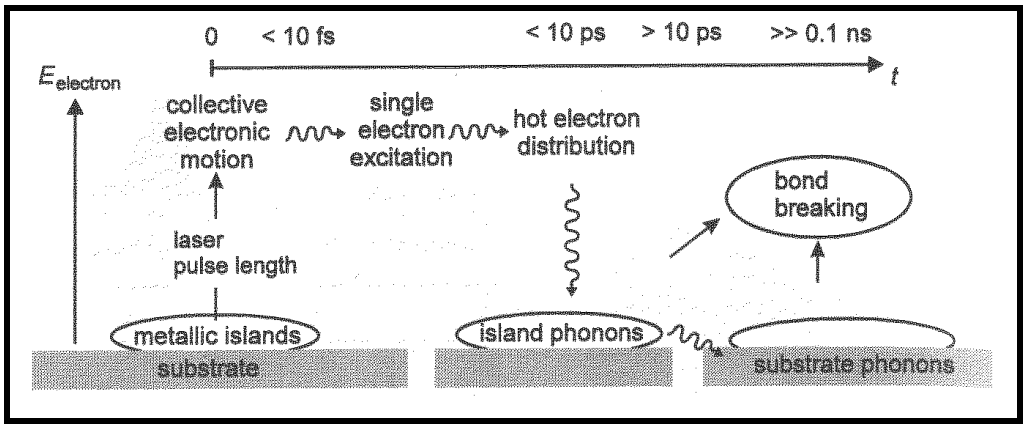

Fig. 59: Schematic drawing of optical excitation (at t = 0) and possible relaxation processes in rough metallic films, consisting of large, surface-bound islands. The ordinate represents the electronic energy $E_{electron}$, while the abscissa shows typical relaxation times for the decay of collective electronic excitation, single electronic excitation and phononic excitation. From [Rub99].

Upon resonant laser excitation, dynamic processes occurring on the *femtosecond* (initial electronic relaxation), *picosecond* (coupling to the lattice) and *nanosecond* (bond breaking processes) timescales are expected.

H.-G. Rubahn pointed out that the particle-plasmon[218] lifetime is expected to be extremely short (femtoseconds), and it is expected to be size-dependent. He mentioned that for clusters with radii a_0 significantly smaller than the mean free path of the electrons in bulk, surface scattering is the dominant damping mechanism in addition to Drude damping[219]. Since the ratio of the surface scattering probability (proportional to the area of the cluster) to the number of scattering electrons (proportional to the volume) scales with $1/a_0$, the plasmon lifetime is expected to be[220]

$$\tau = \left(\frac{v_F}{l} + \frac{A \cdot v_F}{a_0} \right)^{-1} \qquad \textbf{(IV.4.1)}$$

where the first term refers to Drude damping and the second to surface scattering. Here, A is a size parameter that takes into account electron screening and surface roughness and varies between[220] 0.38 and $4/\pi$. For large clusters, retardation effects (radiation damping, excitation of higher multipole plasmons) are expected to broaden the plasmon resonances, i.e.

[218] Particle-plasmons are being called „surface plasmons" in [Rub99]. Here it is called a Mie-plasmon, if the diameter of the particle is smaller than the wavelength of the laser light.

[219] Drude damping is the known damping mechanism due to scattering on defects, impurities, grain boundaries, etc.

[220] [KV95]

shorten the lifetime with increasing a_0 ('extrinsic' or electrodynamic size effects). The total damping rate is then given by

$$\Gamma_{total} = \Gamma_{Drude} + \Gamma_{surface} + \Gamma_{Mie} \qquad \textbf{(IV.4.2)}$$

The additional term to the size dependence of the lifetime of the dipole resonance can be readily calculated via classic Mie theory, explained and used e.g. in [Sch02].

As an overview, the calculated plasmon lifetimes as a function of cluster size ('classic size effect') are shown in Fig. 60, including *intrinsic* and *extrinsic* damping mechanisms as well as A = 0.45 (dashed line) and A = 1 (solid line). The former value has been taken from density functional calculations for Na spheres. For very small clusters this calculation certainly is inadequate and a quantum treatment is required. A few discrete values from such a treatment are included in this figure.

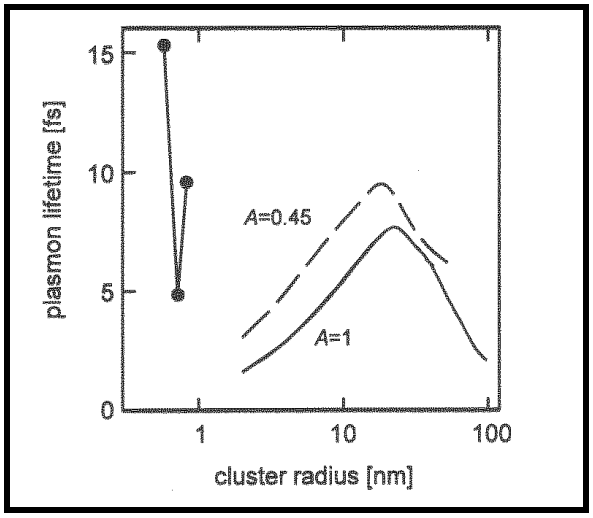

Fig. 60: Lifetimes of collective electronic excitations in large sodium clusters. The solid circles are from a quantum mechanical calculation. On the right-hand side the classic size effect is calculated according eq. (IV.4.2) with the A-parameter discussed in the text.

Thus, whatever the real dimensions of the islands might be, the lifetime that was measured is at least *an order of magnitude* longer than reported in [Rub99] or [Sch02]. It is therefore not possible to fully explain the electron dynamics in this system by means of (Mie-) plasmons.

2) Hot electron distribution

Fann et al.[221] reported the thermalisation[222] dynamics of hot electron gas in thin[223] gold films. They found that the thermalisation process takes up

[221] [FSTB92]
[222] Thermalisation means the distribution of energy and momentum by scattering, until a Fermi-Dirac distribution is reached
[223] Thickness: 30nm

to some hundred femtoseconds, i.e. the electron-phonon scattering starts already before the gas is thermalised. This is due to the fact that the heat transfer from the hot electron gas to the substrate cannot take place via electron-electron scattering, but only via electron-phonon scattering. Additionally, they showed that the more electrons are excited (e.g. by higher laser fluence) the faster the thermalisation process is, because of a higher number of available electrons, with which the nonthermal electrons can scatter.

Because of the weak coupling of the electron system of the particles to the substrate, and the laser fluence of about 10μJ/cm^2 for the blue pulse, a very hot electron gas has been built in the thin deposited silver layer that was investigated. The electrons in that hot gas may not thermalise fast due to the low number of scatter partners. They relax therefore slower than in bulk silver, the hot electron gas may not cool down fast and thus the electrons show the long lifetimes seen in Fig. 57. The almost constant lifetimes at all energies indicate the electron-phonon scattering, which has no energy dependence. The geometry seems to be of a kind to strongly suppress any damping mechanisms, which would lead to a fast relaxation.

Those two given descriptions do not explain all details of the unknown behaviour, which can result to such long lifetimes. However, one may keep in mind, the results seen in chapter IV.3.c (page 97) at Ag[17ML]/GaAs(100). There, the situation was explained, in which the lifetime of an adsorbate gap state was detected to be of the order of ~1000fs, although found values in literature of similar systems described only lifetimes in the sub-hundred femtoseconds.

In case this will be confirmed by other techniques, it would surely become very important for future applications. One can think of a system (e.g. laser crystal or SHG crystal), which may be pumped for ~100fs, before having any losses. It is also possible to test any catalysis reaction on such a surface, aiming to amplify the chemical reactivity. One even may build a memory on such a small dimension, with the advantage of small resistivity and highly localised charge particles.

c. Other phenomena

It was observed at different samples, that the same quantity of silver deposited on MgO resulted in another surface structure (Fig. 61, "Stranski-Krastanov" or "Frank-Van der Merwe"), where those long lifetimes could not be detected, but other phenomena.

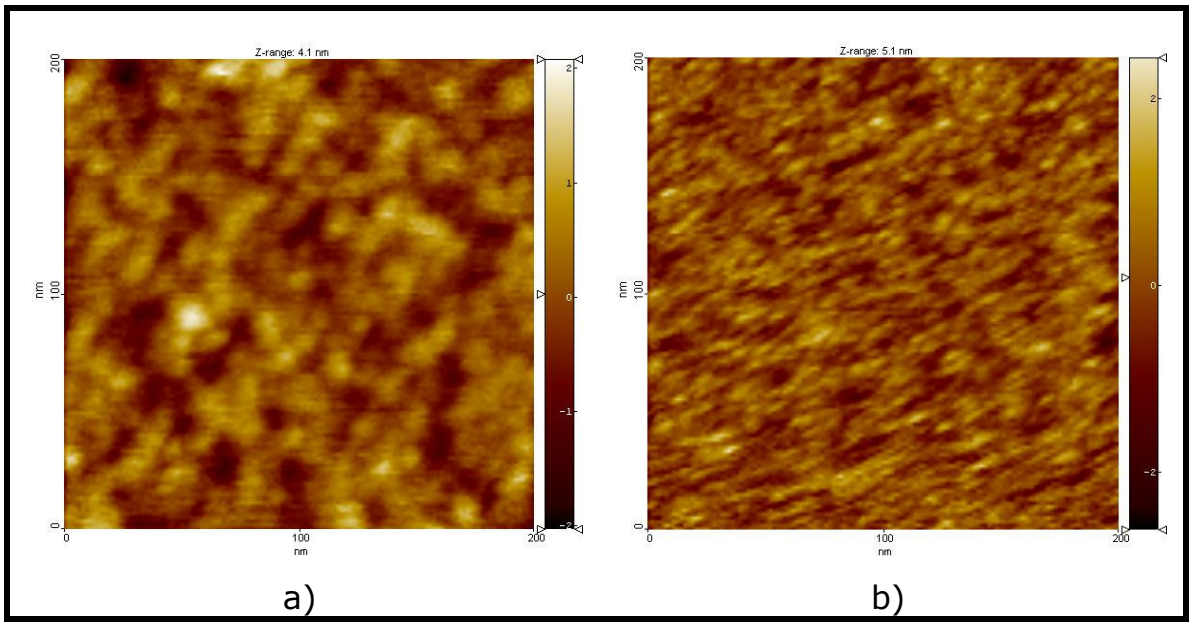

Fig. 61: AFM-picture of silver on MgO

a) Ag[4ML]/MgO(100). The surface is already almost covered, and the heights lie between 0.2nm and 1.2nm, with the peak at 0.8nm.

b) Ag[6ML]/MgO(100). The surface is almost covered, and heights are 1.2nm ± 0.6nm. Area sizes: 200nm x 200nm.

Pictures made by B. Pluchet, Group of Prof. Dr. Ch. Ziegler, Kaiserslautern / Germany.

The AFM-pictures demonstrate, that the surface is almost fully covered at 4ML Ag. One recognizes an agglomeration of many grains. At such a surface, one could not detect very long lifetimes. This points again to the assumption, that one needs the mentioned islands for having long lifetimes.

At systems having those surfaces, an intensity-dependent change of the distribution of excited electrons was observed. At *low* laser intensities, more electrons were counted at *higher* electron energies than with *high* laser intensities, and vice-versa for the lower part of the spectrum. This resulted in measurements like in Fig. 62a).

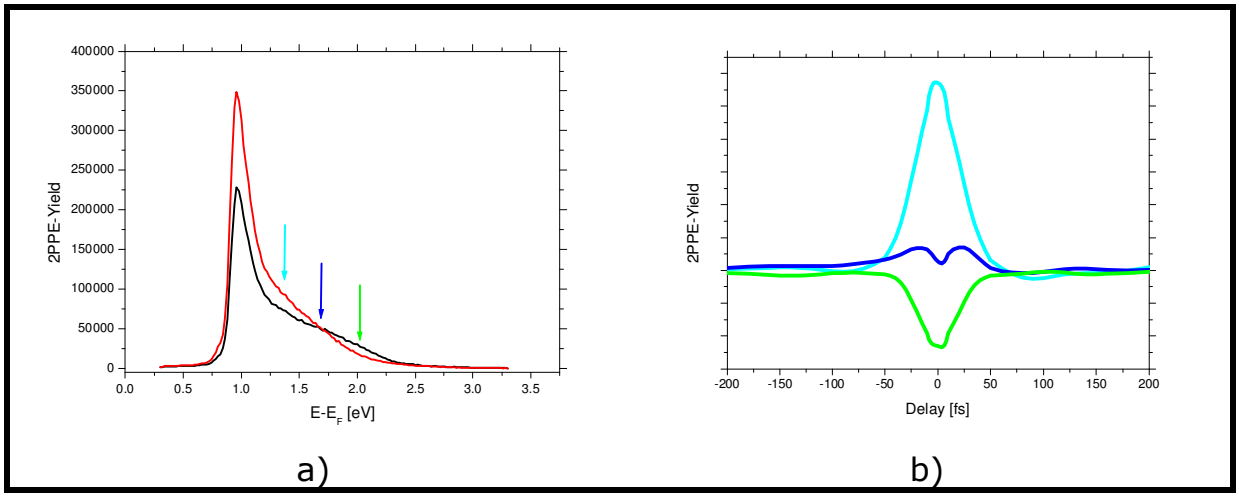

Fig. 62: Intensity-dependence of spectra and TR-2PPE-curves at Ag/MgO(100) systems, having the surface structure shown in Fig. 61.

a) Spectra at two different laser intensities. The laser intensity, producing the red spectrum, is larger than that one for the black spectrum.

b) The TR-2PPE-curves at the energy positions of the three arrows.

It is easy to predict the TR-2PPE-curves (Fig. 62b) at high energies (>~1.7eV above E_F): At *large delays* both pulses are separated, the intensity is always small, and there is no change comparing to normal observation. At *small delays*, both pulses impinge at the same time, leading to high laser intensity and thus to lower (!) electron population at this energy[224]. The consequence is a curve like the green one in Fig. 62b). It is clear, that a meaningful TR-2PPE-measurement is not possible. Even at low electron energies, it may be questionable if a TR-2PPE measurement represents a real lifetime value, due to the influence of this intensity dependence.

[224] Because, the high electron gas temperature after the excitation by both pulses may not cool down so fast.

V. Outlook

The sum of all those experiments, made it obvious that the dynamics of optically excited electrons are critically sensitive to the morphology of the system. In this work, it was not yet possible to produce uniform epitaxial single crystal metal layers on a substrate with a large bandgap. Thus, the main activity, in order to prove the theory of Giuliani and Quinn, must involve the finding of a substrate and of evaporation parameters to produce adequate ultra-thin layers. However, not only the morphology hinders to prove the theory, but also former unexpected effects, like (Mie-) plasmons or QWS. It will be an interesting task to find a system, where those influences may be eliminated one after the other. Activities to improve these measurements are already running.

Up to now, it is still not clear, whether the theory of Giuliani and Quinn is right. They predicted for a two-dimensional system, an additional logarithmical, energy dependent factor to the relaxation time. And it is also still not evident what influence to the measurement of silver is coming from the excitation and relaxation of plasmons.

VI. Zusammenfassung

Im Mittelpunkt der vorliegenden Dissertation steht die Untersuchung der Dynamik von optisch angeregten (heißen) Elektronen in dünnen bis ultra-dünnen Schichten. Dabei interessiert vor allem das zeitliche Verhalten der Energie- und Impulsdissipation der angeregten Elektronen. Die relevanten Zeiten spielen sich dabei auf der Femtosekunden – Zeitskala ab. Die zeitaufgelöste zwei - Photonen Photoemissionsspektroskopie ist bekannt dafür, ein geeignetes Werkzeug zu sein, um solche dynamischen Prozesse in Echtzeit zu analysieren.

Diese Arbeit erweitert das Wissen auf den Gebieten der Elektronen-Relaxation in ultra-dünnen Silberschichten auf verschiedenen Substraten, in Adsorbatzuständen und in der Bandlücke eines Halbleiters. Sie trägt bei zum Verständnis über den Spintransports durch eine Grenzfläche zwischen einem Metall und einem Halbleiter.

Durch Einschränkung des untersuchten Kristalls in mindestens einer Richtung wurde in dieser Arbeit begonnen, die bereits publizierten theoretischen Vorhersagen zu bestätigen. Man erwartet dabei eine Änderung im Relaxationsverhalten der Elektronen beim Übergang von einem 3d Festkörper zu einer 2d (ultra-dünnen) Schicht, da man theoretisch unterhalb einer bestimmten Schichtdicke ein zweidimensionales Gas vorfindet. Genau dieses Verhalten konnte in der vorliegenden Arbeit bestätigt werden. Die heißen Elektronen in einer ca. 3nm dünnen Silberschicht auf Graphit zeigten über den ganzen verfügbaren Messenergiebereich eine zeitliche Änderung zu längeren Relaxationszeiten hin. Dies ist das erste Mal, dass die zeitliche Entwicklung der Relaxation optisch angeregter Elektronen beim Übergang von einem 3d zu einem 2d-System beobachtet werden konnte.

Um den Einfluss des Substrates möglichst zu verhindern, wurde Silber auf dem Halbleiter GaAs untersucht, welcher eine direkte Bandlücke von 1.5eV am Γ-Punkt aufweist. Bei der Untersuchung des Relaxationsverhaltens heißer Elektronen in verschiedenen ultra-dünnen Silberschichten auf diesem Halbleiter zeigte sich, dass bei dieser Schottky-Barriere Plasmonen im Silber und an der Grenzfläche, sowie kaskadierende Elektronen aus höheren Energien einen wesentlichen Einfluss auf die Energiedissipation haben. Dies ist hauptsächlich eine

Folge der Bandverbiegung des Halbleiters und der im GaAs angeregten Elektronen.

Die Begrenzung der Silberschicht auf dem GaAs in einer Richtung hatte als Konsequenz die erwartete Bildung von Quantum Well Zuständen (QWS) in der Bandlücke. Diese Adsorbatzustände haben quantisierte Energie- und Impulswerte, welche direkt mit der Schichtdicke und der sich darin befindlichen stehenden Elektronenwellen gekoppelt sind. Bei den Untersuchung konnten dabei nicht nur bestehende Messwerte ergänzt und bestätigt, sondern darüber hinaus auch die zeitliche Evolution eines QWS bestimmt werden. Es zeigte sich, dass dieser QWS hauptsächlich über Elektronen gefüllt werden kann, die von der Leitungsbandunterkante des Halbleiters in das Silber hineindiffundieren und dort über energetische Kaskadenzerfälle relaxieren.

Mit dem System des Silbers auf GaAs und der bekannten Tatsache, dass eine Elektronenanregung in GaAs mit zirkularpolarisiertem Licht der Energie 1.5eV spinpolarisierte Elektronen im Leitungsband erzeugt, war die Möglichkeit gegeben, einen Beitrag zum aktuellen Thema der Spininjektion zu erbringen. Das Ziel der Spininjektion ist der Transfer von spinpolarisierten Elektronen aus einem Ferromagneten in einen Halbleiter hinein, um damit spinabhängige Schalter und Speicher zu entwickeln. Mit den Messungen konnte demonstriert werden, wie spinpolarisierte Elektronen vom GaAs aus über die Grenzfläche zum Silber ihren Spin beibehalten.

Als drittes Untersuchungssystem wurden ultra-dünne Silberschichten auf dem Isolator MgO betrachtet, der eine Bandlücke von 7.8eV aufweist. Auch in diesem System konnte ein Änderung in den Relaxationszeiten beim Übergang von einer dicken zu einer ultra-dünnen Schicht beobachtet werden. Des Weiteren zeigte sich eine extrem lange Relaxationszeit bei einer Schichtdicke von 0.6 – 1.2nm. Diese um einen Faktor zehn längere Zeit als bei dicken Schichten ist eine Folge zweier Faktoren: erstens der Reduktion des Phasenraums wegen der eingeschränkten Bewegungs-freiheit der Elektronen in z-Richtung, und zweitens als Folge der langsameren Thermalisierung des Elektronengas, da wenig Streupartner zur Verfügung stehen.

VII. Abstract

This thesis deals with the investigation of the dynamics of optically excited (hot) electrons in thin and ultra-thin layers. The main interests concern about the time behaviour of the dissipation of energy and momentum of the excited electrons. The relevant relaxation times occur in the femtosecond time region. The two-photon photoemission is known to be an adequate tool in order to analyse such dynamical processes in real-time.

This work expands the knowledge in the fields of electron relaxation in ultra-thin silver layers on different substrates, as well as in adsorbate states in a bandgap of a semiconductor. It contributes facts to the comprehension of spin transport through an interface between a metal and a semiconductor.

The primary goal was to prove the predicted theory by reducing the observed crystal in at least one direction. One expects a change of the electron relaxation behaviour while altering the crystal's shape from a 3d bulk to a 2d (ultra-thin) layer. This is due to the fact that below a determined layer thickness, the electron gas transfers to a two-dimensional one. This behaviour could be proven in this work. In an about 3nm thin silver layer on graphite, the hot electrons show a jump to longer relaxation time all over the whole accessible energy range. It is the first time that the temporal evolution of the relaxation of excited electrons could be observed during the transition from a 3d to a 2d system.

In order to reduce or even eliminate the influence coming from the substrate, the system of silver on the semiconductor GaAs, which has a bandgap of 1.5eV at the Γ-point, was investigated. The observations of the relaxation behaviour of hot electron in different ultra-thin silver layers on this semiconductor could show, that at metal-insulator-junctions, plasmons in the silver and in the interface, as well as cascading electrons from higher lying energies, have a huge influence to the dissipation of momentum and energy. This comes mainly from the band bending of the semiconductor, and from the electrons, which are excited in GaAs.

The limitation of the silver layer on GaAs in one direction led to the expected generation of quantum well states (QWS) in the bandgap. Those

adsorbate states have quantised energy- and momentum values, which are directly connected to the layer thickness and the standing electron wave therein. With the experiments of this work, published values could not only be completed and proved, but it could also be determined the time evolution of such a QWS. It came out that this QWS might only be filled by electrons, which are moving from the lower edge of the conduction band of the semiconductor to the silver and suffer cascading steps there.

By means of the system silver on GaAs, and of the known fact that an excitation of electrons in GaAs with circularly polarised light of the energy 1.5eV does produce spin polarised electrons in the conduction band, it became possible to bring a contribution to the hot topic of spin injection. The main target of spin injection is the transfer of spin polarised electrons out of a ferromagnet into a semiconductor, in order to develop spin dependent switches and memories. It could be demonstrated here that spin polarised electrons from GaAs can move through the interface into silver, could be photoemitted from there and their spin was still being detectable.

As a third investigation system, ultra-thin silver layers were deposited on the insulator MgO, which has a bandgap of 7.8eV. Also in *this* system, one could recognize a change in the relaxation time while reducing the dimension of the silver layer from thick to ultra-thin. Additionally, it came out an extreme large relaxation time at a layer thickness of 0.6 – 1.2nm. This time is an order of magnitude longer than at thick films, and this is a consequence of two factors: first, the reduction of the phase space due to the confined electron gas in the z-direction, and second, the slowlier thermalisation of the electron gas due to less accessible scattering partners.

VIII. Appendix

1. The crystal structure

a. The uncovered crystal

The crystal structures of three dimensional bulk lattices (in the solid state) are well known[225] and will not be described here. Instead, it will be explained how a surface and a two-dimensional layer[226] look like.

In the whole text, a multilayer[227] and a surface are considered as the same, and are both called "surface".

The surface is normally taken as the outer three monolayers (= layers of atoms). However, this assumption is often too strictly, and whenever it is necessary, the surface is just taken as the outer layers, without any declaration of height.

To illustrate such a surface the use of the same geometrical description is appropriate, as it is used for a bulk. What is called a Bravais lattice in 3d is being called a 2d surface net (or 2d Bravais net). A 3d-cell is here now a 2d-mash. There are exactly five different possible Bravais nets (see Fig. 63).

[225] See for example [Kit96]
[226] Which normally lies on a three dimensional bulk (substrate)
[227] A "multilayer" is an arrangement of some films, having the height of one atom each, and lying one above the other. Another term for it is "monolayers"

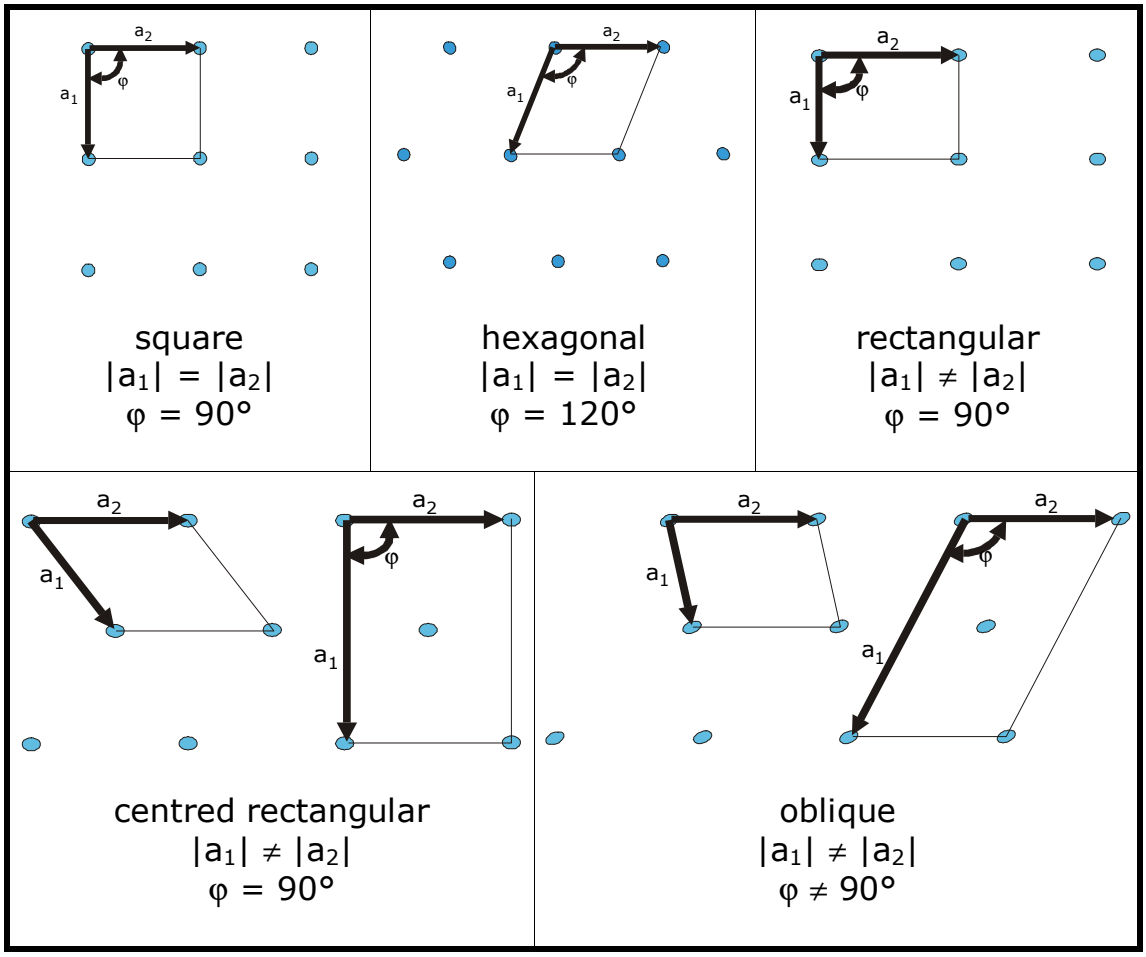

Fig. 63: The five possible surface nets in two dimensions, for example on a surface. All points in a lattice can be reached from the origin by translation vectors $T = m \cdot a_1 + n \cdot a_2$ ([Kit96])

The net of the (underlying) substrate is used to be compared to the surface net. If e.g. one considers the (111)-plane of a cubic crystal, then the net of the substrate is hexagonal (see Fig. 64), and the surface net is being related to those axes.

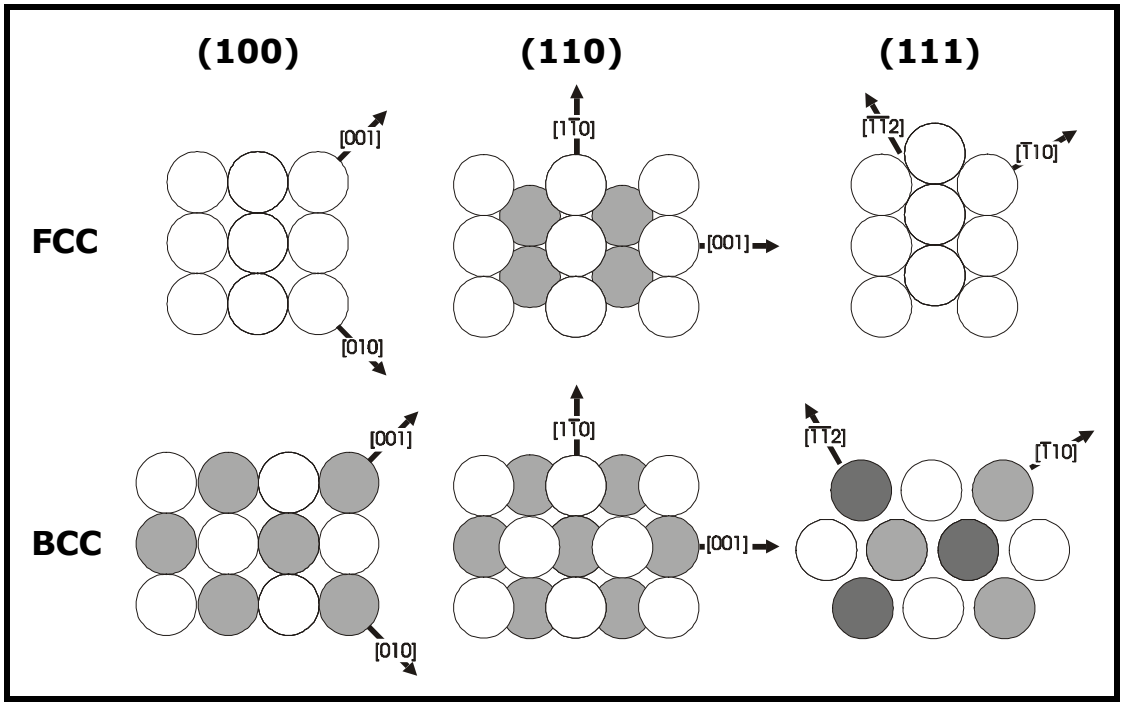

Fig. 64: Low-index ideal surfaces of a hard-sphere cubic crystal. White, grey bright and grey dark indicate the first, second and third atom layers, respectively. View from top. ([Zan88])

By calling the primitive translation vectors of the substrate net as b_1 and b_2, those vectors and an operator P can express the vectors a_1 and a_2 of the surface structure:

$$\begin{pmatrix} a_1 \\ a_2 \end{pmatrix} = P \begin{pmatrix} b_1 \\ b_2 \end{pmatrix} \qquad \textbf{(VIII.1.1)}$$

Assuming the angles to be equal, it is convenient to use the short formula of E.A. Wood (R="rotated by"):

$$\left(\frac{a_1}{b_1} \times \frac{a_2}{b_2} \right) R\alpha \qquad \textbf{(VIII.1.2)}$$

For example $\left(\sqrt{3} \times \sqrt{3}\right) R30°$.

A more concrete example is the crystal surface MgO(100), which served as a substrate for some measurements explained in this work. This ideal (or simply relaxed) surface is identified easily by reference to the bulk plane of termination. The periodicity and orientation of the surface net is the same as the underlying bulk lattice; it is called (1x1) structure: MgO(100)-(1x1).

Beside this simply relaxed surface structure, there are surfaces, which show a more complicated configurations, namely a so-called *relaxation* or even a *reconstruction*. Those rearrangements may reduce the energies of

the outer-layer atoms by displacement and thus are more preferred. See Fig. 65 for one of the possible relaxations and one of the reconstructions. In Fig. 66 one can see a reconstruction for GaAs(110). For further details see e.g. [Kit96].

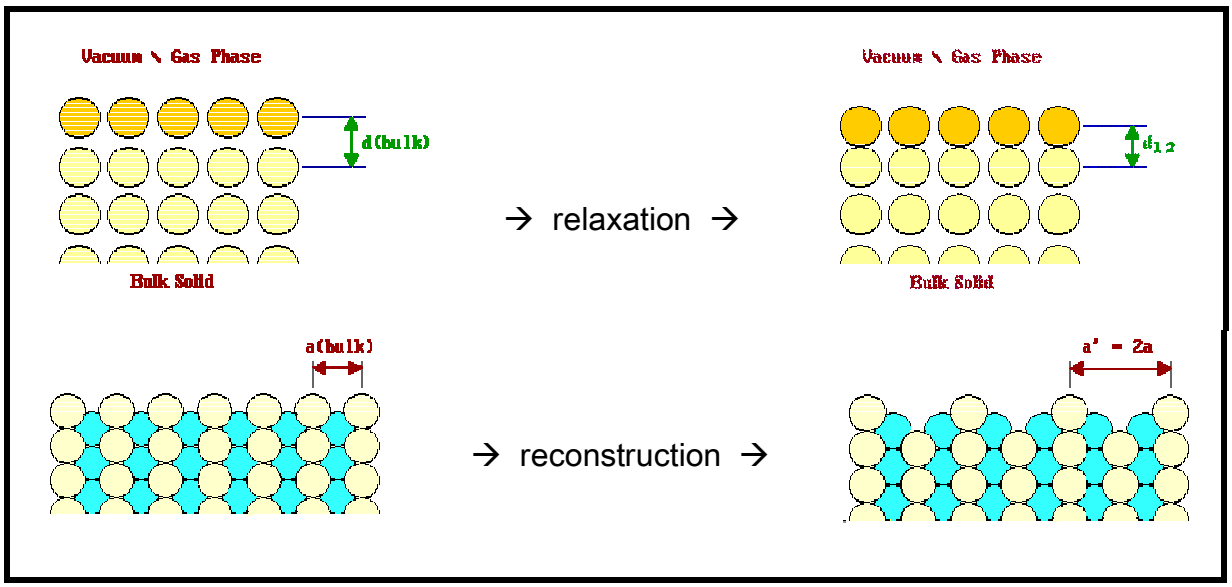

Fig. 65: Illustration for a possible relaxation and for a possible reconstruction.

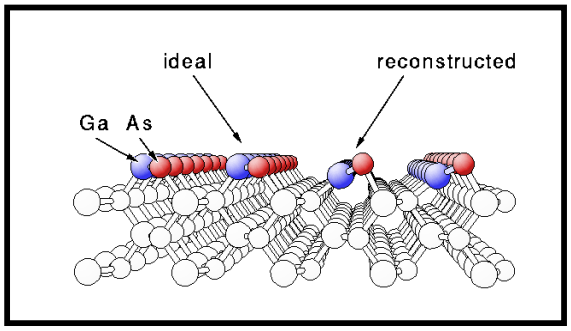

Fig. 66: A scheme of a reconstruction on GaAs(110). On the left side, an ideal surface is shown. Right beside it reconstructed atoms are drawn.

Before going to analyse the covered crystal structure, it is of huge importance to look at other types of events appearing at a crystal and its surface: dislocations, point defects, and vacancies. Some of their consequences had also been described in chapter I.b (the electronic structure of an insulator surface).

A *dislocation* is a linear defect in a crystal, i.e., it involves a large number of atoms arranged along a line. Typically, it extends over many tens of Angstroms. The region in the neighbourhood of the dislocation experiences a noticeable distortion relative to the normal crystalline arrangement. Far away from the dislocation, the crystal regains its regularity.

Point defects are irregularities in the crystal structure, localised in the lattice. An example is a foreign atom, or impurity, in the crystal. An impurity is *substitutional* if it occupies a lattice site from which the host atom has been expelled, and *interstitial* if it occupies a position between the host atoms. The region surrounding an impurity is strained, the extent of the strain depends on the kind of impurity atom and its location.

Vacancies are empty lattice sites from which the regular atom has been removed. This happens for example by thermal excitation. When the regular atom leaves, the region surrounding a vacancy is distorted, caused by relaxation of the lattice, in order to partially fill the void left by the atom. So-called *Schottky defects* appear when the displaced atom migrates in successive steps and eventually settles at the surface. In the second type, called a *Frenkel defect*, an atom moves from a lattice place to an interstitial position. This defect includes atom and vacancy, needs therefore a large amount of energy, and for this reason, it is usually not present in metals except under special circumstances. As a result, vacancies usually exist only near free surfaces, grain boundaries, and dislocations, rather than inside a perfect crystal, because only at surfaces, boundaries, or dislocations they can be created without a concomitant formation of interstitials.

b. The covered crystal and the three principle growth modes of deposited material

In nature, it is normal that a surface is never clean. There is always any kind of contamination on it. Any additional atoms or molecules like water, nitrogen, or something else. This is clear, because of the exposure to the air.

In the artificial circumstances of a lab, the main goal is to prevent any sort of dirt on the examined sample. However, also there, one has to fight against contamination. That is, why an ultra-high vacuum system was used, see chapter III.1 oben.

Additionally, there were many investigations, which let to produce a controlled deposition of adatoms and molecules. The instrumental requirement to deposit material on a substrate and to control the cleanness or order of it is explained in chapter III.1.b. Here the geometry of deposited adatoms, lying on a clean surface of a crystal is going to be described.

The term "deposition" usually means epitaxial growth of adsorbed atoms. Taking the word epitaxy[228] literally, it stands only for ordered, structured

[228] Greek: επι = ´on´, ταξις = ´arrangement´

films. But this expression is often used also in contexts, where not well ordered, structured layers are considered.

In principle, one can distinguish between epitaxy of atoms of the same chemical element as the underlying substrate, and those atoms, which differ in their chemical property from the substrate. The first category is called *monoepitaxy*, the second *heteroepitaxy*.

Generally, one hops the crystal growth proceeds in a two-dimensional fashion; one monolayer after another (layer-by-layer), up to a desired thickness of overlayer material. This actually appears for Sn/InSb(100), Co/Cu(100) or a lot of other systems. However, it is not the usual situation observed for either the growth of metals on metals or for the growth of metals on semiconductors. Instead, one often finds that the deposited material build three-dimensional clumps, which only later merge into a thick polycrystalline film.

If the growth mode show a layer-by-layer arrangement, one can speak of a coverage of "x monolayers", otherwise it is better to speak of "nominal x monolayers", this means, there is the same amount of adatoms, as if there were flat layers.

Whatever measurement method are used, if the surface consists of not completed or not smooth, epitaxial coverage, the detection will always be a mixture of different layers. Some analysing techniques use exactly this behaviour as an advantage, for example RHEED (Reflection High Energy Electron Diffraction), see Fig. 67. In a RHEED experiment, a 5-50keV-electron beam is directed towards the sample at extreme grazing incidence. Electrons are scattered at the top 1-2 atomic layers of the crystal, under these conditions. A screen monitors the variation of the specular beam intensity as a function of time. Remarkably, the signal exhibits extremely regular oscillations, whose period exactly corresponds to the growth.

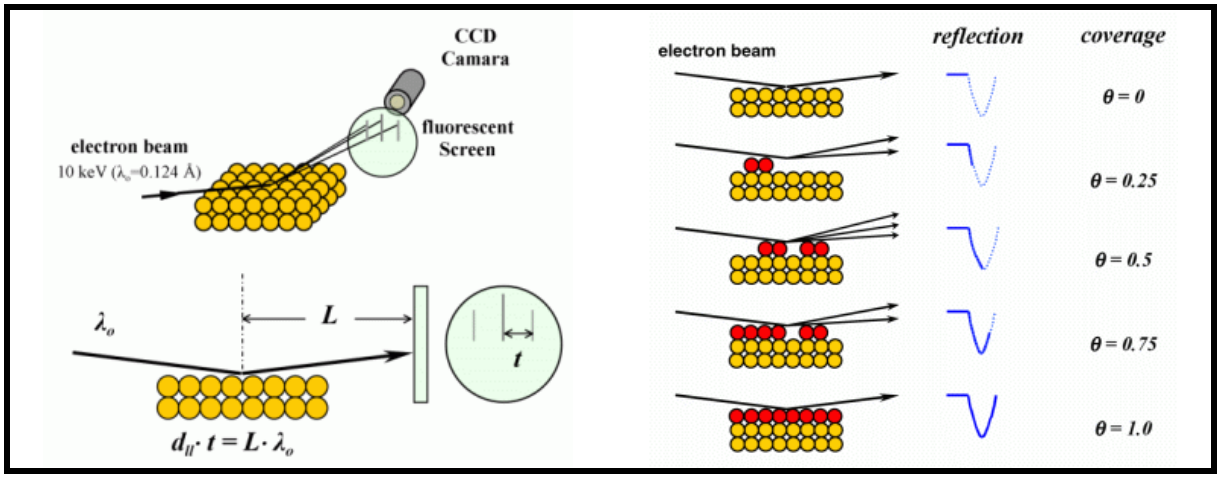

Fig. 67: RHEED scheme and intensity oscillation. From [Kai]

In all cases of deposited layers, whether they are smooth or not, it is easy to describe the height of such a deposition. Assuming e.g. silver (Ag), which has a lattice constant of about 4.09Å in bulk. The lattice is fcc. This leads to a monolayer spacing of about 2.045Å, see Fig. 68.

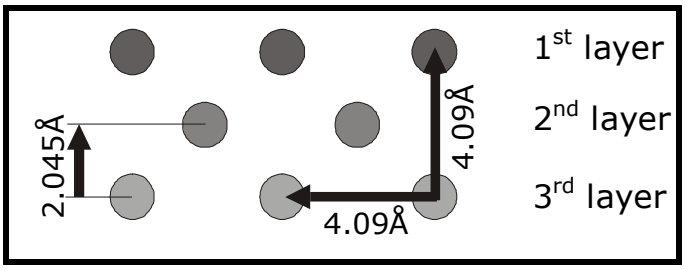

Fig. 68: Side view of a part of a fcc-lattice. The lattice constant is 4.09Å. Therefore, the layer-to-layer spacing is 2.045Å

Extensive experimental results point to the existence of three distinct growth modes:

Frank-Van der Merwe growth FV growth follows the layer-by-layer scenario. Each layer is being completed before the next layer starts to grow. **Example Ag/Fe/MgO(100)**	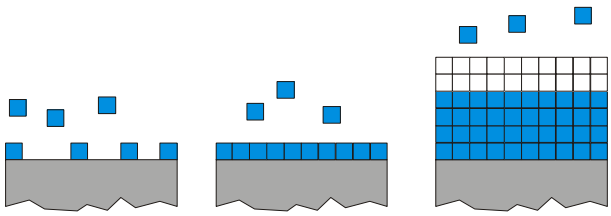
Stranski-Krastanov growth SK growth lies between the other both: a few monolayers adsorb in layer-by-layer fashion before three-dimensional clumps begin to form. **Example Ag/MgO(100)**	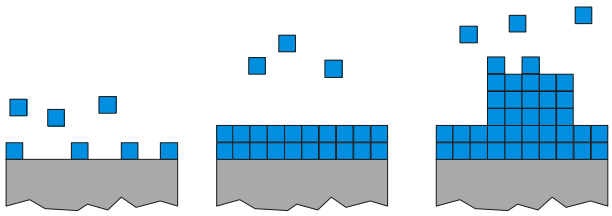
Volmer-Weber growth VW growth is the opposite of FV. Three-dimensional crystallites nucleate immediately upon contact and the overlayer may not completely cover the exposed substrate surface until a huge amount of atoms have been deposited. **Example: Ag/GaAs**	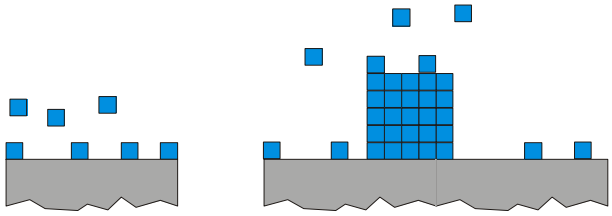

Fig. 69: The three principal growth modes

The different deposition methods, like MBE, MOCVD, as well as the thermodynamical processes of material attachment on a surface are described very well at other places. Nevertheless, some very exciting subjects of the current research concerning deposition may not be missing here. Beside flat layers, which spread them out over a microscopic or macroscopic area, some groups try and reach to produce smaller structures like “wires” and “dots”.

It is very interesting for electronics to have small wires with macroscopic length and diameter of only one atom, because of the assumption to get very small power consuming, due to joule’s heat. A promising success became the research on vicinal steps. The groups, which investigate

this[229], prepare a surface of a crystal in such a manner, that they get a lot of sharp, long and smooth steps on the top layer without any kinks. Afterwards they add some adatoms, which diffuse and attach in best case at those steps and produce long quantum wires.

Another very interesting topic, which opened a great amount of new themes, is the investigation of nanoparticles. This research area is usually divided into two main fields: particles, which lie or are imbedded on a surface, and those, which are freestanding, for example in a gas stream.

To produce the former ones - lying or imbedded particles - different methods are used. An example for lying particles on a substrate, are the arrays of nanoparticles, which are produced e.g. in the group of F.R. Aussenegg[230]. They work with e-beam lithography to build symmetrical metal arrays of different length, different particle sizes, and different particle heights. They can tune the optical properties, like plasmon resonances, in a wide range. One important advantage is, that the particles may be shaped very regular.

W. Pfeiffer et al.[231] produce imbedded particles of silver and gold in HOPG. The graphite (HOPG) substrate is bombarded by argon ions and subsequently oxidised in air. This treatment results in the formation of pits in the topmost layer of the graphite with a controlled diameter of several nanometers. By offering of metal vapour, those holes become filled by small metal particles. The irregularity may be a disadvantage of this method, because it generates an inhomogeneous line broadening in photoemission spectra, for example.

The freestanding clusters are created for example by spark discharge of metal filaments. M. Fierz[232] held them in a nitrogen gas jet. He could separate them by size, and could charge them in a radioactive tube. One benefit by doing some experiments with particles in a gas jet is, that one can get rid of effects of a surrounding, like a surface.
G. Schmid et al.[233] uses another technique. He builds clusters of up to 55 metal atoms, which are bound in a surrounding ligand net.

[229] E.g. Horn-von Hoegen et al. [HMK+98]
[230] [Lam99]. See Fig. 13a) on page 35, which show a part of such an array
[231] [MPT+00]
[232] [Fie01]
[233] [SB00]

2. Surface states, image states, QWS

The physics of an electron, caught in a two-dimensional layer or in a quantum-well structure, is quite the same as that of an electron in a surface state or an image state. Especially, the derivations of Pendry und Gurman[234] and of Echenique und Pendry[235] demonstrate the relationship, of both subjects. The authors found also an instructive way of explaining surface states, which should be given here, shortly.

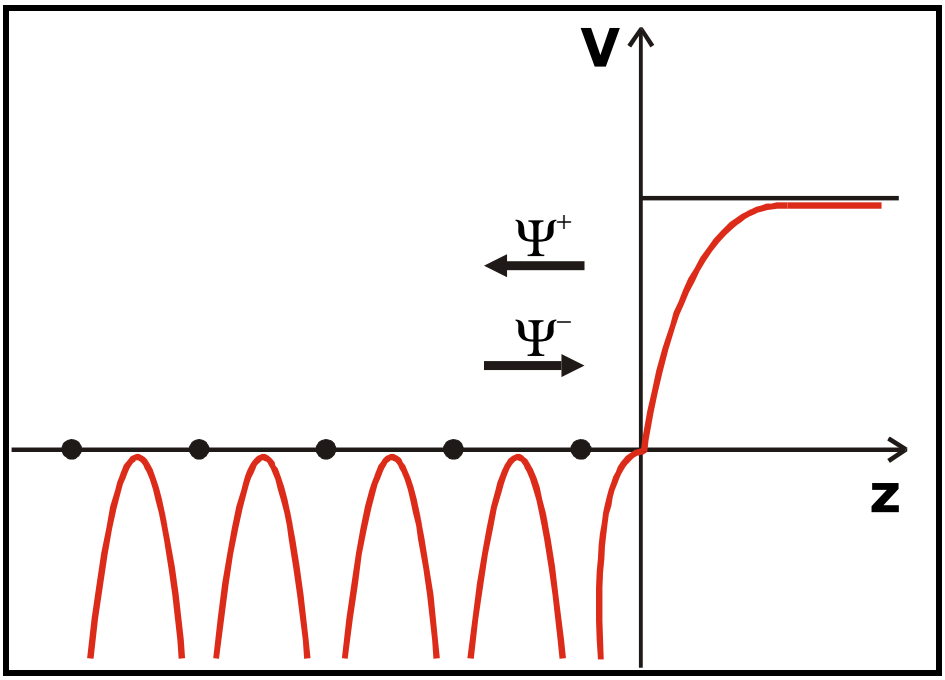

Fig. 70: The electron potential at the surface. The explanation of the waves (Ψ^+,Ψ^-) are described in the text.

They consider a surface state as a wave, caught between a band gap of the bulk crystal and the surface barrier. If this wave ψ_+ carry an unit flux *in the direction of the bulk*, a part of it will be Bragg reflected due to the band gap: $r_c e^{i\phi_c}\psi_-$

The wave ψ_- carries an unit flux *away from bulk* to the surface barrier, with r_c the amplitude and $e^{i\phi_c}$ the phase change comparing to ψ_+. During its round trip, the wave will meet the surface barrier, and will be reflected back, again *in the direction of the bulk*: $r_b e^{i\phi_b}\ r_c e^{i\phi_c}\psi_+$

[234] [PG75]
[235] [EP78]

By adding all amplitudes[236] of the multiple scatterings, one gets the total amplitude of ψ_+:

$$A = \frac{1}{1 - r_b r_c e^{i(\phi_b + \phi_c)}} \qquad \textbf{(VIII.2.1)}$$

A pole in that term describes a bound state at the surface: a **surface state**. The waves ψ_+ and ψ_- are in general Bloch waves.

With the formula above, one may write down the conditions for a surface state:

$$\begin{aligned} r_b\, r_c &= 1 \\ \phi_b + \phi_c &= 2\pi n \end{aligned} \qquad \textbf{(VIII.2.2)}$$

Because of conservation of flux:

$$r_b \le 1,\ r_c \le 1 \qquad \textbf{(VIII.2.3)}$$

Therefore:

$$r_b = r_c = 1 \qquad \textbf{(VIII.2.4)}$$

This means, that the energy (E) of the waves, and their momentum parallel to the surface (k_{II}) have to prevent both a propagation into the crystal and the escaping of the flux into the vacuum. (The conservation of the momentum parallel to the surface might prevent the escaping already, even if the energy lies above the vacuum level).

The phases are functions of the energy, and it is demonstrated[237], that while sweeping the energy through a band gap of the crystal, the term ϕ_c varies by about π, and therefore there is a good chance to find a surface state in this gap.

With that derivation, it follows quite easily the existence of *surface states* and of *image states*[238].

---

[236] The sum of all amplitudes, from first to n^{th} wave ${}^{n}\psi_+$ is:

$$\begin{aligned} A &= 1 + r_b r_c e^{i(\phi_b+\phi_c)} + r_b^2 r_c^2 e^{2i(\phi_b+\phi_c)} + \ldots + r_b^n r_c^n e^{n\cdot i(\phi_b+\phi_c)} + \ldots \\ &= \sum_{k=0}^{\infty} r_b^k r_c^k e^{k\cdot i(\phi_b+\phi_c)} \\ &\equiv \sum_{k=0}^{\infty} a^k = \frac{1}{1-a} \quad (|a| < 1) \end{aligned}$$

[237] [PG75]

[238] Image states are not being explained here further

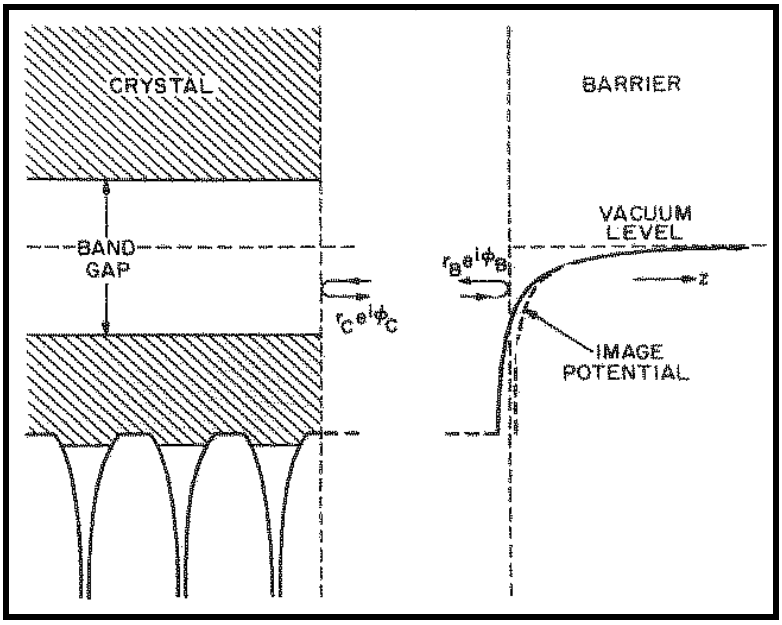

Fig. 71: The illustration of the creation of surface states and image states. It shows the situation of waves, which are reflected at the surface barrier and the bulk, and build up standing waves in the gap. From [Smi85].

Quantum well states may also be calculated using the same terms[239]:

The QW states are evaluated by the *phase accumulation model* combined with the *two-band nearly free electron approximation* (TBNFE). The phase accumulation in QW can be written as

$$\phi^*(\mathrm{E}) + 2\mathrm{k}(\mathrm{E}) \cdot \mathrm{nd} = 2\mathrm{m}\pi \qquad \textbf{(VIII.2.5)}$$

where $\phi^* = \phi_b^* + \phi_c^*$ is the phase change upon reflections at vacuum (ϕ_b^*) and substrate (ϕ_c^*) interfaces; k(E) is the wave number of a QW electron, n·d (d=2.045Å for silver) is the film thickness, and n, m are integers. The quantum number of QW series in Fig. 48 on page 101 is given by ν=m-n. Using the Ag band structure k(E), the energy dependence of $\phi^*(\mathrm{E})$ is deduced to reproduce the observed occupied and unoccupied QW energies (Fig. 48, page 101). The total phase change for unoccupied QW states is not a simple linear extrapolation of that for the occupied QW states. The reflection at the vacuum potential barrier can be calculated for a free electron within the *Wentzel-Kramers-Brillouin* approximation as

$$\phi_b(\mathrm{E}) = \pi[3.4\mathrm{eV}/(\mathrm{E_V} - \mathrm{E})^{1/2} - 1] \qquad \textbf{(VIII.2.6)}$$

Therefore, the confinement condition depends on the work function E_V. In the TBNFE model, the phase change (ϕ_b) for free electrons is replaced by

[239] [ONP02]

$$\phi_b^* = 2\arctan(l_b / \xi) \qquad \textbf{(VIII.2.7)}$$

where $l_b = k\tan(\phi_b/2)$ is a logarithmic derivative of the wave function at the vacuum barrier, and $\xi = k + g/(a_0/a_g - 1)$ is the modified momentum using coefficients a_0, a_g of two band solutions. ϕ_c^* is estimated from $\phi_c^* = \phi^* - \phi_b^*$, but could be taken in the current case as the same as ϕ_b^*, because the wave function penetrates into the gap as bad as into the vacuum.

The simple QW description given above assumes that the thin film can be treated as a *homogenous* medium, and that the QW states are simply the stationary states corresponding to standing waves perpendicular to the surfaces.

3. List of some spectroscopic methods

- XPS: X-Ray Photoelectron Spectroscopy
  ħω ~ 1keV, penetrating depth ~ 20-30Å
- ESCA: Electron Spectroscopy for Chemical Analysis
- UPS: Ultraviolet Photoelectron Spectroscopy
  ħω ~ 20-40eV, penetrating depth ~ 6-8Å
- EXAFS: Extended X-Ray Absorption Fine Structures
  To determine structures
- 2PPE: Two-Photon Photoemission
  To observe different electronic states
- AES: Auger Electron Spectroscopy
  To analyse the chemical state of the surface

In surface physics there has been built up a kind of universal law, connecting the electron energy and the escape depth, illustrated in Fig. 72. It is not only valid for the escape depth, but also for the penetration depth and the mean free path.

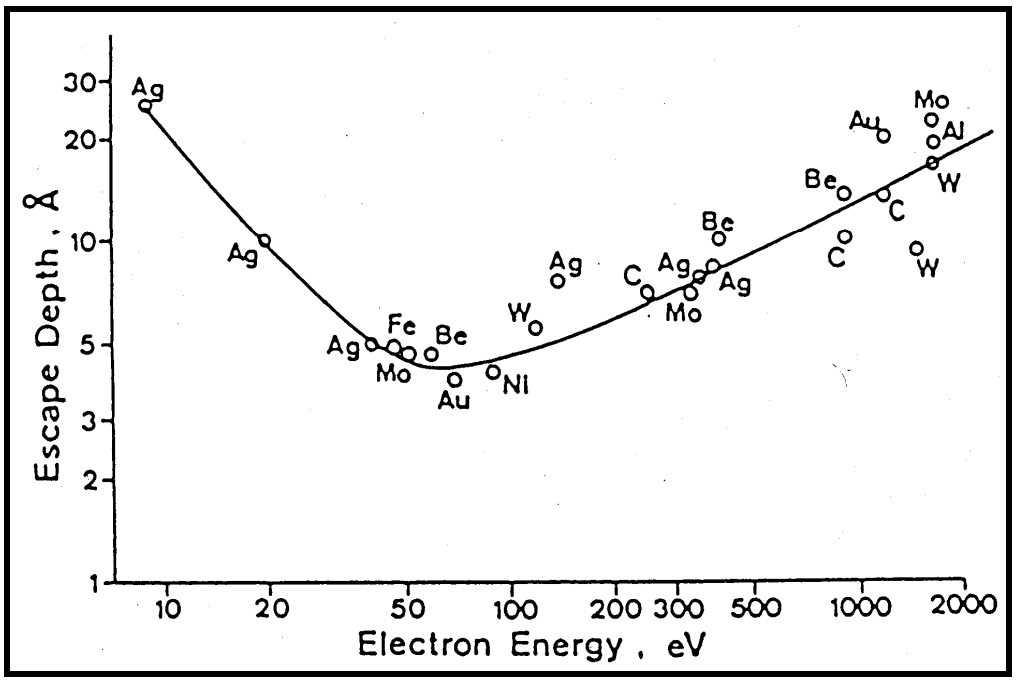

Fig. 72: Universal curve of the electron mean free path

4. The theoretical description of the TR-2PPE curve

The time-resolved measurements produce as signal the already mentioned autocorrelation curve (see Fig. 24 on page 59). It is built up by the two short laser pulses and the electron system. In first order approximation, one may take the influence of the electrons as very small, and just affecting the width of this autocorrelation curve, but not its shape. This approach is of course not always right; see for example the Ag/GaAs data. However, it is good enough in order to study the principle appearance of the TR-2PPE signal. In a second step (chapter VIII.4.b unterhalb), the influence caused by electrons will be taken into account.

a. The autocorrelation of two laser pulses[240]

1) Parallel-polarised beams (pp-polarised, or ss-polarised)

Without loss of generality, one takes the two electric fields of the laser pulses $E_1(t)$ and $E_2(t)$ as equal and called them $E(t)=E_{1,2}(t) = A(t)\cdot\cos(\omega t)$, with the *envelop curve* A(t). Because of the two-step process of the TR-2PPE measurement, one has to add (= superpose) both electric fields for each step, and multiply then those sums. One can therefore write the resulting intensity as:

$$\begin{aligned} I_{AC}(\tau) &= const \cdot \int_{-\infty}^{+\infty} \left|\left[E_1(t)+E_2(t-\tau)\right]\cdot\left[E_1(t)+E_2(t-\tau)\right]\right|^2 dt \\ &= const \cdot \int_{-\infty}^{+\infty} \left|\left[E(t)+E(t-\tau)\right]^2\right|^2 dt \qquad \textbf{(VIII.4.1)} \\ &= const \cdot \int_{-\infty}^{+\infty} \left|\left[A(t)\cdot\cos(\omega t)+A(t-\tau)\cdot\cos[\omega(t-\tau)]\right]^2\right|^2 dt \end{aligned}$$

Some interference terms arise, which are taken all along:

[240] To be exact, one speaks here of a "collinear autocorrelation", because of the fact that both correlated beams merge collinearly.

$$\begin{aligned} I_{AC}(\tau) &= \int A^4(t)\cdot\cos^4(\omega t) + A^4(t-\tau)\cdot\cos^4\left[\omega\left(t-\tau\right)\right]dt \\ &+ 6\cdot\int A^2(t)\cdot A^2(t-\tau)\cdot\cos^2(\omega t)\cdot\cos^2\left[\omega\left(t-\tau\right)\right]dt \\ &+ 4\cdot\int A^3(t)\cdot A(t-\tau)\cdot\cos^3(\omega t)\cdot\cos\left[\omega\left(t-\tau\right)\right]dt \\ &+ 4\cdot\int A(t)\cdot A^3(t-\tau)\cdot\cos(\omega t)\cdot\cos^3\left[\omega\left(t-\tau\right)\right]dt \end{aligned} \qquad \textbf{(VIII.4.2)}$$

With the assumption of a "slowly varying envelop" A(t), where A(t) does not change strongly during one optical period, one is able to rewrite the integrals:

$$\begin{aligned} \int A^4(t)\cdot\cos^4(\omega t)dt &\approx \int A^4(t)dt\cdot\frac{1}{T}\int_0^{+T}\cos^4(\omega t)dt \\ &= \frac{3}{8}\int A^4(t)dt \end{aligned} \qquad \textbf{(VIII.4.3)}$$

The terms with $\omega\tau$ survive, and after some trigonometrical calculations, one reaches the all-inclusive formula:

$$\begin{aligned} I_{AC}(\tau) &= 2\cdot\frac{3}{8}\cdot\int A^4(t)dt \\ &+ 4\cdot\frac{3}{8}\cdot\int A^2(t)\cdot A^2(t-\tau)dt \\ &+ 2\cdot\frac{3}{8}\cdot\cos(2\omega\tau)\cdot\int A^2(t)\cdot A^2(t-\tau)dt \\ &+ 4\cdot\frac{3}{8}\cdot\cos(\omega\tau)\cdot\int A^3(t)\cdot A(t-\tau)+A^3(t-\tau)\cdot A(t)dt \end{aligned} \qquad \textbf{(VIII.4.4)}$$

Consider now two cases:

$$\begin{aligned} I_{AC}(\tau\to\infty) &= 2\cdot\frac{3}{8}\cdot\int A^4(t)dt \\ I_{AC}(\tau\to 0) &= 16\cdot\frac{3}{8}\cdot\int A^4(t)dt \end{aligned} \qquad \textbf{(VIII.4.5)}$$

It could be seen that there is a *(constant) background* signal ($I_{AC}(\tau\to\infty)>0$), and the *ratio between background and peak* is **1:8**. That special result can only be measured, by using a phase- and time-resolved set-up[241].

[241] Never used in this work

Usually, one does not have to take care of the phase, due to the fact that it is being smeared out during the measurement. The terms containing **cos(ωt)** and **cos(2ωt)** become averaged, and only the first two terms remain. The mentioned cases turn into

$$\begin{aligned} I_{AC}(\tau \to \infty) &= 2 \cdot \frac{3}{8} \cdot \int A^4(t) dt \\ I_{AC}(\tau \to 0) &= 6 \cdot \frac{3}{8} \cdot \int A^4(t) dt \end{aligned} \qquad \textbf{(VIII.4.6)}$$

Therefore, one gets the ratio **1:3**, as always seen in the measurements (e.g. Fig. 39, page 87).

2) Cross-polarised beams (ps-polarised, or sp-polarised)

In a cross-polarised set-up, the electric fields of both pulses hit the sample perpendicular to each other. It is no longer allowed to simply add both of them like scalars, but like vectors $\vec{E}(t,\tau) = \vec{E}_p(t) + \vec{E}_s(t-\tau)$. Thus, because they stand normal, Pythagoras' law determines the absolute value

$$\left|\vec{E}(t,\tau)\right| = \sqrt{\left|\vec{E}_p(t)\right|^2 + \left|\vec{E}_s(t-\tau)\right|^2} \qquad \textbf{(VIII.4.7)}$$

Now, it is possible to follow the same steps like in the parallel-polarised case above:

$$\begin{aligned} I_{AC}(\tau) &= const \cdot \int_{-\infty}^{+\infty} \left|\vec{E}(t,\tau)^2\right|^2 dt \\ &= const \cdot \int_{-\infty}^{+\infty} \left|\left|\vec{E}_p(t)\right|^2 + \left|\vec{E}_s(t-\tau)\right|^2\right|^2 dt \\ &= const \cdot \int_{-\infty}^{+\infty} \left|\left|A(t)\cdot\cos(\omega t)\right|^2 + \left|A(t-\tau)\cdot\cos\left[\omega\left(t-\tau\right)\right]\right|^2\right|^2 dt \end{aligned} \qquad \textbf{(VIII.4.8)}$$

Again $E_{p,s}(t) = A_{p,s}(t)\cdot\cos(\omega t)$, and additionally: $A_p \equiv A_s$.

$$\begin{aligned} I_{AC}(\tau) &= \int A^4(t)\cdot\cos^4(\omega t) + A^4(t-\tau)\cdot\cos^4\left[\omega\left(t-\tau\right)\right] dt \\ &+ 2\cdot\int A^2(t)\cdot A^2(t-\tau)\cdot\cos^2(\omega t)\cdot\cos^2\left[\omega\left(t-\tau\right)\right] dt \end{aligned} \qquad \textbf{(VIII.4.9)}$$

As before, one goes on with the "slowly varying envelop" approximation, and gets then finally:

$$I_{AC}(\tau) = 2\cdot\frac{3}{8}\cdot\int A^4(t)dt + 2\cdot\frac{3}{8}\cdot\cos(2\omega\tau)\cdot\int A^2(t)\cdot A^2(t-\tau)dt \qquad \textbf{(VIII.4.10)}$$

It is easy to see that many of the terms from above could be eliminated. The formula shows a *constant background* and a *time-dependent part*. The ratio of the two extreme cases ($I_{AC}(\tau\to\infty)$ and $I_{AC}(\tau\to 0)$) yields the result **1:2**. Unfortunately, one cannot determine the phase-integrated result, because of the loss of information using the "slowly varying envelop" approximation. It is known, that the phase-integrated curve behaves also as **1:2**.

All results may be summarised in the following table. See also Fig. 73:

	parallel-polarised pp, ss	**cross-polarised ps, sp**
phase-resolved	1:8	1:2
phase-integrated	1:3	1:2

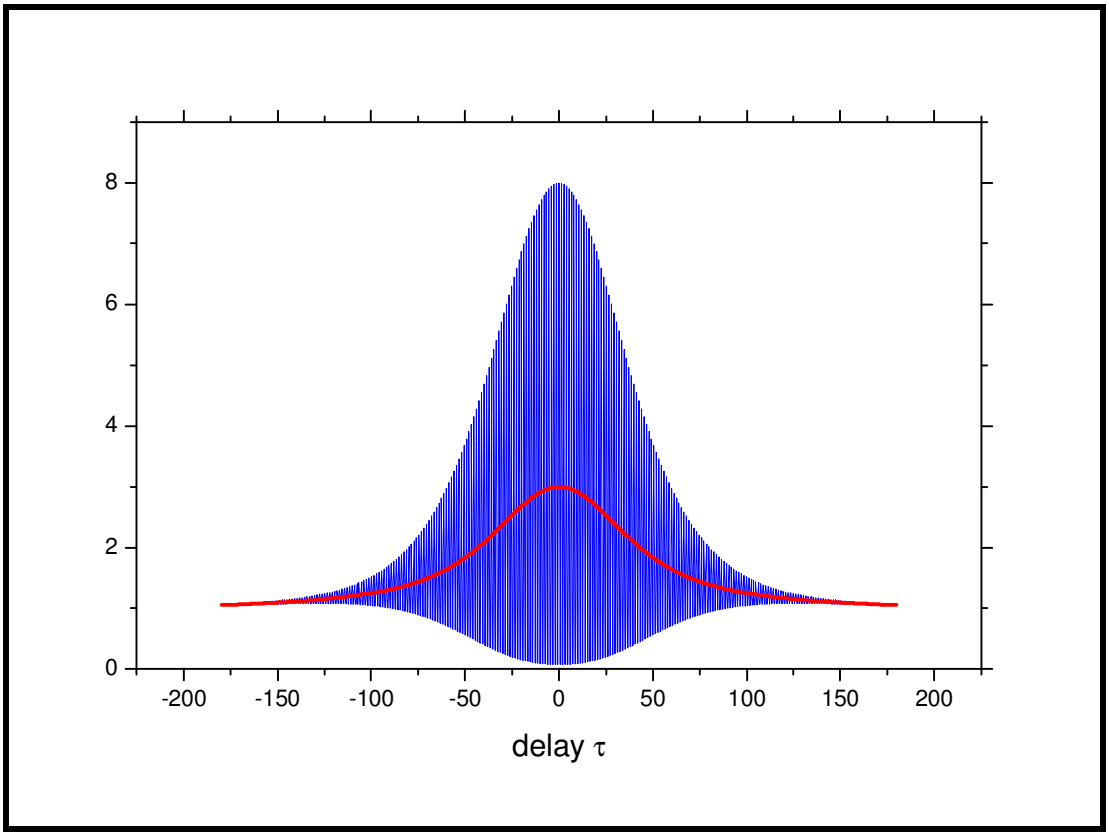

Fig. 73: The autocorrelation curve for *parallel-polarised* (pp or ss) electric fields. The blue curve indicates the phase-resolved, and red the phase-integrated result.

b. The influence of the electronic system

As mentioned at the beginning of this chapter, the influence of the electronic answer to the impinging of two laser pulses cannot be included in the simple calculations of section a). However, there is a more adequate theory to analyse the physics behind the measurement.

The following is just a brief overview[242]; the full explanation with many examples and consequences may be seen in [Bau97] and [Ohm02].

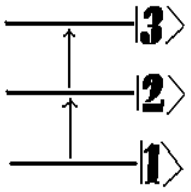

The *classical* description of a transition, using the Fermi Golden Rule, is a non-dynamical theory, i.e. there is *no time-dependent part*. Therefore, a more passable way to analyse the data is required. From the assumption of a three level system (initial state **|1>**, intermediate state **|2>**, final state **|3>**), one may go on to consider *time-dependent perturbations*. Take the ansatz:

$$i\hbar\frac{d}{dt}|\psi\rangle = (H_0 + V)|\psi\rangle \qquad \textbf{(VIII.4.11)}$$

with

$$\psi = c_1(t)e^{-i\omega_1 t}|1\rangle + c_1(t)e^{-i\omega_2 t}|2\rangle + c_1(t)e^{-i\omega_3 t}|3\rangle \qquad \textbf{(VIII.4.12)}$$

and the sum of the electric fields of both pulses (as above: $E(t)=A(t)\cdot e^{i\omega t}$)

$$V = A_a e^{i\omega_a t} + A_b(t-\tau)e^{i\omega_b(t-\tau)} \qquad \textbf{(VIII.4.13)}$$

Inserting ψ leads to

$$\sum_k \dot{c}_k e^{-i\omega_k t}|k\rangle = V|\psi\rangle \qquad \textbf{(VIII.4.14)}$$

and thus

$$\begin{aligned} \dot{c}_j &= -i\cdot\sum_k V_{jk}c_k \\ V_{jk} &= \tfrac{1}{\hbar}\langle j|V|k\rangle e^{i(\omega_j-\omega_k)t} \end{aligned} \qquad \textbf{(VIII.4.15)}$$

The abbreviation $\rho_{ij} = c_i(t)\cdot c_j^*(t)$ may be interpreted as *density matrix*. Its diagonal elements ρ_{ii} give the probability of the system being in the state |i>, while ρ_{ij} represent the optically induced coherence between |i> and

[242] Coming from [Ohm99]

|j>. The derivative $\dot{\rho}_{ij} = \dot{c}_i c_j^* + c_i \dot{c}_j^*$ of the density matrix is Hermitian ($\dot{\rho}_{ij} = \dot{\rho}_{ji}^*$), and it is possible to rewrite it with means of previous equations:

$$\begin{aligned} \dot{\rho}_{ij} &= -i \cdot \left(\sum_k V_{ik} c_k \right) \cdot c_j^* + i \cdot \sum_k V_{kj} c_k \\ &= -i \cdot \sum_k V_{ik} \rho_{kj} + i \cdot \sum_k V_{kj} \rho_{ik} \end{aligned} \qquad \textbf{(VIII.4.16)}$$

This is a relation of the form $\dot{\rho} = -\hbar[V, \rho]$. The coupling of the electron system to an external bath, which leads to possible dissipative affections (like decay of energy and/or momentum) to the density at the three levels, induces the necessary of a decay term $\dot{\rho}_{diss}$. Examples for it are

- No decay from final state: $(\dot{\rho}_{diss})_{33} = 0$
- An exponential decay channel from intermediate level: $(\dot{\rho}_{diss})_{22} = -\Gamma \rho_{22}$
- A refilling process into the initial state: $(\dot{\rho}_{diss})_{11} = \Gamma \rho_{22}$

Hence one gets finally the

Liouville-von Neumann (LvN) equation:

$$\dot{\rho} = -\hbar[V, \rho] + \dot{\rho}_{diss} \qquad \textbf{(VIII.4.17)}$$

Annotation: the diagonal elements (ρ_{ii}) of the density matrix describe the population in level i. They are called "population density", and are always real. The off-diagonal elements (ρ_{ij}, $i \neq j$), expressing the connections between two levels, are labelled as "coherences", and may be real or imaginary.

The Liouville-von Neumann equation may be expanded into nine coupled differential equations, one for each element of the density matrix. For the completeness, the nine equations shall be written here. Those equations are also known as the

Bloch equations:

$$\begin{aligned}
1)\quad & \dot{\rho}_{11} = -i \cdot V_{12} \cdot (\rho_{21} - \rho_{12}) && + \Gamma \rho_{11} \\
2)\quad & \dot{\rho}_{22} = -i \cdot V_{12} \cdot (\rho_{12} - \rho_{21}) + i \cdot V_{23} \cdot (\rho_{32} - \rho_{23}) && - \Gamma \rho_{22} \\
3)\quad & \dot{\rho}_{33} = -i \cdot V_{23} \cdot (\rho_{23} - \rho_{32}) && \\
4)\quad & \dot{\rho}_{13} = -i \cdot V_{12} \cdot \rho_{23} + i \cdot V_{23} \cdot \rho_{12} && - \Gamma_{13} \rho_{13} \\
5)\quad & \dot{\rho}_{12} = i \cdot V_{12} \cdot (\rho_{11} - \rho_{22}) + i \cdot V_{32} \cdot \rho_{13} && - \Gamma_{12} \rho_{12} \\
6)\quad & \dot{\rho}_{23} = i \cdot V_{23} \cdot (\rho_{22} - \rho_{33}) - i \cdot V_{21} \cdot \rho_{13} && - \Gamma_{23} \rho_{23} \\
7-9)\quad & \dot{\rho}_{ij} = \dot{\rho}_{ji}^* &&
\end{aligned} \qquad \textbf{(VIII.4.18)}$$

On this occasion, some assumption have been taken, which were already mentioned above:

- $\Gamma \equiv \Gamma_{22} = 1/\tau_{ee}$ is taken as main relaxation path from *second* into the *first* level (~inelastic lifetime)
- $V_{13} = 0$, means that the transition from *first* to *third* level is vanishing
- $\Gamma_{33} = 0$: no relaxation from *third* level

Those factors Γ_{ij} of the dissipative terms, are exactly the known spectral line width, used for example in photoemission spectra investigations. They can be described as $\Gamma_{ij} = \Gamma_i + \Gamma_j$, with the cited (page 60) relation

$$\frac{\Gamma}{2} = \frac{1}{T_2} = \frac{1}{2 \cdot T_1} + \frac{1}{T_2^*} \qquad \textbf{(VIII.4.19)}$$

Knowing the LvN equations enables to code a simulation routine, which needs just some assumption (like these above) and delivers directly the dynamical population density in the intermediate level (see Fig. 73 on page 143). It is then relatively easy to compare the measured data with this simulation. For an instructive example of how one gets information out of such simulated and compared fittings, see [Bau97].

Concerning the last mentioned formula, there is one thing, which demonstrates an advantage of the used method (TR-2PPE) to other optical means. While for example, second harmonic generation (SHG) could not distinguish, whether an excited electron has been dephased or has been inelastic scattered, this technique allows to decide the origin of the dynamical process behind. One can determine the inelastic relaxation T_1 as well as the dephasing T_2, and even the elastic relaxation (pure dephasing) T_2^*.

5. Selected types of F-centres

Because of the certain importance of F-centres in the investigations of systems using MgO as a substrate, it is good to know the full-range of possible F-centres, and their absorbance / emittance capability. The following table enumerates the frequently appearing F-centres.

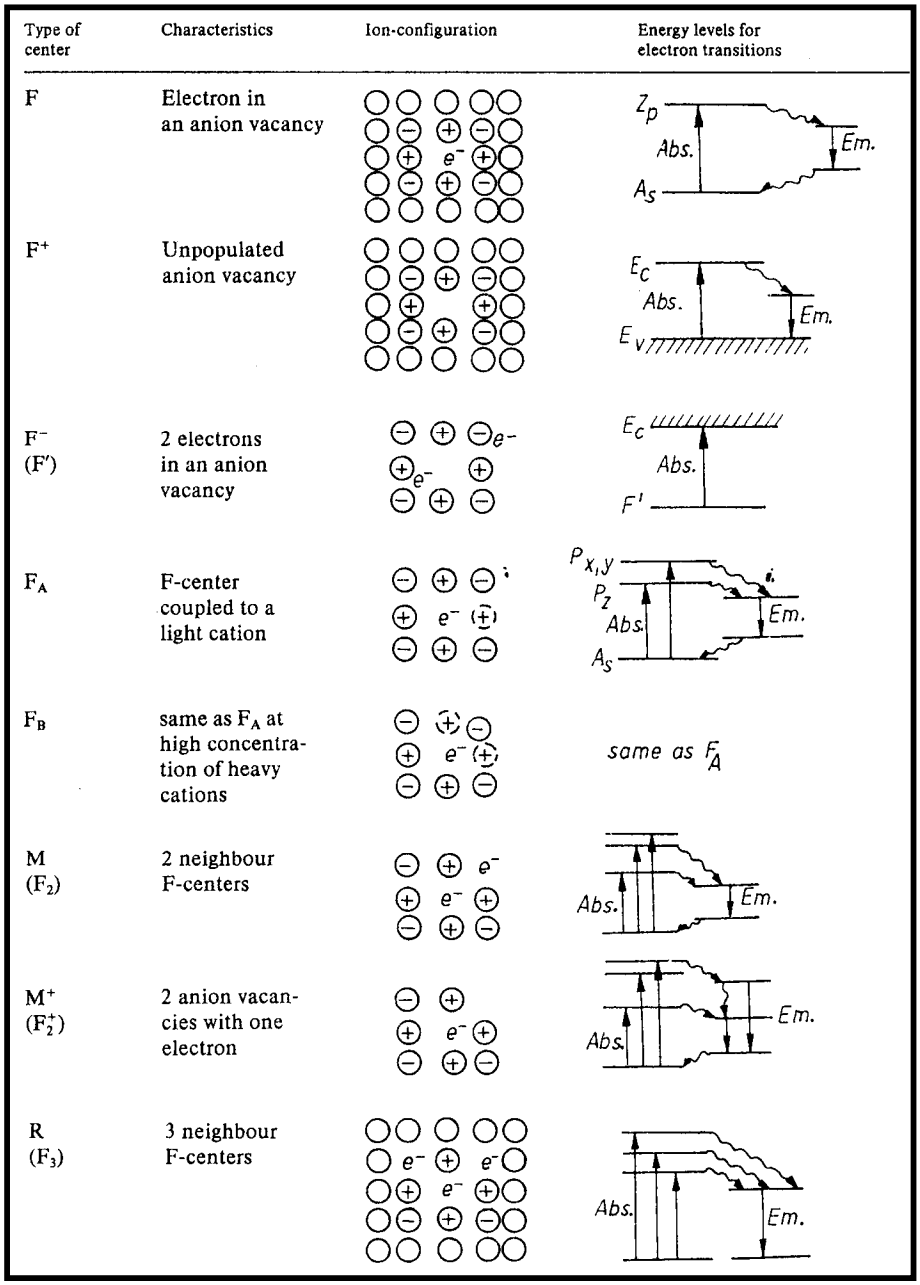

Fig. 74: The most frequently appearing F-centres and their excitations. This table has been taken from [BFG90].

6. Some physical constants

Data from [Lid95], [Bas95], [Ohm02]

Silver Ag

- Penetration depth λ of light:
  - Red (800nm): 11.6 nm
  - Blue (400nm): 15.2 nm
  - UV (267nm): 17.1 nm
- Lattice constants a: 4.09 Å (fcc)
- Mass density ρ: 10.2 $g \cdot cm^{-3}$
- Work function ϕ: 4.26 eV (polycrystalline)
  4.64 eV (100)
  4.52 eV (110)
  4.74 eV (111)

Graphite HOPG

- Lattice constants a: 2.46 Å (hex.)
- Mass density ρ: 2.3 $g \cdot cm^{-3}$

Gallium-arsenide GaAs

- Penetration depth λ of light:
  - Red (800nm): 730 nm
  - Blue (400nm): 14 nm
- Lattice constants a: 5.65 Å (hex.)
- Mass density ρ: 5.3 $g \cdot cm^{-3}$

Magnesium Oxide MgO

- Penetration depth λ of light:
  - Red (800nm): µm - mm
  - Blue (400nm): µm - mm
- Lattice constants a: 4.21 Å (rock-salt)
- Mass density ρ: 3.6 $g \cdot cm^{-3}$

IX. Literature

[AALR81] **Abrahams E.**, Anderson P.W., Lee P.A. and Ramakrishnan T.V.
Phys. Rev. B 24, 6783, 1981
Quasiparticle lifetime in disordered two-dimensional metals

[ABP+00] **Aeschlimann M.**, Bauer M., Pawlik S., Knorren R., Bouzerar G., Bennemann K.H.
Appl. Phys. A 71, 485-491, 2000
Transport and dynamics of optically excited electrons in metals

[ABP+97] **Aeschlimann M.**, Bauer M., Pawlik S., Weber W., Burgermeister R., Oberli D., Siegmann H.C.
Phys. Rev. Lett. 79, 5158, 1997
Ultrafast spin-dependent electron dynamics in fcc Co

[ACF+96] **Arciprete F.**, Colonna S., Fanfoni M., Patelly F., and Balzarotti A.
Phys. Rev. B 53, 12948, 1996
Observations of interface states by high-resolution electron-energy-loss spectroscopy in metal-GaAs(110) junctions

[Aes96] **Aeschlimann M.**
Habilitation, Zurich, 1996
Time Resolved Studies of Electron Relaxation at Metal Surfaces

[AS98] **Anton R.** and Schneidereit I.
Phys. Rev. B 58, 13874, 1998
In Situ TEM investigations of dendritic growth of Au on HOPG

[AYYT95] **Angerer J.Qi.W.**, Yaganeh M.S., Yodh A.G., and Theis W.M.
Phys. Rev. Lett. 75, 3174, 1995
Observation of Midgap Interface States in Buried Metal/GaAs Junctions

[BA02] **Bauer M. and Aeschlimann M.**
J. of Electron Spectr. and Rel. Phen. 124 (2002) 225-243
Dynamics of excited electrons in metals, thin films and nanostructures

[Bab37] **Baber W.G.**
Proc. R. Soc. London Ser. A 158, 383, 1937

[Bas95] **Bass M. editor in chief**
Handbook of optics (I, II, III), 2nd edition, McGraw-Hill
Sponsored by the Optical Society of America

[Bau97] **Bauer M.**
Ph.D. Thesis, Zurich, 1997
Real-time Investigation of the Lifetime of Electronic Excitations at Clean and Adsorbate-covered Metal Surfaces

[Bee02] **Beesley J.**
Private Communications, 2002

[Ben98] **Bennemann K.H.**
The International series of monographs on physics 98, Oxford science publications, 1998
Nonlinear optics in metals

[BFG90] **Brückner V.**, Feller K.-H., Grummt U.-W.
Akad. Verlagsgesellschaft Geest&Portig K.-G., Leipzig, 1990
Applications of Time-resolved Optical Spectroscopy

[BFI87] **Brorson S.D.**, Fujimoto J.G., Ippen E.P.
Phys. Rev. Lett. 59, 1962, 1987

[Bla96] **Blatter Ch.**
ETH Zurich, 1996
Lecture: Theorie der Wärme

[BRA95] **Borensztein Y.**, Roy M., and Alameh R.
Europhys. Lett. 31, 311, 1995

[BS64] **Berlund C.N.**, Spicer W.E.
Phys. Rev. A 136, 1030 and 1044, 1964

[Bur98] **Burgermeister R**.
Ph.D. Thesis, Zurich, 1998
Spin- and Time-resolved Two-Photon Photoemission

[CGE+98] **Cao J.**, Gao Y., Elsayed-Ali H.E., Miller R.J.D., Mantell D.A.
Phys. Rev. B 58, 10948, 1998

[Cha71] **Chaplik A.V.**
Sov. Phys. – JETP 33, 997, 1971

[Col93] **Collet J.H.**
Phys. Rev. B 47, 10279, 1993
Screening and exchange in the theory of the femtosecond kinetics of the electron-hole plasma

[Deg96] **Degiorgi L.**
Lecture on "optical properties of solids", ETH Zurich, 1996/1997

[DJ94] **Didier F.**, Jupille J.
Surf. Sci. 307-309, 587-590, 1993
Layer-by-Layer growth mode of silver on magnesium oxide (100)

[Dru00] **Drude P.**
Annalen der Physik 1, 369, 2000

[DSCM84] **Dubois L.H.**, Schwartz G.P., Camley R.E., Mills D.L.
Phys. Rev. B 29, 3208, 1984
Inelastic scattering of electrons from ionic crystals with a highly conducting overlayer

[EFN84] **Eckardt H.**, Fritsche L., Noffke J.
J. Phys. F 14, 97, 1984

[EH93] **Evans D.A.** and **Horn K.**
J. of Electron Spect. a. Related Phenomena 62, 59-72, 1993
Ag/GaAs(110) revisited: a photoemission study

[EP78] **Echenique P.M.**, Pendry J.B.
J. Phys. C: Solid State Phys., Vol. 11, 1978
The Existence and detection of Rydberg states at surfaces

[ESK00] **Ekardt W.**, Schöne W.-D., Keyling R.
Appl. Phys. A 71, 529-535, 2000
The determination of the lifetime of hot electrons in metals by time-resolved two-photon photoemission: the role of transport effects, virtual states, and transient excitons

[FE74] **Feibelman P.J.**, Eastman D.E.
Phys. Rev. B 10, 4932, 1974

[Fee89] **Feenstra R.M.**
Phys. Rev. Lett. 63, 1412, 1989

[Fee92] **Feenstra R.M.**
Appl. Surf. Sci. 56-58, 104, 1992

[Fer56] **Ferell R.A.**
Phys. Rev. 101, 554, 1956

[Fie01] **Fierz M.**
Ph.D. Thesis, Zurich, 2001
Ultrafast electron dynamics in gas-suspended nanoparticles

[FMG84] **Fork R.L.**, Martinez O.E., and Gordon J.P.
Optics Lett. 9, 159, 1984

[Fre99] **Freund H.-J.**
Faraday Discuss. 114, 1-31, 1999
Oxide surfaces

[FSFS94] **Fischer N.**, Schuppler S., Fauster Th., and Steinmann W.
Surf. Sci. 314, 89, 1994

[FSTB92] **Fann W.S.**, Storz R., Tom H.W.K. and Bokor J.
Phys. Rev. Lett. 46, 13592, 1992
Electron thermalization in gold

[GQ82] **Giuliani G.F.** and **Quinn J.**
Phys. Rev. B 26, 4421, 1982
Lifetime of a quasiparticle in a two-dimensional electron gas

[GZ94] **Göpel W., Ziegler C.**
Teubner Verlagsgesellschaft, 1994
Struktur der Materie: Grundlagen, Mikroskopie und Spektrokopie

[GZ96] **Göpel W., Ziegler C.**
Teubner Verlagsgesellschaft, 1996
Einführung in die Materialwissenschaften: Physikalisch-chemische Grundlagen und Anwendungen

[Hai95] **Haight R.**
Surf. Sci. Rep. 21, 275-325, 1995
Electron Dynamics at Surfaces

[HB86] **Haight R.**, and Bokor J.
Phys. Rev. Lett. 56, 2846, 1986
Direct Observation of Adsorbate-Induced Band-Gap States on GaAs(110)

[HKWE96] **Hertel T.**, Knoesel E., Wolf M., and Ertl G.
Phys. Rev. Lett. 76, 535, 1996

[HMK+98] **Horn-von Hoegen M.**, Meyer zu Heringdorf F.-J., Kähler D., Schmidt Th., Bauer E.
Thin solid films 336, 16-21, 1998
Adsorption induced giant faceting of vicinal Si(001)

[HMWM97] **Hohlfeld J.**, Müller J.G., Wellershoff S.-S., Matthias E.
Appl. Phys. B 64, 387, 1997

[Hüf01] **Hüfner S.**
Universität Saarbrücken
„Hochauflösende Photoelektronenemission": Talk on 3.12.01 in the „Physikalisches Kolloquium" in Kaiserslautern

[Hüf95] **Hüfner S.**
Springer Verlag, Berlin, Heidelberg, 1995
Photoelectron Spectroscopy: Principles and Applications

[Jac83] **Jackson J.D.**
Verlag de Gruyter, 2nd edition, Berlin, New York
Klassische Elektrodynamik

[JC72] **Johnson P.B.** and **Christy R.W.**
Phys. Rev. B 6, 4370, 1972

[JKLB92] **Jalochowski M.**, Knoppe H., Lilienkamp G., and Bauer E.
Phys. Rev. B 46, 4693-4701, 1992
Photoemission from ultrathin metallic films: Quantum size effect, electron scattering, and film structure

[JL75] **Jaklevic, R.C.**, Lambe J.
Phys. Rev. B 12, 4146, 1975
Experimental study of quantum size effects in thin metal films by electron tunnelling

[Kai] "http://www.material.tohoku.ac.jp/~kaimenb/B_RHEED.html"

[Kev83] **Kevan S.D.**
Phys. Rev. Lett. 50, 526, 1983

[KHM+01] **Kennerknecht C.**, Hövel H., Merschdorf M., Voll S., Pfeiffer W.
Appl. Phys. B 73, 425-429, 2001
Surface plasmon assisted photoemission from Au nanoparticles on graphite

[Kit96] **Kittel Ch.**
R. Oldenbourg Verlag München Wien 1996
Einführung in die Festkörperphysik

[KNMN95] **Kobayashi H.**, Namba K., Mori T., and Nakato Y.
Phys. Rev. B 52, 5781, 1995
Energy distribution of interface states in the band gap of GaAs determined from x-ray photoelectron spectra under biases

[Kno97] **Knösel E.**
Ph.D. Thesis, Berlin, 1997
Ultrakurzzeit-Dynamik elektronischer Anregungen auf Metalloberflächen

[KV95] **Kreibig U.** and **Vollmer M.**
Springer Series in Materials Science, Vol. 25, Springer Verlag, Berlin, 1995
Optical Properties of Metal Clusters

[Lan01] **Lange J.**
Diploma Thesis, Essen / Kaiserslautern, 2001
Interferometrische 2PPE-Messungen an Metalloberflächen

[Lan57] **Landau L.**
Soviet Physics JETP 3, 920, 1957

[LBD+01] **LaBella V.P.**,Bullock D.W., Ding Z., Emery C., Venkatesan A., Oliver W.F., Salamo G.J., Thibado P.M., and Mortazavi M.
Science 2001 May 25; 292: 1518-1521. (in Reports)
Spatially Resolved Spin-Injection Probability for Gallium Arsenide

[LHS+99] **Leitenstorfer A.**, Hunsche S.,Shah J., Nuss M.C., and Knox W.H.
Phys. Rev. Lett. 82, 5140, 1999
Femtosecond Charge Transport in Polar Semiconductors

[Lid95] **Lide D.R.**
Handbook of Chemistry and Physics
CRC Press, special student edition, 1995

[Lie93] **Liebsch A.**
Phys. Rev. B 48, 11317, 1993
Surface-plasmon dispersion and size dependence of Mie resonance: Silver versus simple metals

[Lie97] **Liebsch A.**
Plenum Press, New York and London, 1997
Electronic Excitations at Metal Surfaces

[Lin54] **Lindhard J.**
Kgl. Danske Videnskab. Selskab
Mat-fys. Medd. 28, No. 8, 1954

[LLA99] **Lamprecht B.**, Leitner A., Aussenegg F.R.
Appl. Phys. B 68, 419, 1999
SHG studies of plasmon dephasing in nanoparticles

[LMP+00] **Lehmann J.**, Merschdorf M., Pfeiffer W., Thon A., Voll S., Gerber G.
J. Chem. Phys. 112, 5428, 2000

[LP36] **Landau L.**, Pomerantschusk I.
Phys. Z. Sowjetunion 10, 649, 1936

[LRWM01] **Lindner R.**, Reichling M., Williams R.T., and Matthias E.
J. Phys.: Condens. Matter 13, 2339–2346, 2001
Femtosecond laser pulse excitation of electrons and excitons in CaF2 and SrF2

[LSHL86] **Ludeke R.**, Straub D., Hympsel F.J., and Landgren G.
J. Vac. Sci. Technol. A 4, 874, 1986

[Lut61] **Luttinger J.M.**
Phys. Rev. 121, 942, 1961

[LW88] **Lindgren S.Å.**, Walldén L.
Phys.Rev.Lett 61, 2894, 1988
Electron-Energy-Band Determination by Photoemission from Overlayer States

[LWFF93] **Li C.**, Wu R., and Freeman A.J., Fu C.L.
Phys. Rev. B 48, 8317, 1993
Energetics, bonding mechanism, and electronic structure of metal-ceramic interfaces: Ag/MgO(001)

[Mah70] **Mahan G.D.**
Phys. Rev. B 2, 4334, 1970

[Mar00] **Mariani C.**
Surf. Sci. 454-456, 417-427, 2000
A high-resolution photoemission study of confined metal systems on InAs(110)

[MPT+00] **Merschdorf M.**, Pfeiffer W., Thon A., Voll S. Gerber G.
Appl. Phys. A 71, 547-552, 2000
Photoemission from multiply excited surface plasmons in Ag nanoparticles

[MRHH99] **Moresco F.**, Rocca M., Hildebrandt T., and Henzler M.
Phys. Rev. Lett. 83, 2238, 1999
Plasmon Confinement in Ultrathin Continuous Ag Films

[MYT+01] **Matsuda I.**,Yeom H. W., Tanikawa T., Tono K., Nagao T., Hasegawa S., and Ohta T.
Phys. Rev. B 63, 125325-1, 2001
Growth and electron quantization of metastable silver films on Si(001)

[NBPH97] **Neuhold G.**, Bartels L., Paggel J.J., Horn K.
Surf. Sci. 376, 1-12, 1997
Thickness-dependent morphologies of thin Ag films on GaAs(110) as revealed by LEED and STM

[NSW+96] **Nilsson A.**, Stöhr J., Wiell T., Aldén M., Bennich P., Wassdahl N., Samant M.G., Parkin S.S.P., Mårtensson N., Nordgren J., Johansson B., Skriver H.L.
Phys. Rev. B 54, 2917, 1996
Determination of the electronic density of states near buried interfaces: Application to Co/Cu multilayers

[Ohm02] **Ohms T.**
Ph.D. Thesis, University of Kaiserslautern, 2002
Spin- and Energy Relaxation of Hot Electrons in Gallium-Arsenide

[Ohm99] **Ohms T.**
Private communications based on works by H. Ueba, 1999

[Oma75] **Omar M.A.**
Addison-Wesley Publishing Company, 1975
Elementary Solid State Physics

[ONP02] **Ogawa S.**, Nagano H., Petek H.
Phys. Rev. Lett. 88, 116801-1, 2002
Optical Intersubband Transitions and Femtosecond Dynamics in Ag/Fe(100) Quantum Wells

[OSP+02]? **Ohms T.**, Scharte M., Porath R., and Aeschlimann M.
PRL, 2002 <= ?
Electron spin dynamics in GaAs/metal interface

[Ott95] **Ott H.-R.**
Vorlesungsskript, ETH Zurich, 1995
Festkörperphysik I

[Paw98] **Pawlik S.**
Ph.D. Thesis, Zurich, 1998
Untersuchung der Elektronendynamik in Metallen mittels zeitaufgelöster Zwei-Photonen-Photoemission

[PBBA98] **Pawlik S.**, Burgermeister R., Bauer M., Aeschlimann M.
Surf. Sci. 402-404, 556, 1998
Direct transition in the system Ag(111) studied by one- and two-photon photoemission

[PBFW84] **Posternak M.**, Baldereschi A., Freemann A.J., Wimmer E.
Phys. Rev. Lett. 52, 863, 1984

[Pen76] **Pendry J.B.**
Surf. Sci. 57, 679, 1976

[PG75] **Pendry J.B.**, Gurman S.J.
Surf. Sci. 49, 87-105, 1975

[PM96] **Pérez-Díaz J.L.** and **Muñoz M.C.**
Phys. Rev. B 53, 13583, 1996
Quantum-well states in metallic-thin-film overlayers

[PMC98] **Paggel J.J.**, Miller T., and Chiang T.-C.
Phys. Rev. Lett. 81, 5632, 1998
Quasiparticle Lifetime in Macroscopically Uniform Ag/Fe(100) Quantum Wells

[PN66] **Pines D.**, Nozieres P.
Benjamin, New York, 1966
The Theory of Quantum Liquids

[PO97] **Petek H. and Ogawa S.**
Prog. In Surf. Science 56, 239, 1997

[Por98] **Porath R.**
Diploma Thesis, Essen / Zurich, 1998
Die Elektronendynamik in niedrigdimensionalen Systemen: Relaxationsdynamik im Silber/Graphit-System

[PRT67] **Palmberg P.W.**, Rhodin T.N., and Todd C.J.
Appl. Phys. Lett. 11, 33, 1967
Epitaxial Growth of Gold and Silver on Magnesium Oxide Cleaved in Ultrahigh Vacuum

[PY01] **Perry S.S.**, Yang X.
Omicron Newsletter, Vol. 5 Nr. 2, II/01, 2001
Variable-Temperature Non-Contact Atomic Force Microscopy Measurements of Copper on MgO(100)

[Qui62] **Quinn J.**
Phys. Rev. 126 (4), 1453-1457, 1962
Range of Excited Electrons in Metals

[Qui63] **Quinn J.**
Appl. Phys. Lett. 2, 167, 1963

[Rae80] **Raether H.**
Springer tracts in modern Physics, Volume 88, 1980
Excitation of Plasmons and Interband Transitions by Electrons

[Rae88] **Raether H.**
Springer tracts in modern Physics, Volume 111, 1988
Surface Plasmons on Smooth and Rough Surfaces and on Gratings

[RGPC97] **Ramírez R., González R., Pareja R., Chen Y.**
Phys. Rev. B 55, 2413-2416, 1997
Semiconducting property of a wide-band-gap oxide crystal: Impact ionization and avalanche breakdown

[RRM+01] **Rickart M.**, Roos B.F.P., Mewes T., Jorzick J., Demokritiv S.O., Hillebrands B.
Surf. Sci. 495, 68-76, 2001
Morphology of epitaxial metallic layers on MgO substrates: influence of submonolayer carbon contamination

[Rub99] **Rubahn H.-G.**
John Wiley & Sons, 1999
Laser Applications in Surface Science and Technology

[SA95] **Schönberger U.**, Aryasetiawan F.
Phys. Rev. B 52, 8788, 1995
Bulk and surface electronic structures of MgO

[SAE+94] **Schmuttenmear C.A**., Aeschlimann M., Elsayed-Ali H.E., Miller R.J.D., Mantell D., Cao J., and Gao Y.
Phys. Rev. B 50, 8957, 1994
Time resolved Two Photon Photoemission from Cu(100): Energy Dependence of Electron Relaxation

[SB00] **Schmid G.**, Beyer N.,
Eur. J. Inorg. Chem. 2000, 835-837
A New Approach to Well-Ordered Quantum Dots

[SBJ95] **Suarez C.**, Bron W.E., Juhasz T.
Phys. Rev. Lett. 75, 4536, 1995

[SBW+02] **Schmidt O.**, Bauer M., Wiemann C., Porath R., Scharte M., Andreyev O., Schönhense G., and Aeschlimann M.
Appl. Phys. B 74 (2002) 223-227
Time-resolved two photon photoemission electron microscopy

[Sch02] **Scharte M.**
Ph.D. Thesis, University of Kaiserslautern, 2002
Lebensdauern von Mie-Plasmonen in Ag-Nanoteilchen

[SCNS96] **Smith A.R.**, Chao K.-J., Niu Q., Shih C.-K.
Science 273, 226-228, 1996
Formation of atomically flat silver films on GaAs with a "silver mean" quasi periodicity

[Shah96] **Shah J.**
Ultrafast spectroscopy of semiconductors and semiconductor nanostructures, Springer 1996

[SKK01] **Stracke P.**, Krischok S., Kempter V.
Surf. Sci. 473, 86-96, 2001
Ag-adsorption on MgO: investigations with MIES and UPS

[SLSS80] **Spicer W.E.**, Lindau I., Skeath P., and Su C.Y.
J. Vac. Sci. Technol. 17, 1019, 1980

[Smi85] **Smith N.V.**
Phys. Rev. B 32, 3549, 1985
Phase analysis of image states and surface states associated with nearly-free-electron band gaps

[SP+01] **Scharte M.**, Porath R., Ohms T., and Aeschlimann M., Lamprecht B., Ditlbacher H., and Aussenegg F.R.
in "Controlling and using light in nanometric domains", A. Lewis, H.K. Wickramasingae, K. Al-Shamery, Ed., Proc. of the SPIE 4456, (2001) 14
Lifetime and dephasing of plasmons in Ag-nanoparticles

[SPO+01] **Scharte M.**, Porath R., Ohms T., and Aeschlimann M., Krenn J.R., Ditlbacher H., and Aussenegg F.R., Liebsch A.
Appl. Phys. B 73, 305-310, 2001
Do Mie plasmons have a longer lifetime on resonance than off-resonance

[SPS98] **Schaffner M.-H.**, Patthey F., Schneider W.-D.
Surf. Sci. 417, 159-167, 1998
Growth study of silver on MgO(100)/Mo(100)

[SSC00] **Sushko P.V.**, Shluger A.L., Catlow C.R.A.
Surf. Sci. 450, 153-170, 2000
Relative energies of surface and defect states: ab initio calculations for the MgO(001) surface

[TKML93] **Tiggesbaumker J.**, Koller L., Meiwes-Broer K.H., and Liebsch A.
Phys. Rev. A 48, 1749, 1993

[TR82] **Tatar R.C.**, Rabii S.
Phys. Rev. B 25, 4126, 1982

[TVS90] **Tjeng L.H.**, Vos A.R. Sawatzky G.A.
Surf. Sci. 235, 269-279, 1990
Electronic structure of MgO studied by angle-resolved ultraviolet photoelectron spectroscopy

[UDKP81] **Uren M.J.**, Davies R.A., Kaveh M. and Pepper M.
J. Phys. C 14, L395, 1981

[UM00] **Ueba H.** and **Mii T.**
Appl. Phys. A 71, 537-545, 2000
Theory of energy- and time-resolved two-photon photoemission from metal surfaces – influence of pulse duration and excitation condition

[UM01] **Ueba H.** and **Mii T.**
Springer Series on Applied Physics: "Time-resolved photoemission from solids", Editors: M. Aeschlimann and M. Wolf, Springer 2001 (in printing)
Theory of Two-Photon Photoemission Spectroscopy

[VPM+96] **Valla T.**, Pervan P., Milun M., Hayden A.B., Woodruff D.P.
Phys. Rev. B 54, 11786, 1996
Electronic structure of silver and copper ultrathin films on V(100): Quantum-well states

[VSB86] **Vitrro R.E.**, Slade M.L., and Brillson L.J.
Phys. Rev. Lett. 57, 487, 1986

[vSN90] **van Schilfgaarde M. and Newman N.**
Phys. Rev. Lett. 65, 2728, 1990
Electronic Structure of Ideal Metal/GaAs Contacts

[WCLH85] **Wern H.**, Courths R., Leschik G., Hüfner S.
Z. Physik B 60, 293, 1985

[Wei87] **Weisbuch C.**
Semiconductors and Semimetals, Vol 24, Academic Press, New York, 1987
Fundamental Properties of III-V Semiconductor Two-Dimensional Quantized Structures: The Basis for Optical and Electronic Device Applications

[Wol01] **Wolf S.A. et al.**
Science 294, 1488, 2001
Spintronics: a spin-based electronics vision for the future

[WSHC86] **Wachs A.L.**, Shapiro A.P., Hsieh T.C., and Chiang T.-C.
Phys. Rev. B 33, 1460, 1986
Observation of film states and surface-state precursors for Ag films on Si(111)

[Zan88] **Zangwill A.**
Cambridge University Press, 1988
Physics At Surfaces

[Zew98] **Zewail A.H.**
J. Phys. Chem. - Special Issue (1998), pp. 4021
Ten years of Femtochemistry: Time Resolution of Physical, Chemical and Biological Dynamics, A.W. Castleman and V. Sundström (eds.)

[ZKJ+99] **Zhukovskii Yu.F.**, Kotomin E.A., Jacobs P.W.M., Stoneham A.M., Harding J.H.
Surf. Sci. 441, 373-383, 1999
Comparative theoretical study of the Ag-MgO(100) and (110) interfaces

X. Thanks to …

I would like to give my special thanks to **Prof. Dr. M. Aeschlimann**, who invited me to do research in his work group, and who gave me the opportunity to learn interesting topics of surface science and ultrafast phenomena. He was never tired to discuss with me about any new arising effect and other difficult details of the experiments.

Sincere thanks go to **Prof. Dr. Ch. Ziegler**. She has kindly accepted to examine my thesis and it was a great pleasure for me to debate with her about topics of chemistry and semiconductors.

I owe my dear friend **Dr. Mathias Scharte** huge thanks for so many reasons. He did not only motivate me with his endless humour, but he also showed me a large variety of interesting activities apart from the work at the university. He was and is still like an elder brother for me.

When we moved to Essen in 1998, it was very important for me to have good friends like **John Beesley** and **Dr. Torsten Ohms** at my side. Both of them had their own special topics they preferred to discuss with me. John and I could talk enthusiastically and infinitely about the differences of Switzerland and Germany. With Torsten it was an amusement to talk about German authorities and their decisions. Thanks to both of you.

Marlies Wessendorf is a wonderful person. I will never forget her. Since she has joined our group, her warm-hearted and lovely nature has inspired all of us. With her knowledge of chemistry, she is an irreplaceable advisor, whenever we physicists have to handle molecules or similar things.

Further thanks go to **Carsten Wiemann**, who helped me to measure a part of this work. I am glad to had the possibility to become acquainted with him, and also with **Jörg Lange**, **Dirk Mittnacht** and **Oleksiy Andreyev**. I wish you all success and joy at your work as well as in your life.

The new group members **Dorothea Hoffmann**, **Sven Passlack** and **Felix Steeb** as well as the former group members **Jörg M. Walter**,

and **Ansgar Lohoff** have helped me in their own way to finish this work. Thanks and all the best at what ever you will do.

The personality of **Dr. Michael Bauer**, **Dr. Hans-Jochen Foth**, **Dirk Hüttenberger** and **Manfred Lüke** gave me the opportunity to see and learn so many different things, which are important for my further work and life.

I am greatly indebted to **Mathias Mondon**, **Blondine Pluget**, **Stefen Berger** and **Stefan Lach**, who did AFM-analyses for parts of this work.

During the periods of Essen and of Kaiserslautern, I had the wonderful chance to work with the helpful technicians **Axel Mühle**, **Harry Sept** and **Richard Walther** and also with the lovely and very obliging secretaries **Ms M. Motzko**, **Ms K. Eibl** and **Ms S. Heider**. I cannot imagine, what would have happened to this work without all of them.

It is important for me to apologize to all my friends for not having mentioned them by name. You are very essential for me.

Last but most important, I would like to thank my parents **Brigitte** and **Sylvain**, my sister **Dalit** and my brother **Michael**, for being there whenever I need them, and for supporting me in whatever I do.

XI. List of publications

Parts of this work are already published or will be published soon:

- **Relaxation of hot electrons in solids of reduced dimensions**
  R. Porath, T. Ohms, M. Scharte, J. Beesley, M. Wessendorf,
  O. Andreyev, C. Wiemann and M. Aeschlimann
  (submitted)

- **Electron spin dynamics in a GaAs/metal interface**
  T. Ohms, R. Porath, M. Scharte, J. Beesley and M. Aeschlimann
  (submitted)

- **Lifetime and dephasing of plasmons in Ag-nanoparticles**
  M. Scharte, R. Porath, T. Ohms, M. Aeschlimann, B. Lamprecht,
  H. Ditlbacher, F.R. Aussenegg
  in "Controlling and using light in nanometric domains", A. Lewis, H.K. Wickramasingae, K. Al-Shamery, Ed.,
  Proc. of the SPIE 4456, (2001) 14

- **Do Mie plasmons have a longer lifetime on resonance than off resonance?**
  M. Scharte, R. Porath, T. Ohms, M. Aeschlimann, J.R. Krenn,
  H. Ditlbacher, F.R. Aussenegg, A. Liebsch
  Appl. Phys. B 73 (2001) 305-310

- **Time-resolved two photon photoemission electron microscopy**
  O. Schmidt, M. Bauer, C. Wiemann, R. Porath, M. Scharte,
  O. Andreyev, G. Schönhense, and M. Aeschlimann
  Appl. Phys. B 74 (2002) 223-227

XII. Curriculum vitae

10.04.1973	Born in Haifa, Israel
04/1980 – 04/1986	Primary school, Zurich, Switzerland
04/1986 – 08/1989	Secondary school, Zurich, Switzerland
09/1989 – 09/1992	High school AKAD, Zurich, Switzerland Degree: Matura (Abitur)
09/1992 – 10/1993	Military services and internships
10/1993 – 08/1998	Studies of physics at the ETHZ (Swiss Federal Institute of Technology Zurich) Topics: solid state physics, magnetism, numerical methods Thesis: Relaxation dynamics of optically excited electrons in mesoscopic systems
09/1998 – 11/2002	Ph.D. in the group of Prof. Dr. M. Aeschlimann at the universities of • Essen, Germany • Kaiserslautern, Germany Thesis: Dynamics of hot electrons in thin films and small structures